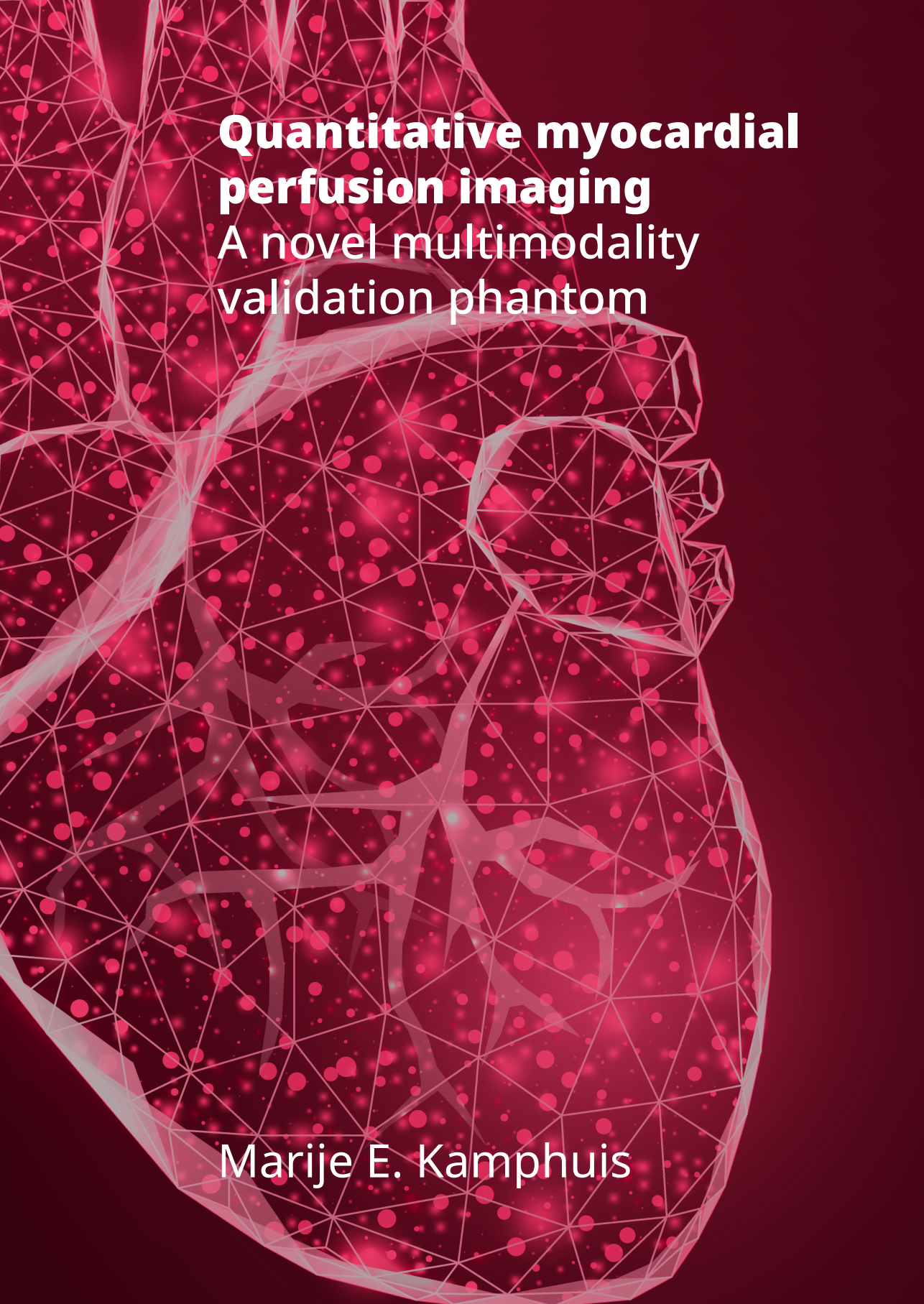

Quantitative myocardial perfusion imaging

A novel multimodality validation phantom

Marije E. Kamphuis

Quantitative myocardial perfusion imaging
A novel multimodality validation phantom

Marije Elise Kamphuis

QUANTITATIVE MYOCARDIAL PERFUSION IMAGING

A NOVEL MULTIMODALITY VALIDATION PHANTOM

DISSERTATION

to obtain
the degree of doctor at the University of Twente,
on the authority of the rector magnificus,
prof. dr. ir. A. Veldkamp,
on account of the decision of the Doctorate Board
to be publicly defended
on Thursday 30 June 2022 at 14.45 hours

by

Marije Elise Kamphuis

born on the 19th of May, 1990
in Delfzijl, The Netherlands

This dissertation has been approved by

Supervisors

prof. dr. ir. C.H. Slump
prof. dr. R.H.J.A. Slart

Co-supervisor

dr. M.J.W. Greuter

Cover design: Vectormer - Freepik.com / Arthur Veugelers
Printed by: Gildeprint
Lay-out: Arthur Veugelers
ISBN: 978-90-365-5378-0
DOI: 10.3990/1.9789036553780

Graduation Committee

Chair / secretary

prof. dr. J.N. Kok
University of Twente

Supervisors

prof. dr. ir. C.H. Slump
University of Twente

prof. dr. R.H.J.A. Slart
University of Twente
University Medical Center Groningen

Co-supervisor

dr. M.J.W. Greuter
University of Twente
University Medical Center Groningen

Committee Members

prof. dr. ir. B.J. Geurts
University of Twente

prof. dr. S. Manohar
University Twente

dr. F.J. Siepel
University of Twente

prof. dr. L.F. de Geus-Oei
Leiden University Medical Center
University of Twente

prof. dr. R. Vliegenthart
University of Groningen
University Medical Center Groningen

Contents

1

Introduction

Coronary artery disease

Coronary artery disease (CAD) presents an enormous societal burden with respect to disease morbidity and mortality, personal hardship, and healthcare expense. In the Netherlands in 2020, the prevalence of CAD was estimated at 777,400 patients, with an increasing prevalence by age.[1,2] Over 8,000 patients die from CAD annually, whereof acute myocardial infarction covers about 60 % of deaths.[1,3] Both national and international morbidity and mortality rates have declined in the past decades due to improved risk factor management and treatment possibilities.[4] However, CAD remains one of the leading causes of death and disability worldwide.[4] In the Netherlands, CAD tops the list of disorders with the highest disease burden (expressed in disability-adjusted life years; 271,300 in 2018).[5] CAD also occurs in the top ten most expensive diseases. In 2017, CAD related cost were 2.3 billion euros, which is about 2.6 % of total national healthcare expenditure.[6]

Obstructive CAD develops when coronary arteries that supply the myocardium (i.e., heart muscle) become damaged or diseased (**Figure 1**). Usually, coronary arteries occlude via atherosclerotic plaque development containing cholesterol deposits and

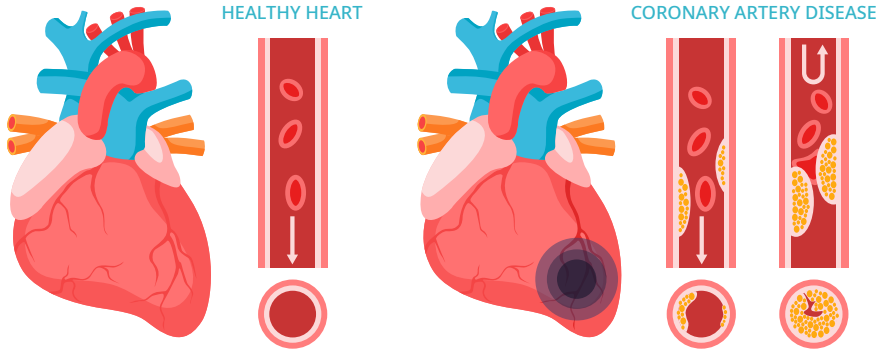

Figure 1 Comparison between a healthy and coronary artery diseased heart. Regional myocardial ischemia can be the result of a flow limitation in a supplying coronary artery upstream, due to atherosclerotic plaque development. Adapted from Natpra - Freepik.com

inflammatory cells.[7] Depending on its severity and stage, the stenosis can cause an impaired blood flow. Succeeding shortage of oxygen and nutrients, further referred to as myocardial ischemia, reduces cardiac contraction and therefore cardiac output. Ischemia can be temporarily present when the myocardium is being additionally challenged, e.g., in stress. In chronic, stable CAD, a stenosis develops gradually over decades. Characteristics of discomfort, such as chest pain and shortness of breath, regularly arise at a time there is already a significant flow limiting stenosis (or multiple). If left untreated, stable CAD may progress into a life-threatening condition when a sudden rupture of plaque causes complete occlusion, resulting in myocardial infarction.[8–10]

The chronic nature of atherosclerotic plaque formation can be altered by risk factor modification, pharmacological therapy, and revascularization surgery (**Figure 2**). These monitoring and intervention efforts may result in disease stabilization or regression.[7] In disease management it is important to correctly indicate which patients suffer from CAD with 'vulnerable' plaque development, and thus benefit more from thorough testing in determining an optimal treatment strategy, that may finally result in invasive intervention. These revascularization interventions include percutaneous coronary intervention with or without stenting and coronary bypass surgery.[11] On the contrary, it is also important to identify those patients with a less severe disease stage and good prognosis, thereby avoiding unnecessary (invasive) testing and intervention. These patients, for example, benefit more from lifestyle adjustments possibly in combination with pharmacological therapies.[7,12] In addition, a certain number of patients with symptoms eventually turn out to have no cardiac related problems and can be reassured and send home or get referred to another specialism. The high impact of treatment decision making on patient outcome is also reflected by outcomes of multiple large clinical trials.[13–16] These trials show that patients with a non-ischemic stenosis have a low risk (<1%) at developing a major adverse cardiovascular event (MACE) at a composite endpoint (e.g., including nonfatal myocardial infarction and cardiovascular death). Stenting such stenosis is undesired as it triples the risk at MACE.[13–16] An ischemic stenosis, on the contrary, should be treated, as untreated the risk at MACE is about 5–10%. Accordingly, adequate and timely diagnostics are essential in overall CAD management.

Figure 2 Schematic representation of treatment decision making process based on (imaging) diagnostics in patients with suspected or known 'stable' coronary artery disease (CAD).[7]

Diagnostics

Several diagnostic workups are common in CAD management depending on the particular patient population (categorized into subgroups by risk stratification), and on local expertise and equipment available. International guidelines recommend using non-invasive imaging techniques prior to invasive coronary angiography to evaluate patients with suspected or established 'stable' CAD who have a low to intermediate pre-test likelihood*.[7,17] In this particular patient population, both anatomical and functional imaging is recommended to further assess a patient's cardiovascular risk profile. Coronary computed tomography angiography (CCTA) visualizes the anatomy of the coronary arteries to detect the presence and severity of a possible stenosis (or multiple).[18] Myocardial perfusion imaging (MPI) is a functional imaging test utilized to detect ischemia and confirm the diagnosis CAD. Especially the manifestation of ischemia is a key indicator for revascularization.

Conventional static myocardial perfusion imaging

Conventional static MPI is performed with single photon emitting computed tomography (SPECT) and positron emission tomography (PET).[7] These nuclear imaging methods aim to identify areas of the left ventricular myocardium with reduced perfusion by comparing a static perfusion scan in rest with a static perfusion scan in (bicycle or pharmacon) stress.[19] During the procedure, a radioactive labeled contrast agent, called a radiotracer, is administered intravenously. Nowadays, common radiotracers in MPI are [^{99m}Tc]Tc-sestamibi or [^{99m}Tc]Tc-tetrofosmin in SPECT and ^{82}Rb, [^{13}N]NH_3 or H_2[^{15}O]O in PET. Depending on the radiotracer used, a certain fraction of the entrained tracer is taken up by the myocardium. The radiotracer emits gamma rays that can be detected by the SPECT or PET camera. Backtracking of the origin of these detected photons forms the basis of perfusion image reconstruction. In SPECT this is performed using single photon detection and in PET using coincidence photon detection, usually incorporated with time-of-flight measurement.[20,21] A region from which relatively less photons are detected can indicate a local perfusion deficit as a result of a significant stenosis upstream. By performing both a scan in rest and stress, it is possible to differentiate between a reversible or irreversible perfusion deficit, implying ischemia or infarction, respectively.[19] **Figure 3** visualizes a basic overview of the conventional static nuclear MPI procedure as part of overall CAD diagnostics.

Conventional static MPI is fairly good in identifying obstructive CAD. In this, PET offers a fundamentally better image resolution compared to SPECT, as reflected in a slightly higher diagnostic performance.[22] Moreover, compared with SPECT, PET imaging provides lower radiation exposure to patients due to the physical properties of the used radiotracers. On the contrary, SPECT is considerably less expensive compared to PET as it does not require a generator or cyclotron on site and is therefore

more widely accessible and utilized.[23–25] Nevertheless, this relative way of perfusion assessment results in underdiagnosis of particular patient subgroups, including patients with microvascular dysfunction and balanced ischemia (where all epicardial arteries are evenly affected or in main stem disease).[25,26] In addition, conventional MPI comprises visual evaluation of perfusion images, which can contribute to dispersion in diagnostic performance between clinicians and centers.[26,27]

Innovation in myocardial perfusion imaging

The medical imaging domain is continuously evolving, from the introduction of novel (aspects in) imaging technology to improvements in acquisition, reconstruction, and

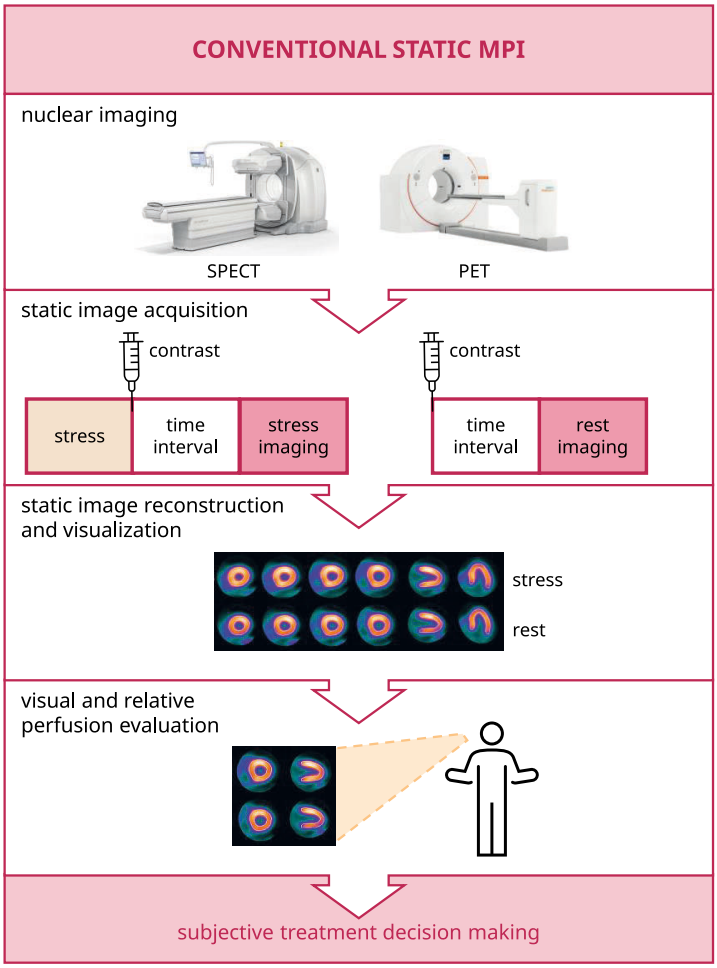

Figure 3 Basic overview of the conventional static myocardial perfusion imaging (MPI) procedure as part of overall CAD diagnostics.

analysis methods. Zoomed in on MPI, the field has been originally dominated by static nuclear imaging. Yet, in recent decades, a shift towards dynamic imaging, hybrid imaging (for attenuation correction) and towards other imaging modalities is ongoing.[28,29] For example, magnetic resonance imaging (MRI) has become a common MPI method and possibilities with ultrasound (US) and computed tomography (CT) are being explored as well. Noteworthy is that current clinical implementation of these multimodal MPI procedures varies widely. For example, centers can choose between stress and rest, or stress-only imaging protocols, a one-day or two-day examination, etc. There are also various options for scanner hardware and associated MPI software to choose from.[19,30]

Another widely supported innovation direction in the medical imaging domain concerns the clinical need for quantitative imaging, thereby aiming to improve, objectify and standardize the analysis and interpretation of image data. Quantitative imaging is introduced into clinical practice through various forms of technical medical innovation (e.g., using artificial intelligence) and such innovation is also ongoing in the field of MPI.[26,27,31] For some time now, the use of semi-quantitative scores has proven to be a reasonably objective measure of cardiac perfusion and ischemia. For example, summed scores of accumulated radiotracer activity in myocardial regions can be calculated for the rest and stress perfusion scans. The summed difference score is the difference between these two scores and represents a measure of ischemia. Although this form of image quantification is a start of a more objective, and standardized decision-making process, the measurement itself remains based on relative perfusion data. Hence, these semi-quantitative scores should be handled with caution and are clinically used as a supplement to visual judgment.[19]

One step further in quantitative MPI covers the assessment of absolute myocardial perfusion measures. Contemporary studies (merely in PET) have reported on the added diagnostic and prognostic value of global and regional myocardial blood flow (MBF) and myocardial flow reserve (MFR) measurements.[32] MBF is measured in mL/min per g of myocardium and MFR is defined as the ratio between peak stress and rest MBF. As a result, absolute blood flow quantification is considered a desirable and widely supported addition to current multimodal MPI diagnostics. In essence, assessment of MBF and MFR could not only strive for a more objective and standardized evaluation of myocardial ischemia, but also improve diagnostics in patients with balanced ischemia and microvascular dysfunction.[30]

Quantitative multimodal myocardial perfusion imaging

Figure 4 illustrates the basic quantitative / absolute MPI procedure, which is a multimodality approach. This procedure differs from conventional MPI in terms of image data acquisition, reconstruction, and analysis. Conventional MPI detects the accumulated tracer uptake in the myocardium for a certain time period after radiotracer

administration (see **Figure 3**). For quantitative, multimodal MPI it is generally a prerequisite to record the kinetics of the injected (radiolabeled) contrast medium over time.* The dynamic scan will therefore start just before the contrast injection. With conventional MPI, the detected accumulated radiotracer uptake in the myocardium is reconstructed into static perfusion images. In quantitative MPI, nonetheless, a dy-

* Quantitative MPI can be performed also without contrast injection, e.g., with arterial spin labeling in MRI.

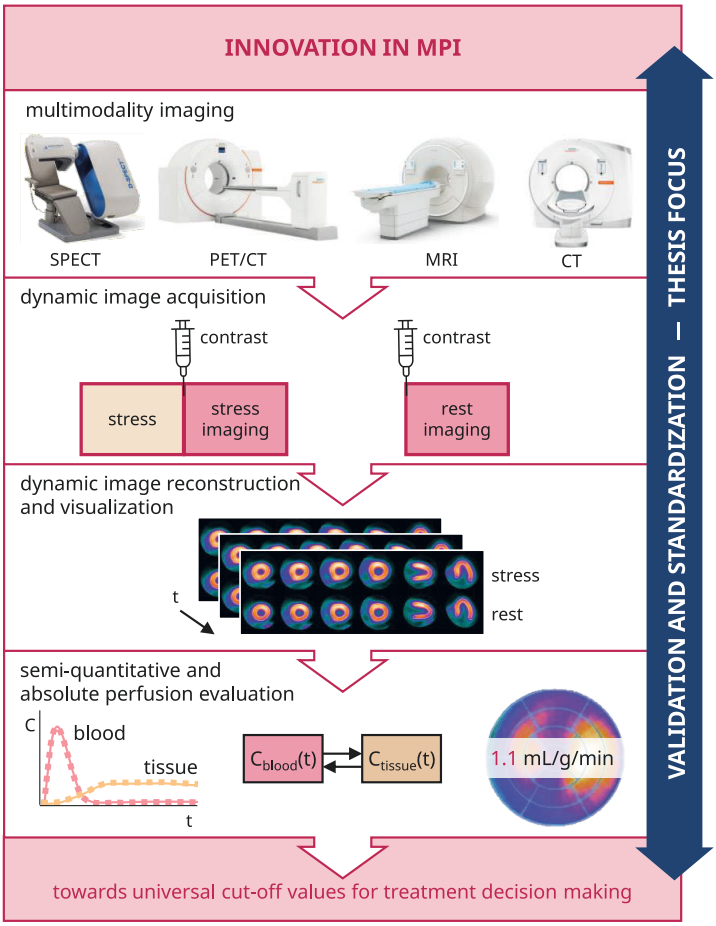

Figure 4 Illustration of ongoing innovation in dynamic, quantitative, and multimodal myocardial perfusion imaging (MPI) and the thesis focus. This thesis contributes to the embedding of such innovations in clinical practice by focusing on the necessary validation and harmonization of quantitative MPI endeavors. To be noted: innovative MPI with ultrasound is beyond the scope of this thesis and is therefore excluded here.

namic perfusion image series is generated, whereby in the case of SPECT and PET, the detected photons over time are rebinned into consecutive time frames. Such dynamic image reconstruction requires an imaging system with a high count sensitivity to maintain a sufficient signal to noise ratio for further analysis. Hence, absolute MPI studies were primarily focused on PET initially. Due to recent advancements in SPECT detector technology, the possibility for absolute MPI is currently also explored for this modality, as well as for MRI, CT and US.[33,34]

The resulting dynamic image series allows for more extensive, quantitative perfusion analysis using tracer kinetic modeling (the term refers to all contrast media).[35] Such models describe the relationship between tracer concentrations in arterial blood and in tissue (see bottom **Figure 4**). In general, the rate of tracer uptake from the arterial blood into the myocardial tissue (K_1; in mL/g/min or in min^{-1}), or vice versa the retention rate (k_2; in mL/g/min or in min^{-1}), can provide an estimation of absolute MBF. These tracer concentrations over time can be derived from the perfusion image data by mapping the average, regional signal intensity in the left ventricular cavity (arterial input) and in surrounding myocardium (tissue response). Corresponding arterial input function (AIF) and regional tissue response functions (TRFs) are usually presented in time activity curves or time intensity curves. These functions serve as input for the tracer kinetic models. Subsequently, blood flow parameters can be estimated from image-derived curve fitting to the model. Tracer kinetic modeling is a long standing, separate field of research, in which model performance and model validation are closely related to our understanding of how the respective radiotracers behave in the human body.[35,36] Many different, and more realistic model approaches have been described in literature, of which nowadays the simpler models find their way into clinical practice.

Clinical challenges

The described innovative, multimodal, and quantitative MPI approaches offer distinctive advantages over current clinical practice, with the ultimate aim to provide for universal cut-off values for revascularization surgery. Nonetheless such innovations also come with certain challenges that need to be addressed to ensure safe and adequate embedding. The following challenges are currently key areas of focus within the international cardiac imaging community:[7,26,37,38]

1. (On-site) validation of quantitative, multimodal MPI, and
2. Harmonization among MPI procedures and standardization between centers.

Current (semi-)quantitative, multimodal MPI comprises a good utility for identification of obstructive CAD. From a recent meta-analysis on diagnostic performance of MPI, a pooled sensitivity of 0.83 (95 % confidence interval: 0.81–0.85) for SPECT, 0.85 (0.80–0.90) for PET, and 0.86 (0.84–0.88) for MRI was observed. Their respected over-

all specificities were 0.77 (0.74–0.80), 0.86 (0.81–0.89), and 0.83 (0.81–0.86).[39] In line with expectations, overall CAD diagnostic performance could be further increased by continuing validation efforts. Yet it is equally important to study harmonization and standardization possibilities between clinical centers as well in order to minimize observed dispersions in diagnostic performance.

Before a clinician can fully rely on a quantitative (or even absolute) perfusion value, its measurement technique ought to be reliable and robust. Due to the wide variation in scanners and software technologies that is part of quantitative, multimodal MPI, it is challenging to realize on-site validation as well as harmonization between clinical centers by patient studies alone.

In patient studies, a direct comparison with the gold standard (i.e., ^{15}O-water PET) is sought for to gain insight in the validity of the particular quantitative perfusion measurement. However, this type of study is required for initial technology validation, but impractical and expensive for other study purposes. Other purposes are for instance studies aimed at procedural optimization, on-site validation, quality assurance, harmonization between workflows, and moreover studies aimed at improving our general understanding on innovative matters. Modeling and simulation are powerful ways to study imaging systems and imaging procedures when direct interaction with the actual system is limited or undesirable.[40] Obviously it is undesirable and unethical to study imaging systems through experimenting on human beings, especially if there are other options available. For example, computer simulations are beneficial in gaining insight into aspects regarding image processing and analysis but are limited in studying the total MPI procedure. From that perspective, animal and phantom studies are well suited as these can mimic the entire procedure in a simplified, yet controlled environment. Hence, animal models and phantom models potentially contribute to this unmet clinical need for ground truth measurement of quantitative, multimodal MPI. In this, animal models possess a high degree of anatomical and (patho)physiological representativeness with respect to the patient. Nonetheless animal models are disadvantageous in terms of the required specialized research facilities and expertise and also associated with high costs and ethical objections. As a result, animal models are predominantly used for preclinical imaging technology validation and not for on-site validation and harmonization between centers. The use of functional imaging phantoms seems therefore well suited for this specific study objective. Even though such phantom model will never fully mimic a patient's relevant anatomy and (patho-)physiology, it may facilitate ground truth flow measurement of quantitative MPI in a controlled and representative environment.

Only when we obtain a better understanding and control of the similarities and dissimilarities in the broad spectrum of quantitative MPI, the implementation of universal cut-off values for treatment decision making becomes within reach.

Thesis outline

The aim of this thesis is to improve current CAD diagnostics by contributing to the required on-site validation and standardization of quantitative, multimodal MPI. In this, we are studying quantitative MPI using a physical model of myocardial perfusion, i.e., a hardware flow phantom. The empirical and iterative development process of this myocardial perfusion phantom forms the core of this thesis.

The following research objectives have been formulated that will be addressed in this thesis:

1. Investigating the usability of contemporary flow phantom models for ground truth perfusion measurement in quantitative, multimodal MPI,
2. Defining multimodal phantom requirements for studying dynamic and quantitative MPI procedures, and
3. Developing a dedicated, multimodality myocardial perfusion phantom.

Chapter 2 presents a systematic review on perfusion/flow phantoms for evaluation of diverse, quantitative perfusion imaging applications. This overview provides insight into already established phantom setups: from design specifications and manufacturing methods, to testing and validation efforts. Subsequent findings have been translated into design requirements and specifications for the myocardial perfusion phantom to be developed.

The development of a proof-of-concept myocardial perfusion phantom is showcased in **Chapter 3**. The phantom is designed for quantitative evaluation of both MPI hardware and software. Due to this preliminary work, we have gained essential expertise in the various development stages, including phantom design, realization, and initial testing and evaluation in dynamic SPECT-MPI.

Chapter 4 incorporates the design and realization of a next iteration in phantom development. In this chapter, we introduce a novel concept on mimicking of radiotracer uptake and retention in the simulated myocardial tissue, which is tested in dynamic SPECT-MPI. Herewith we envision to simulate contrast media specific kinetics at a detailed level, bringing ground truth assessment of absolute, multimodal MPI hardware and software one step closer.

Phantom evaluation as presented in **Chapter 5** builds on the previously developed phantom prototype. On the one hand, this evaluation focuses on the verification of phantom design choices, including the justification for the novel concept in mimicking tracer kinetics. On the other hand, the evaluation comprises preliminary verification of initial phantom results obtained in dynamic SPECT-MPI. The tracer kinetic phantom data are compared to patient data and to a general tracer kinetic model.

In **Chapter 6** we explore multimodal feasibility of the developed myocardial perfusion phantom. Modest adjustments have been made to the overall phantom setup to facilitate initial phantom measurements with dynamic MPI in CT, PET, and MRI. In this way we obtain a better understanding of multimodal phantom requirements.

In **Chapter 7** we conclude with future steps in the iterative phantom development process and describe phantom application possibilities. Moreover, recommendations are given regarding the necessary follow-up steps for multimodal phantom verification and validation. Finally, we argue our vision for next generation perfusion phantoms and illustrate the need to build phantom references to pave the road for validation and harmonization of quantitative MPI in the comprehensive clinical practice.

References

1. Centraal Bureau voor Statistiek. Doodsoorzakenstatistiek. CBS Open Data. https://bronnen.zorggegevens.nl/Bron?naam=Doodsoorzakenstatistiek. Published 2021. Accessed February 8, 2021.
2. Rijksinstituut voor Volksgezondheid en Milieu. Coronaire hartziekten: Leeftijd en geslacht. Volksgezondheid en zorg informatie. https://www.vzinfo.nl/coronaire-hartziekten/leeftijd-en-geslacht. Published 2022. Accessed September 3, 2022.
3. Rijksinstituut voor Volksgezondheid en Milieu. Coronaire hartziekten: Sterfte. Volksgezondheid en zorg informatie. https://www.vzinfo.nl/coronaire-hartziekten/sterfte. Published 2022. Accessed September 3, 2022.
4. Piepoli MF, Hoes AW, Agewall S, et al. 2016 European Guidelines on cardiovascular disease prevention in clinical practice: The Sixth Joint Task Force of the European Society of Cardiology and Other Societies on Cardiovascular Disease Prevention in Clinical Practice. Eur Heart J. 2016;37(29):2315-2381. doi:10.1093/eurheartj/ehw106
5. Hilderink HBM, Plasmans MHD, Poos MJJC, Eysink PED, Gijsen R. Dutch DALYs, current and future burden of disease in the Netherlands. Arch Public Heal. 2020;78(1):85. doi:10.1186/s13690-020-00461-8
6. Rijksinstituut voor Volksgezondheid en Milieu. Coronaire hartziekten: Kosten. Zorguitgaven coronaire hartziekten naar sector 2017. https://www.vzinfo.nl/coronaire-hartziekten/kosten. Published 2022. Accessed March 9, 2022.
7. Knuuti J, Wijns W, Saraste A, et al. 2019 ESC Guidelines for the diagnosis and management of chronic coronary syndromes: The Task Force for the diagnosis and management of chronic coronary syndromes of the European Society of Cardiology (ESC). Eur Heart J. 2020;41(3):407-477. doi:10.1093/eurheartj/ehz425
8. Antman EM, Loscalzo J. Ischemic Heart Disease. In: Jameson JL, Fauci AS, Kasper DL, Hauser SL, Longo DL, Loscalzo J, eds. Harrison's Principles of Internal Medicine, 20e. New York, NY: McGraw-Hill Education; 2018. http://accessmedicine.mhmedical.com/content.aspx?aid=11600468856.
9. Delzell JEJ, Chumley HS. Coronary Artery Disease. In: Usatine RP, Smith MA, Mayeaux E.J. J, Chumley HS, eds. The Color Atlas and Synopsis of Family Medicine, 3e. New York, NY: McGraw-Hill Education; 2019. http://accessmedicine.mhmedical.com/content.aspx?aid=1164345014.
10. Mayo Clinic. Coronary artery disease. https://www.mayoclinic.org/diseases-conditions/coronary-artery-disease/symptoms-causes/syc-20350613. Published 2020. Accessed March 9, 2022.
11. Members AF, Windecker S, Kolh P, et al. 2014 ESC/EACTS Guidelines on myocardial revascularization: The Task Force on Myocardial Revascularization of the European Society of Cardiology (ESC) and the European Association for Cardio-Thoracic Surgery (EACTS). Eur Heart J. 2014;35(37):2541-2619. doi:10.1093/eurheartj/ehu278
12. Members TF, Montalescot G, Sechtem U, et al. 2013 ESC guidelines on the management of stable coronary artery disease: The Task Force on the management of stable coronary artery disease of the European Society of Cardiology. Eur Heart J. 2013;34(38):2949-3003. doi:10.1093/eurheartj/eht296

13. Iqbal J, Zhang Y-J, Holmes DR, et al. Optimal Medical Therapy Improves Clinical Outcomes in Patients Undergoing Revascularization With Percutaneous Coronary Intervention or Coronary Artery Bypass Grafting. Circulation. 2015;131(14):1269-1277. doi:10.1161/CIRCULATIONAHA.114.013042
14. Xaplanteris P, Fournier S, Pijls NHJ, et al. Five-Year Outcomes with PCI Guided by Fractional Flow Reserve. N Engl J Med. 2018;379(3):250-259. doi:10.1056/NEJMoa1803538
15. Chung ES, Leon AR, Tavazzi L, et al. Results of the Predictors of Response to CRT (PROSPECT) Trial. Circulation. 2008;117(20):2608-2616. doi:10.1161/CIRCULATIONAHA.107.743120
16. Kelbæk H, Høfsten DE, Køber L, et al. Deferred versus conventional stent implantation in patients with ST-segment elevation myocardial infarction (DANAMI 3-DEFER): an open-label, randomised controlled trial. Lancet. 2016;387(10034):2199-2206. doi:https://doi.org/10.1016/S0140-6736(16)30072-1
17. Lawton JS, Tamis-Holland JE, Bangalore S, et al. 2021 ACC/AHA/SCAI Guideline for Coronary Artery Revascularization: A Report of the American College of Cardiology/American Heart Association Joint Committee on Clinical Practice Guidelines. Circulation. 2022;145(3):e18-e114. doi:10.1161/CIR.0000000000001038
18. Boxt L, Abbara S. Cardiac Imaging: The Requisites. 4th ed. Elsevier; 2015.
19. Hesse B, Tägil K, Cuocolo A, et al. EANM/ESC procedural guidelines for myocardial perfusion imaging in nuclear cardiology. Eur J Nucl Med Mol Imaging. 2005;32(7):855-897. doi:10.1007/s00259-005-1779-y
20. Cherry SR, Sorenson JA, Phelps ME. chapter 17 - Single Photon Emission Computed Tomography. In: Cherry SR, Sorenson JA, Phelps MEBT-P in NM (Fourth E, eds. Philadelphia: W.B. Saunders; 2012:279-306. doi:https://doi.org/10.1016/B978-1-4160-5198-5.00017-4
21. Cherry SR, Sorenson JA, Phelps ME. chapter 18 - Positron Emission Tomography. In: Cherry SR, Sorenson JA, Phelps MEBT-P in NM (Fourth E, eds. Philadelphia: W.B. Saunders; 2012:307-343. doi:https://doi.org/10.1016/B978-1-4160-5198-5.00018-6
22. Jaarsma C, Leiner T, Bekkers SC, et al. Diagnostic Performance of Noninvasive Myocardial Perfusion Imaging Using Single-Photon Emission Computed Tomography, Cardiac Magnetic Resonance, and Positron Emission Tomography Imaging for the Detection of Obstructive Coronary Artery Disease: A Meta-Anal. J Am Coll Cardiol. 2012;59(19):1719-1728. doi:https://doi.org/10.1016/j.jacc.2011.12.040
23. Maaniitty T, Knuuti J, Saraste A. 15O-Water PET MPI: Current Status and Future Perspectives. Semin Nucl Med. 2020;50(3):238-247. doi:https://doi.org/10.1053/j.semnuclmed.2020.02.011
24. Singh V, Di Carli MF. SPECT Versus PET Myocardial Perfusion Imaging in Patients with Equivocal CT. Curr Cardiol Rep. 2020;22(6):43. doi:10.1007/s11886-020-01287-0
25. Al Badarin FJ, Malhotra S. Diagnosis and Prognosis of Coronary Artery Disease with SPECT and PET. Curr Cardiol Rep. 2019;21(7):57. doi:10.1007/s11886-019-1146-4
26. Dewey M, Siebes M, Kachelrieß M, et al. Clinical quantitative cardiac imaging for the assessment of myocardial ischaemia. Nat Rev Cardiol. 2020;17(7):427-450. doi:10.1038/s41569-020-0341-8

27. Saraste A, Knuuti J. ESC 2019 guidelines for the diagnosis and management of chronic coronary syndromes. Herz. 2020;45(5):409-420. doi:10.1007/s00059-020-04935-x
28. Koepfli P, Hany TF, Wyss CA, et al. CT Attenuation Correction for Myocardial Perfusion Quantification Using a PET/CT Hybrid Scanner. J Nucl Med. 2004;45(4):537 LP - 542. http://jnm.snmjournals.org/content/45/4/537.abstract.
29. Slart RHJA, Bax JJ, van Veldhuisen DJ, van der Wall EE, Dierckx RAJO, Jager PL. Imaging Techniques in Nuclear Cardiology for the Assessment of Myocardial Viability. Int J Cardiovasc Imaging. 2006;22(1):63-80. doi:10.1007/s10554-005-7514-8
30. Sciagrà R, Lubberink M, Hyafil F, et al. EANM procedural guidelines for PET/CT quantitative myocardial perfusion imaging. Eur J Nucl Med Mol Imaging. 2021;48(4):1040-1069. doi:10.1007/s00259-020-05046-9
31. Verberne HJ, Acampa W, Anagnostopoulos C, et al. EANM Procedural Guidelines for Radionuclide Myocardial Perfusion Imaging with SPECT and SPECT / CT. 2015.
32. Juárez-Orozco LE, Tio RA, Alexanderson E, et al. Quantitative myocardial perfusion evaluation with positron emission tomography and the risk of cardiovascular events in patients with coronary artery disease: A systematic review of prognostic studies. Eur Heart J Cardiovasc Imaging. 2018;19(10):1179-1187. doi:10.1093/ehjci/jex331
33. Nkoulou R, Fuchs TA, Pazhenkottil AP, et al. Absolute Myocardial Blood Flow and Flow Reserve Assessed by Gated SPECT with Cadmium–Zinc–Telluride Detectors Using ^{99m}Tc-Tetrofosmin: Head-to-Head Comparison with ^{13}N-Ammonia PET. J Nucl Med. 2016;57(12):1887 LP - 1892. doi:10.2967/jnumed.115.165498
34. Otaki Y, Manabe O, Miller RJH, et al. Quantification of myocardial blood flow by CZT-SPECT with motion correction and comparison with 15O-water PET. J Nucl Cardiol. 2021;28(4):1477-1486. doi:10.1007/s12350-019-01854-1
35. Cherry SR, Sorenson JA, Phelps ME. chapter 21 - Tracer Kinetic Modeling. In: Cherry SR, Sorenson JA, Phelps MEBT-P in NM (Fourth E, eds. Philadelphia: W.B. Saunders; 2012:379-405. doi:https://doi.org/10.1016/B978-1-4160-5198-5.00021-6
36. Carson RE. Tracer kinetic modeling in PET. In: Positron Emission Tomography. Springer; 2005:127-159.
37. Hyafil F, Gimelli A, Slart RHJA, et al. EANM procedural guidelines for myocardial perfusion scintigraphy using cardiac-centered gamma cameras. Eur J Hybrid Imaging. 2019;3(1). doi:10.1186/s41824-019-0058-2
38. Knuuti J, Kajander S, Mäki M, Ukkonen H. Quantification of myocardial blood flow will reform the detection of CAD. J Nucl Cardiol. 2009;16(4):497-506. doi:10.1007/s12350-009-9101-1
39. Xu J, Cai F, Geng C, Wang Z, Tang X. Diagnostic Performance of CMR, SPECT, and PET Imaging for the Identification of Coronary Artery Disease: A Meta-Analysis. Front Cardiovasc Med. 2021;8:621389. doi:10.3389/fcvm.2021.621389
40. Van Meurs W. Modeling and Simulation in Biomedical Engineering - Applications in Cardiorespiratory Physiology. (Penn M, Mulcahy M, Fogarty DE, McLaughlin D, eds.). McGraw-Hill; 2011.
41. Aramendía-Vidaurreta V, Echeverría-Chasco R, Vidorreta M, Bastarrika G, Fernández-Seara M. Quantification of Myocardial Perfusion With Vasodilation Using Arterial Spin Labeling at 1.5T. J Magn Reson Imaging. 2021;53(3). doi:10.1002/jmri.27396

36. Carson RE. Tracer kinetic modeling in PET. In: Positron Emission Tomography. Springer; 2005:127-159.
37. Hyafil F, Gimelli A, Slart RHJA, et al. EANM procedural guidelines for myocardial perfusion scintigraphy using cardiac-centered gamma cameras. Eur J Hybrid Imaging. 2019;3(1). doi:10.1186/s41824-019-0058-2
38. Knuuti J, Kajander S, Mäki M, Ukkonen H. Quantification of myocardial blood flow will reform the detection of CAD. J Nucl Cardiol. 2009;16(4):497-506. doi:10.1007/s12350-009-9101-1
39. Xu J, Cai F, Geng C, Wang Z, Tang X. Diagnostic Performance of CMR, SPECT, and PET Imaging for the Identification of Coronary Artery Disease: A Meta-Analysis. Front Cardiovasc Med. 2021;8:621389. doi:10.3389/fcvm.2021.621389
40. Van Meurs W. Modeling and Simulation in Biomedical Engineering - Applications in Cardiorespiratory Physiology. (Penn M, Mulcahy M, Fogarty DE, McLaughlin D, eds.). McGraw-Hill; 2011.
41. Aramendía-Vidaurreta V, Echeverría-Chasco R, Vidorreta M, Bastarrika G, Fernández-Seara M. Quantification of Myocardial Perfusion With Vasodilation Using Arterial Spin Labeling at 1.5T. J Magn Reson Imaging. 2021;53(3). doi:10.1002/jmri.27396

2

Marije E. Kamphuis
Marcel J. W. Greuter
Riemer H. J. A. Slart
Cornelis H. Slump

European Radiology Experimental
volume 4, Article number: 15 (2020)

Quantitative imaging: systematic review of perfusion/flow phantoms

Abstract

Background We aimed at reviewing design and realization of perfusion/flow phantoms for validating quantitative perfusion imaging (PI) applications to encourage best practices.

Methods A systematic search was performed on the Scopus database for "perfusion", "flow", and "phantom", limited to articles written in English published between January 1999 and December 2018. Information on phantom design, used PI and phantom applications was extracted.

Results Of 463 retrieved articles, 397 were rejected after abstract screening and 32 after full-text reading. The 37 accepted articles resulted to address PI simulation in brain ($n = 11$), myocardial ($n = 8$), liver ($n = 2$), tumour ($n = 1$), finger ($n = 1$), and non-specific tissue ($n = 14$), with diverse modalities: ultrasound ($n = 11$), computed tomography ($n = 11$), magnetic resonance imaging ($n = 17$), and positron emission tomography ($n = 2$). Three phantom designs were described: basic ($n = 6$), aligned capillary ($n = 22$), and tissue-filled ($n = 12$). Microvasculature and tissue perfusion were combined in one compartment ($n = 23$) or in two separated compartments ($n = 17$). With the only exception of one study, inter-compartmental fluid exchange could not be controlled. Nine studies compared phantom results with human or animal perfusion data. Only one commercially available perfusion phantom was identified.

Conclusion We provided insights into contemporary phantom approaches to PI, which can be used for ground truth evaluation of quantitative PI applications. Investigators are recommended to verify and validate whether assumptions underlying PI phantom measurements are justified for their intended phantom application.

Background

Perfusion imaging (PI) is a powerful method for assessing and monitoring tissue vascular status, and alterations therein. Hence, PI is generally aimed at distinguishing healthy from ischemic and infarcted tissue. PI applications cover various imaging modalities such as ultrasound (US), computed tomography (CT), positron emission tomography (PET), and magnetic resonance imaging (MRI) that can record perfusion parameters in a wide spread of tissues including brain, liver, and myocardial tissue. A distinction can be made between contrast-enhanced and non-contrast PI approaches. The pertinent signal intensity in tissue can be recorded as a function of time or after a time interval, called dynamic or static PI respectively. This systematic review focuses on dynamic PI, as this approach supports quantitative analysis and absolute quantification of perfusion. In dynamic PI, it is possible to construct mathematical models that fit image data with model parameters in order to explain observed response functions in tissue. For example, time-intensity curves highlight the distribution of contrast material into the tissue over time. Model outcomes include computation of absolute blood flow (BF), blood volume (BV), and/or mean transit times (MTTs).[1] Multiple BF models of tissue perfusion exist, including model-based deconvolution, model independent singular value decomposition and maximum upslope models.[2] These BF models are increasingly used in addition to standard semiquantitative analysis, as these show potential towards better accuracy and standardized assessment of perfusion measures.[3–5]

Without a validated standard, interpretation of quantitative results can be challenging. Validation and/or calibration of absolute perfusion measures is required to ensure unrestricted and safe adoption in clinical routine.[6–8] Validation approaches include *in vivo*, *ex vivo*, *in vitro*, and *in silico* studies and combinations hereof. Each approach has advantages and disadvantages, and may differ in level of representativeness, controllability of variables, and practical applicability. Our focus was on *in vitro* studies, i.e., physical phantom studies. Phantom studies contribute to ground truth evaluation of single aspects on quantitative PI applications in a simplified, though controlled, environment. Phantom studies also allow for the comparison and optimization of imaging protocols and analysis methods. We hereby observe a shift from the use of static to dynamic perfusion phantoms (i.e., with a flow circuit), as the latter enables in depth evaluation of time-dependent variables.

In general, it can be challenging to translate findings from phantom studies into clinical practice. For example, it can be questionable whether certain choices and simplifications in perfusion phantom measurements are justified. Intra- and interdisciplinary knowledge sharing on phantom designs, experimental findings, and clinical implications can be used to substantiate this. Hence, this systematic review presents

an overview on contemporary perfusion phantoms for evaluation of quantitative PI applications to encourage best quantitative practices.

Methods

A systematic search on general and contemporary perfusion phantoms was conducted using Scopus database online, which includes MEDLINE and EMBASE. The query included "perfusion", "flow", and "phantom". Inclusion was limited to English written articles and reviews published between January 1999 and December 2018.

Two investigators independently screened titles and abstracts (M.E.K. and M.J.W.G.), whereby *in vivo*, *ex vivo* and *in silico* related perfusion studies were excluded, even as non-related *in vitro* studies (e.g., static and large-vessel phantoms). We hereby note that thermal and optical PI techniques fall outside the scope of this review. The same investigators performed full-text screening and analysis. Study inclusion required incorporation of microvascular flow mimicking and we excluded single-vessel phantom studies. In addition, references were scrutinized on cross-references. Observer differences were resolved by discussion.

The perfusion phantom overview concerns three main aspects regarding ground truth evaluation of quantitative PI, as schematically depicted in **Figure 1**. Details on perfusion phantom design, studied PI application and overall phantom application

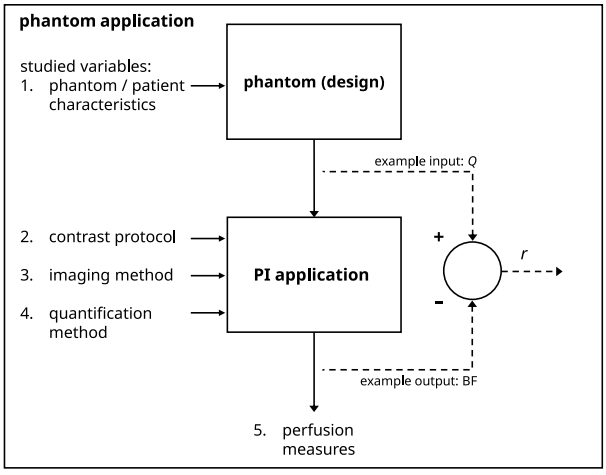

Figure 1 System representation of ground truth validation process of quantitative perfusion imaging (PI). The diverse input variables that might affect quantitative perfusion outcomes are indicated by point 1–4. *Q* serves as an example input variable and refers to set phantom flow in mL/min. Blood flow (BF; in mL/min) is an example of possible output perfusion measures, and *r* is the residual between both. The latter can be translated into a measure of accuracy. The figure summarizes the central topics of this review paper.

were extracted from each paper. We categorized phantom design features in terms of simulated anatomy, physiology, and pathology. Anatomy simulation lists information on the studied tissue type and surrounding tissue. Physiology simulation contains the used phantom configuration, the corresponding tissue compartment model, the applied flow profile and range, and the simulation of motion (e.g., breathing and cardiac motion). Pathology simulation indicates the presence of perfusion deficit simulation.

Extracted parameters for the studied PI application encounters the used contrast protocol, imaging system, and BF model. We also listed the studied input and output variables for the diverse phantom applications. Input variables were categorized as follows:

1. phantom / patient characteristics,
2. contrast protocol
3. imaging method, and
4. quantification method (see **Figure 1**)

Output variables included the following perfusion measures:

- arterial input function (AIF)
- tissue response function (TRF)
- MTT
- BV
- BF

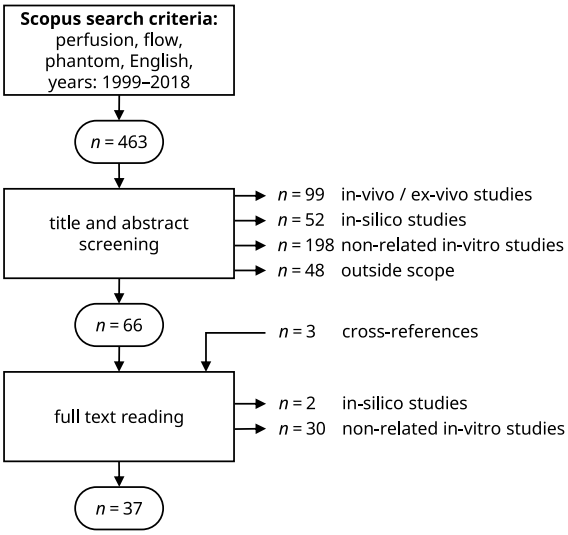

Figure 2 Flow chart of study selection process.

If mentioned by the authors, we listed published results on phantom performance, which describes the relation between the "ground truth" flow measure and the obtained quantitative PI outcomes. Finally, we documented in which studies phantom data are compared with human, animal, or mathematical data, and which phantoms are commercially available.

Results

Phantom data assessment

We have retrieved 463 articles using Scopus, of which 397 were rejected after abstract screening and another 32 after full-text reading. The search resulted in 37 accepted articles including cross-references (**Figure 2**). **Table 1** summarizes our main findings on phantom designs and applications in diverse PI domains.

Phantom design

Anatomically, the phantoms simulate perfusion of various tissue types, including organ specific tissue (brain, $n = 11$ articles; myocardial, $n = 8$; liver, $n = 2$; tumour, $n = 1$; finger, $n = 1$) and non-specific tissue ($n = 14$). Several phantoms additionally mimic surrounding tissue (**Table 1**). All phantoms comprise a simplified "physiologic" model of perfusion that can be translated into a single tissue compartment model. **Figure 3** schematically illustrates the basics of six distinguished phantom configurations, which specify three phantom types: basic ($n = 6$ articles); aligned capillaries ($n = 22$); and tissue filled ($n = 12$). The observed phantom designs simulate the microvasculature and tissue as one combined volume ($n = 23$ articles) or two physically separated volumes ($n = 17$) (e.g., via a semipermeable membrane). Note that papers can present more than one phantom, and phantom designs may slightly differ from the schematic representations.

Basic phantoms generally consist of a single volume with ingoing and outgoing tubes, disregarding physiological simulation of microcirculation and tissue. In capillary phantoms, the microvasculature is simulated as a volume filled with unidirectional aligned hollow fibres or straws (e.g., a dialysis cartridge). The amount, diameter, and permeability of these fibres vary. *Tissue-filled phantoms* incorporate tissue mimicking material inside the volume, which subsequently leads to formation of a "microvasculature". Used materials include sponge[20,21,33,44], (micro)beads[19,31,40], gel[18,39], and printed microchannels.[32,43] Remarkably, in most studies, fluid exchange between simulated microvasculature and tissue (i.e., transfer rates K_1 and k_2) was uncontrollable, except for the study performed by Ohno et al.[33] In this study, the compliance of the capacitor space could be altered to control k_2 to some extent. Low et al.[43] and Ebrahim et al.[32] have mathematically simulated the desired phantom flow configuration, before printing the microchannels. However, these models did not simulate fluid exchange between microvasculature and tissue. Continuous flow was applied in

Table 1 Perfusion phantom design and realization in validating quantitative perfusion imaging (PI).

Publication	Phantom design						PI application			Phantom application							
1st author, year [reference]	Configuration (see Fig. 3)	Flow profile	Flow range	Motion simulation	Surrounding tissue simulation	Perfusion deficit simulation	Imaging modality	Contrast protocol	Blood flow model	Input variables	AIF	TRF	MTT	BV	BF	Data comparison	Commercial
General phantoms																	
Andersen, 2000 [9]	1A	c	0.015–0.57 cm/s				MRI		FAIR	1, 4		◇			◇		
Brauweiler, 2012 [10]	1A	p	180 mL/min		◇		CT	◇		2, 3	◇	◇					
Li, 2002 [11]	1A,2B	c	500–1300 mL/min				US	◇	MBD	1	◇	◇	◇	◇		m	
Peladeau-Pigeon, 2013 [12]	1B	c,p	210–450 mL/min		◇		MRI, CT	◇	MBD (Fick, modif. Toft)	1–3	◇	◇			◇	m	◇
Driscoll, 2011 [13]	1B	p	150–270 mL/min		◇		CT	◇		1–3	◇	◇					◇
Kim, 2016 [14]	2B	c	0–2 mL/min	◇			US			1,3		◇					
Anderson, 2011 [15]	2B	c	50 mL/min				MRI	◇		1		◇					
Meyer-Wiethe, 2005 [16]	2B	c	4.5–36 mL/min				US	◇	Replenishment	1,3,4		◇					
Veltmann, 2002 [17]	2B	c	10–45 mL/min				US	◇	Replenishment	1,2		◇			◇		
Kim, 2004 [18]	2B,3A	p	0.09, 1.6–1.8 cm/s				MRI		1-TCM	1,3		◇					
Lee, 2016 [19]	3A	c	0–3 mL/min				MRI		DWI	1		◇					
Chai, 2002 [20]	3A	c	50–300 mL/min				MRI		ASL	1		◇				h	
Potdevin, 2004 [21]	3A	p	2.6–10.4 mL/min		◇		US	◇	Replenishment	1,2		◇	◇			m	
Lucidarme, 2003 [22]	2B	p	100–400 mL/min				US	◇	Replenishment	1		◇				a	

c continuous, p pulsatile FAIR Flow-sensitive alternating inversion recovery, MBD Model-based deconvolution, 1-TCM Single tissue compartment model, DWI diffusion weighted imaging, ASL Arterial spin labeling, SVD Singular value decomposition, MSM Maximum slope model 1 = phantom / patient characteristics, 2 = contrast protocol, 3 = imaging method, 4 = flow quantification method AIF Arterial input function, TRF Tissue Response function, MTT Mean transit time, BV Blood volume, BF Blood flow h human, a animal, m mathematical.

(cont.▶)

Table 1 (Continued) Perfusion phantom design and realization in validating quantitative perfusion imaging (PI).

Publication	Phantom design						PI application			Phantom application							
1st author, year [reference]	Configuration (see Fig. 3)	Flow profile	Flow range	Motion simulation	Surrounding tissue simulation	Perfusion deficit simulation	Imaging modality	Contrast protocol	Blood flow model	Input variables	AIF	RF	MTT	BV	BF	Data comparison	Commercial
Brain phantoms																	
Boese, 2013 [23]	1A	p	800 mL/min			◇	CT	◇	MBD	1–3	◇	◇		◇	◇		
Hashimoto, 2018 [24]	2A	c	60 mL/min		◇		CT	◇	SVD	2,3			◇	◇	◇	m	
Suzuki, 2017 [25]	2A	c	60 mL/min		◇		CT	◇	SVD	3	◇	◇	◇	◇	◇	m	
Noguchi, 2007 [26]	2A	c	0–2.16 cm/s				MRI		ASL	1		◇			◇		
Wang, 2010 [27]	2B	c	45–180 mL/min				MRI		ASL	1		◇			◇	m,h	
Cangür, 2004 [28]	2B	c	1.8–21.6 mL/min		◇		US	◇		1		◇					
Klotz, 1999 [29]	2B	c	50–140 mL/min		◇		CT	◇	MSM	1	◇	◇			◇	h	
Claasse, 2001 [30]	2B	p	180–540 mL/min				US	◇	MBD	1,2		◇	◇			a	
Mathys, 2012 [31]	3A	c	200–600 mL/min		◇		CT	◇	SVD, MSM	1–4	◇	◇		◇	◇		
Ebrahimi, 2010 [32]	3A	c	012–1.2 mL/min				MRI	◇	SVD	1	◇	◇	◇	◇	◇	m	
Ohno, 2017 [33]	3B	p	240–480 mL/min				MRI		ASL	1		◇			◇		

c continuous, p pulsatile FAIR Flow-sensitive alternating inversion recovery, MBD Model-based deconvolution, 1-TCM Single tissue compartment model, DWI diffusion weighted imaging, ASL Arterial spin labeling, SVD Singular value decomposition, MSM Maximum slope model 1 = phantom / patient characteristics, 2 = contrast protocol, 3 = imaging method, 4 = flow quantification method AIF Arterial input function, TRF Tissue Response function, MTT Mean transit time, BV Blood volume, BF Blood flow h human, a animal, m mathematical. *(cont.▶)*

Table 1 (Continued) Perfusion phantom design and realization in validating quantitative perfusion imaging (PI).

Publication	Phantom design						PI application			Phantom application							
1st author, year [reference]	Configuration (see Fig. 3)	Flow profile	Flow range	Motion simulation	Surrounding tissue simulation	Perfusion deficit simulation	Imaging modality	Contrast protocol	Blood flow model	Input variables	AIF	RF	MTT	BV	BF	Data comparison	Commercial
Myocardial phantoms																	
Zarinabad, 2014 [34]	2A	c	1–5 mL/min/g				MRI	◇	MBD (Fermi)	1,4	◇	◇			◇	m,h	
Chiribiri 2013 [8]	2A	c	1–10 mL/min/g				MRI	◇		1,2	◇	◇					
Zarinabad, 2012 [35]	2A	c	1–5 mL/min/g				MRI	◇	MBD (Fermi), SVD	1,3,4	◇	◇			◇	m,h	
O'Doherty, 2017 [36]	2A	c	3 mL/min/g				PET, MRI	◇	1-TCM	2,3	◇	◇			◇		
O'Doherty, 2017 [37]	2A	c	1–5 mL/min/g				PET, MRI	◇	1-TCM	1,3	◇	◇			◇		
Otton, 2013 [38]	2A	c	2–4 mL/min/g				MR, CT	◇		1,3	◇	◇					
Ressner, 2006 [39]	3A	c	5–10 cm/s	◇			US	◇		1,2		◇			◇	h	
Ziemer, 2015 [40]	3A	p	0.96–2.49 mL/min/g		◇		CT	◇	MSM	1,4	◇	◇			◇		
Finger phantom																	
Sakano, 2015 [41]	2B	c	6–30 mL/min				US	◇		1,3		◇					
Liver phantoms																	
Gauthier, 2011 [42]	2B	c	130 mL/min				US	◇		3		◇	◇			h	
Low, 2018 [43]	3A	-	20.5 mL/min				CT	◇		1							
Tumour phantom																	
Cho, 2012 [44]	3A,3B	p	-				MRI		DWI	1,4		◇					

c continuous, p pulsatile FAIR Flow-sensitive alternating inversion recovery, MBD Model-based deconvolution, 1-TCM Single tissue compartment model, DWI diffusion weighted imaging, ASL Arterial spin labeling, SVD Singular value decomposition, MSM Maximum slope model 1 = phantom / patient characteristics, 2 = contrast protocol, 3 = imaging method, 4 = flow quantification method AIF Arterial input function, TRF Tissue Response function, MTT Mean transit time, BV Blood volume, BF Blood flow h human, a animal, m mathematical.

26 phantom studies and pulsatile/peristaltic flow in 11 phantom studies. Flow settings vary per study and target organ and are presented in three different units (**Table 1**). In case of brain and myocardial perfusion phantom models, flow experiments do not always cover the whole physiological range (**Figure 4**). In addition, we observed two phantom studies that incorporated clutter motion (i.e., small periodic motion), but no studies included breathing or cardiac motion (**Table 1**). Regional perfusion deficit simulation (pathology) was only executed by Boese et al.[23] Several studies mimicked some sort of global perfusion deficits by reducing the total flow or perfusion rate.

Studied PI applications

Table 1 depicts 17 studies focusing on MRI, 11 on ultrasound imaging, 11 on CT, and 2 on PET; 4 studies presented a direct comparison of MRI with PET or CT. A contrast-enhanced protocol was used in 28 studies. The used BF model for perfusion quantification varies per imaging modality and contrast protocol.

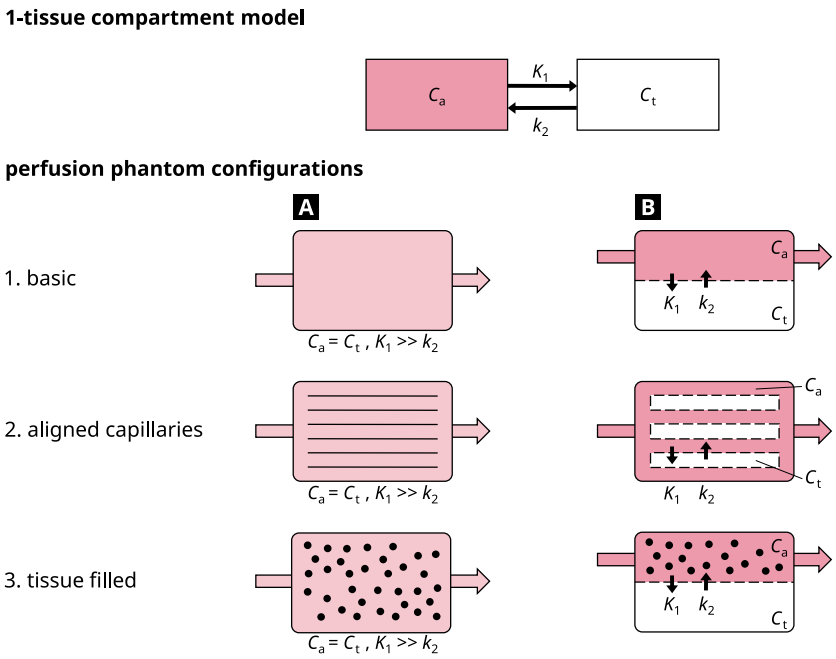

Figure 3 Schematic representation of the 1-tissue compartment model and six derived phantom configurations. A distinction is made between three phantom types: basic, aligned capillaries and tissue filled (black spheres). Moreover, the microvasculature and tissue can be simulated as one combined (**A**) or two separated volumes (**B**) (e.g. via a porous membrane). C_a and C_t represent the concentration of the compound of interest (is being imaged) in the simulated blood plasma and tissue, respectively. K_1 and k_2 comprise the two transfer coefficients. Formation of in- and outgoing flow (arrow) and compartment flow varies per individual phantom design.

Phantom applications

Variables related to phantom/patient characteristics ($n = 32$), contrast protocol ($n = 12$), imaging method ($n = 16$), and quantification method ($n = 7$) were studied in relation to various quantitative perfusion measures (**Table 1**). Most papers describe the influence of flow settings on quantitative perfusion outcomes, followed by variation in contrast volume and acquisition protocol. Several studies compare outcomes to human/patient data ($n = 7$), animal data ($n = 2$), and mathematical simulations ($n = 9$) (**Table 1**). In addition, we have identified one commercially available perfusion phantom that is described by Driscoll et al.[13] and applied by Peladeau-Pigeon et al.[12] The relation between the "ground truth" flow measure and quantitative PI outcomes is summarised in **Table 2**. Remarkable is the diversity in used measures of perfusion and comparison (e.g., absolute errors, correlations statistics).

Discussion

A systematic search of the literature (from 1999 to 2018) was performed on contemporary perfusion phantoms. Detailed information was provided on three main aspects for ground truth evaluation of quantitative PI applications. We have elaborated on thirty-seven phantom designs, whereby focusing on anatomy, physiology, and pathology simulation. In addition, we have listed the imaging system, contrast protocol and BF model for the studied PI applications. Finally, we have documented for each phantom application the investigated input and output variables, data comparison efforts and commercial availability. Hence, this review presents as main result

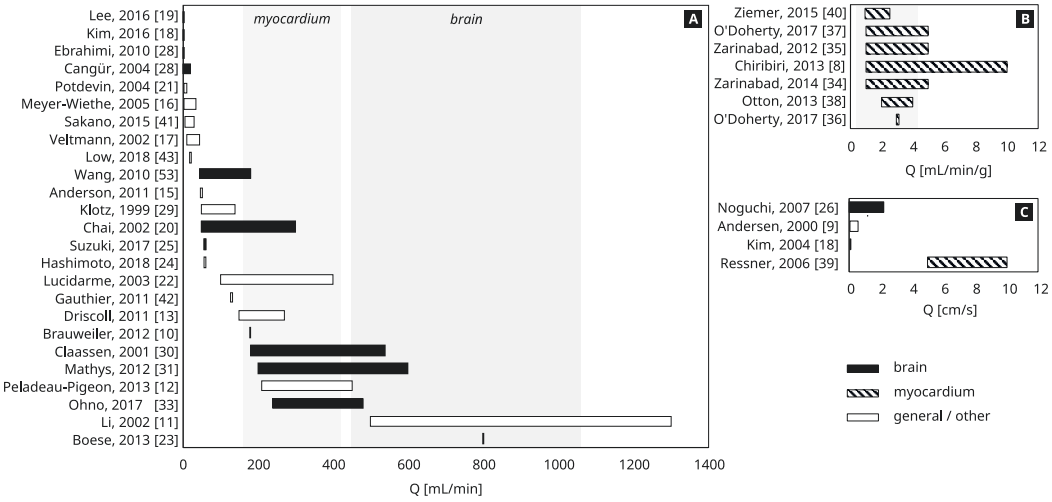

Figure 4 Overview of used flow ranges and units in assessed perfusion phantom studies. (**A**) shows the studied flow ranges in mL/min, (**B**) in mL/min/g, and (**C**) in cm/s. The grey blocks represent physiological flow ranges for brain and myocardial tissue.[45,46]

Table 2 Indication of phantom performance for specified flow range.

1st author, year [reference]	Perfusion measure(s)	Phantom performance	Q
Direct comparison with Q			
Klotz, 1999 [29]	BF	$r = 0.990$	50–140 mL/min
Wang, 2010 [27]	BF	$r > 0.834$	45–180 mL/min
Mathys, 2012 [31]	BF	$r = 0.995$	200–600 mL/min
Peladeau-Pigeon, 2013 [12]	BF	$r = 0.992$	210–450 mL/min
Ohno, 2017 [33]	BF	$r > 0.90$	240–480 mL/min
Ziemer, 2015 [40]	BF	$r = 0.98$	0.96–2.49 mL/g/min
O'Doherty, 2017 [36]	BF	$r = 0.99$	1–5 mL/g/min
Andersen, 2000 [9]	BF	$\varepsilon \approx 0.015 \pm 0.03$ cm/s $\varepsilon \approx 0.001 \pm 0.03$ cm/s	0.015 ± 0.002 cm/s 0.570 ± 0.003 cm/s
Ressner, 2006 [39]	BF	$\varepsilon > 40$ % $\varepsilon < 20$ %	1–3 cm/s 5–7 cm/s
Zarinabad, 2012 [35]	BF	$\varepsilon = 0.007 \pm 0.002$ mL/g/min $\varepsilon = 0.23 \pm 0.26$ ml/g/min	0.5 mL/g/min 5 mL/g/min
Zarinabad, 2014 [34]	BF	$\varepsilon < 0.03$ mL/g/min $\varepsilon < 0.05$ ml/g/min	2.5–5 mL/g/min 1–2.5 mL/g/min
Suzuki, 2017 [25]	BF	$\varepsilon \approx 0.0589 \pm 0.0108$ mL/g/min	0.1684 mL/g/min
Hashimoto, 2018 [24]	BF	$\varepsilon \approx 0.0446 \pm 0.0130$ mL/g/min	0.1684 mL/g/min
Ebrahimi, 2019 [32]	BF	BF/Q > 0.6	0.12–1.2 mL/min
Indirect comparison with Q			
Veltmann, 2002 [17]	r_{kin}	$r > 0.984$, $\chi^2 < 0.019$	10–45 mL/min
Chai, 2002 [20]	ΔSI ratio	$r = 0.995$	50–300 mL/min
Cangür, 2004 [28]	TTP PSI AUC PG FWHM	$r = -0.964$ $r = 0.683$ $r = 0.668$ $r = 0.907$ $r = -0.63$	1.8–21.6 mL/min
Myer-Wiethe, 2005 [36]	ΔSI	$r = 0.99$	4.5–36 mL/min
Lee, 2016 [38]	f_p	$r > 0.838$	1–3 mL/min
O'Doherty, 2017 [37]	SI	$r = 0.99$ $r = 0.99$	1–5 mL/g/min (MRI) 1.2–5.1 mL/g/min (MRI vs PET)
Kim, 2016 [14]	AUC	Efficiency < 50 %	0.1–2.0 mL/min
Claassen, 2001 [30]	AUC, PSI, MTT	No clear correlation with Q	

Phantom performance is predominantly listed in correlation statistics (r,χ^2) and absolute errors (ε). A distinction is made between direct and indirect comparison with a 'ground truth' flow measure (Q), which consists of theoretical or experimental values.
BF Blood flow, TTP Time to peak, MTT Mean transit time, AUC Area under the curve, (P)SI Peak signal intensity, f_p Perfusion fraction, r_{kin} Replenishment kinetics, FWHM Full width at half maximum, PG Positive gradient.

an overview on perfusion phantom approaches and emphasises on the choices and simplifications in phantom design and realization.

Although physical perfusion phantom models involve various tissues and applies to diverse PI applications, we observe similarities in overall phantom designs and configurations. These configurations can be categorised in three types (6/40 basic, 22/40 capillary, and 12/40 tissue filled) and two representations of microvasculature and tissue (23/40 as one combined and 17/40 as two separated compartments). Differences in these six phantom configurations are reflected in the resulting flow dynamics, e.g., how a contrast material is distributed and how long it stays inside the simulated organ tissue. None of the assessed phantoms could control inter-compartmental fluid exchange. Ideally, one would be able to fine-tune the exact flow dynamics in perfusion phantom models to achieve patient realistic (and contrast material specific) response function simulation. The required level of representativeness depends on the intended analyses, being closely related to the input parameters and boundary conditions of the BF model used. Since all assessed phantoms are limited to single tissue compartment models, phantom validation of higher order BF models should be performed with caution. It is generally important to verify whether assumptions in these phantom models are justified for the intended phantom application. This also concerns decisions regarding motion, pulsatile flow, and perfusion deficit simulation. For example, in myocardial perfusion phantom models it could be relevant to incorporate respiratory and cardiac motion for certain analyses[47,48], while for other tissues motion could be disregarded more easily.

The need for standardisation and validation of (quantitative) PI applications is widely recognised.[49,50] Perfusion phantom studies contribute to this endeavour since these studies enable direct comparison between imaging systems and protocols. We only observed one commercial perfusion phantom in our search result. We foresee an increased clinical impact when phantoms become validated and widely available. In our opinion, phantom validation efforts are sometimes reported insufficiently and ambiguously. The concept of *phantom validation* can be difficult since it is application-dependent and prone to subjectivity. The latter becomes apparent in the use of the words "considered", "reasonable", and "acceptable" (by whom, to whom, according to which criteria?).[51] We therefore suggest using Sargent's theory on model verification and validation.[52] Van Meurs' interpretation of this theory, including a practical checklist, is also applicable to physical, biomedical models (in adjusted form).[51] For example, according to the checklist, investigators should verify whether the applied flow range covers the full physiological range. Our results (see **Figure 4**) show great diversity in measured flow ranges. In addition, investigators are advised to consult physiologists and clinicians along the process and compare findings with

clinical data. In nine studies, phantom data are indeed compared with human or animal perfusion data (see **Table 1**).

When analysing phantom results, we noticed that investigators use different measures to evaluate quantitative PI outcomes, which hampers comparability (see **Table 2**). Some investigators express the relation between quantitative PI outcomes and the "ground truth" flow in correlation statistics or plots and others in absolute errors. Due to the diversity in outcome measures, applied flow ranges, and number of measurements carried out, interpretation of these results should be handled with caution. A uniform, unambiguous measure to evaluate both phantom validity and the accuracy and precision of quantitative PI outcomes is desired.

This study has limitations. Our search was limited to articles published between 1999 and 2018, yet we are aware that the development and use of perfusion phantoms date further back. Contemporary studies build on these designs, which makes it relevant to elaborate on perfusion phantom experiments in advanced PI systems. Furthermore, we have decided to leave out detailed information on phantom design and fabrication (e.g., material choices and dimensions), since this information can be found in the appropriate references. Besides, phantom manufacturing is highly subject to change. We expect to see more three-dimensional printed perfusion phantoms in the coming years.[43,53,54]

In conclusion, this systematic review provides insights into contemporary perfusion phantom approaches, which can be used for ground truth evaluation of quantitative PI applications. It is desirable to indicate an unambiguous measure for phantom validity. Furthermore, investigators in the field are recommended to perform phantom measurements in the full physiological flow range, consult physiologists and clinicians along the process, and compare findings with clinical data. In this way, one can verify and validate whether made choices and simplifications in perfusion phantom models are justified for the intended application, hence increasing clinical impact.

References

1. Barbier EL, Lamalle L, Decorps M (2001) Methodology of brain perfusion imaging. J Magn Reson Imaging. 13:496–520. https://doi.org/10.1002/jmri. 1073
2. Eck BL, Muzic RF, Levi J et al (2018) The role of acquisition and quantification methods in myocardial blood flow estimability for myocardial perfusion imaging CT. Phys Med Biol. 63:185011. https://doi.org/10.1088/1361-6560/aadab6
3. Bengel FM (2011) Leaving relativity behind. J Am Coll Cardiol. 8:749–751. https://doi.org/10.1016/j.jacc.2011.02.068
4. Sviri GE, Britz GW, Lewis DH, Newell DW, Zaaroor M, Cohen W (2006) Dynamic perfusion computed tomography in the diagnosis of cerebral vasospasm. Neurosurgery 59:319–324. https://doi.org/10.1227/01.NEU.0000222819.18834.33
5. Morton G, Chiribiri A, Ishida M et al (2012) Quantification of absolute myocardial perfusion in patients with coronary artery disease. J Am Coll Cardiol 60:1546–1555. https://doi.org/10.1016/j.jacc.2012.05.052
6. Slomka P, Xu Y, Berman D, Germano G (2014) Quantitative analysis of perfusion studies: strengths and pitfalls. J Nucl Cardiol 71:3831–3840. https://doi.org/10.1007/s12350-011-9509-2
7. Burrell S, MacDonald A (2006) Artifacts and pitfalls in myocardial perfusion imaging artifacts and pitfalls in myocardial perfusion imaging. J Nucl Med Technol 34:193–212
8. Chiribiri A, Schuster A, Ishida M et al (2013) Perfusion phantom: an efficient and reproducible method to simulate myocardial first-pass perfusion measurements with cardiovascular magnetic resonance. Magn Reson Med 69:698–707. https://doi.org/10.1002/mrm.24299
9. Andersen IK, Sidaros K, Gesmar H, Rostrup E, Larsson HB (2000) A model system for perfusion quantification using FAIR. Magn Reson Imaging. 18:565–574. https://doi.org/10.1016/S0730-725X(00)00136-3
10. Brauweiler R, Eisa F, Hupfer M, Nowak T, Kolditz D, Kalender WA (2012) Development and evaluation of a phantom for dynamic contrast-enhanced imaging. Invest Radiol. 47:462–467. https://doi.org/10.1097/RLI.0b013e318250a72c
11. Li P-C, Yeh C-K, Wang S-W (2002) Time-intensity-based volumetric flow measurements: an in vitro study. Ultrasound Med Biol. 28:349–358. https://doi.org/10.1016/S0301-5629(01)00516-6
12. Peladeau-Pigeon M, Coolens C (2013) Computational fluid dynamics modelling of perfusion measurements in dynamic contrast-enhanced computed tomography: Development, validation and clinical applications. Phys Med Biol. 58:6111–6131. https://doi.org/10.1088/0031-9155/58/17/6111
13. Driscoll B, Keller H, Coolens C (2011) Development of a dynamic flow imaging phantom for dynamic contrast-enhanced CT. Med Phys. 38:4866–4880. https://doi.org/10.1118/1.3615058
14. Kim M, Abbey CK, Insana MF (2016) Efficiency of U.S. tissue perfusion estimators. IEEE Trans Ultrason Ferroelectr Freq Control. 63:1131–1139. https://doi.org/10.1109/TUFFC.2016.2571979

15. Anderson JR, Ackerman JJH, Garbow JR (2011) Semipermeable hollow fiber phantoms for development and validation of perfusion-sensitive MR methods and signal models. Concepts Magn Reson Part B Magn Reson Eng. 39B:149–158. https://doi.org/10.1002/cmr.b.20202
16. Meyer-Wiethe K, Cangür H, Seidel G (2005) Comparison of different mathematical models to analyze diminution kinetics of ultrasound contrast enhancement in a flow phantom. Ultrasound Med Biol. 31:93–98. https://doi.org/10.1016/j.ultrasmedbio.2004.05.006
17. Veltmann C, Lohmaier S, Schlosser T et al (2002) On the design of a capillary flow phantom for the evaluation of ultrasound contrast agents at very low flow velocities. Ultrasound Med Biol. 28:625–634. https://doi.org/10.1016/S0301-5629(02)00499-4
18. Kim EJ, Kim DH, Lee SH, Huh YM, Song HT, Suh JS (2004) Simultaneous acquisition of perfusion and permeability from corrected relaxation rates with dynamic susceptibility contrast dual gradient echo. Magn Reson Imaging. 22:307–314. https://doi.org/10.1016/j.mri.2004.01.012
19. Lee JH, Cheong H, Song J-A et al (2016) Perfusion assessment using intravoxel incoherent motion-based analysis of diffusion-weighted magnetic resonance imaging. Invest Radiol. 51:520–528. https://doi.org/10.1097/RLI.0000000000000262
20. Chai JW, Chen JH, Kao YH et al (2002) Spoiled gradient-echo as an arterial spin tagging technique for quick evaluation of local perfusion. J Magn Reson Imaging. 16:51–59. https://doi.org/10.1002/jmri.10128
21. Potdevin TC, Fowlkes JB, Moskalik AP, Carson PL (2004) Analysis of refill curve shape in ultrasound contrast agent studies. Med Phys. 31:623–632. https://doi.org/10.1118/1.1649534
22. Lucidarme O, Franchi-abella S, Correas J, Bridal SL, Kurtisovski E (2003) Blood flow quantification with contrast-enhanced US: "Entrance in the Section" phenomenon — phantom and rabbit study. Radiology. 228:473–479. https://doi.org/10.1148/radiol.2282020699
23. Boese A, Gugel S, Serowy S et al (2012) Performance evaluation of a C-Arm CT perfusion phantom. Int J Comput Assist Radiol Surg. 8:799–807. https://doi.org/10.1007/s11548-012-0804-4
24. Hashimoto H, Suzuki K, Okaniwa E, Iimura H, Abe K, Sakai S (2017) The effect of scan interval and bolus length on the quantitative accuracy of cerebral computed tomography perfusion analysis using a hollow-fiber phantom. Radiol Phys Technol. 11:13–19. https://doi.org/10.1007/s12194-017-0427-0
25. Suzuki K, Hashimoto H, Okaniwa E et al (2017) Quantitative accuracy of computed tomography perfusion under low - dose conditions, measured using a hollow - fiber phantom. Jpn J Radiol. 35:373–380. https://doi.org/10.1007/s11604-017-0642-y
26. Noguchi T, Yshiura T, Hiwatashi A et al (2007) Quantitative perfusion imaging with pulsed arterial spin labeling: a phantom study. Magn Reson Med Sci. 6:91–97. https://doi.org/10.2463/mrms.6.91
27. Wang Y, Kim SE, Dibella EVR, Parker DL (2010) Flow measurement in MRI using arterial spin labeling with cumulative readout pulses - theory and validation. Med Phys. 37:5801–5810. https://doi.org/10.1118/1.3501881

28. Cangür H, Meyer-Wiethe K, Seidel G (2004) Comparison of flow parameters to analyse bolus kinetics of ultrasound contrast enhancement in a capillary flow model. Ultraschall Med. 25:418–421. https://doi.org/10.1055/s-2004-813796
29. Klotz E, König M (1999) Perfusion measurements of the brain: using dynamic CT for the quantitative assessment of cerebral ischemia in acute stroke. Eur J Radiol. 30:170–184. https://doi.org/10.1016/S0720-048X(99)00009-1
30. Claassen L, Seidel G, Algermissen C (2001) Quantification of flow rates using harmonic grey-scale imaging and an ultrasound contrast agent: an in vitro and in vivo study. Ultrasound Med Biol. 27:83–88. https://doi.org/10.1016/S0301-5629(00)00324-0
31. Mathys C, Rybacki K, Wittsack HJ et al (2012) A phantom approach to interscanner comparability of computed tomographic brain perfusion parameters. J Comput Assist Tomogr. 36:732–738. https://doi.org/10.1097/rct.0b013e31826801df
32. Ebrahimi B, Swanson SD, Chupp TE (2010) A microfabricated phantom for quantitative MR perfusion measurements: validation of singular value decomposition deconvolution method. IEEE Trans Biomed Eng. 57:2730–2736. https://doi.org/10.1109/TBME.2010.2055866
33. Ohno N, Miyati T, Chigusa T et al (2015) Technical note: development of a cranial phantom for assessing perfusion, diffusion, and biomechanics. Med Phys 44:1646–54. https://doi.org/10.1002/mp.12182
34. Zarinabad N, Hautvast GLTF, Sammut E et al (2014) Effects of tracer arrival time on the accuracy of high-resolution (Voxel-wise) myocardial perfusion maps from contrast-enhanced first-pass perfusion magnetic resonance. IEEE Trans Biomed Eng. 61:2499–2506. https://doi.org/10.1109/TBME.2014.2322937
35. Zarinabad N, Chiribiri A, Hautvast GLTF et al (2012) Voxel-wise quantification of myocardial perfusion by cardiac magnetic resonance. Feasibility and Methods Comparison. Magn Reson Med. 68:1994–2004. https://doi.org/10.1002/mrm.24195
36. O'Doherty J, Chalampalakis Z, Schleyer P, Nazir MS, Chiribiri A, Marsden PK (2017) The effect of high count rates on cardiac perfusion quantification in a simultaneous PET-MR system using a cardiac perfusion phantom. EJNMMI Phys. 4:31. https://doi.org/10.1186/s40658-017-0199-y
37. O'Doherty J, Sammut E, Schleyer P et al (2017) Feasibility of simultaneous PET-MR perfusion using a novel cardiac perfusion phantom. Eur J Hybrid Imaging. 1:1–14. https://doi.org/10.1186/s41824-017-0008-9
38. Otton J, Morton G, Schuster A et al (2013) A direct comparison of the sensitivity of CT and MR cardiac perfusion using a myocardial perfusion phantom. J Cardiovasc Comput Tomogr. 7:117–124. https://doi.org/10.1016/j.jcct.2013.01.016
39. Ressner M, Brodin LA, Jansson T, Hoff L, Ask P, Janerot-Sjoberg B (2006) Effects of ultrasound contrast agents on doppler tissue velocity estimation. J Am Soc Echocardiogr. 19:154–164. https://doi.org/10.1016/j.echo.2005.09.025
40. Ziemer BP, Hubbard L, Lipinski J, Molloi S (2015) Dynamic CT perfusion measurement in a cardiac phantom. Int J Cardiovasc Imaging. 31:1451–1459. https://doi.org/10.1007/s10554-015-0700-4

41. Sakano R, Kamishima T, Nishida M, Horie T (2015) Power Doppler signal calibration between ultrasound machines by use of a capillary-flow phantom for pannus vascularity in rheumatoid finger joints: a basic study. Radiol Phys Technol.8:120-124. https://doi.org/10.1007/s12194-014-0299-5
42. Gauthier TP, Averkiou MA, Leen ELS (2011) Perfusion quantification using dynamic contrast-enhanced ultrasound: the impact of dynamic range and gain on time-intensity curves. Ultrasonics. 51:102–106. https://doi.org/10.1016/j.ultras.2010.06.004
43. Low L, Ramadan S, Coolens C, Naguib HE (2018) 3D printing complex lattice structures for permeable liver phantom fabrication. Bioprinting. 10. https://doi.org/10.1016/j.bprint.2018.e00025
44. Cho GY, Kim S, Jensen JH, Storey P, Sodickson DK, Sigmund EE (2012) A versatile flow phantom for intravoxel incoherent motion MRI. Magn Reson Med 67:1710–1720. https://doi.org/10.1002/mrm.23193
45. Murthy VL, Bateman TM, Beanlands RS et al (2017) Clinical quantification of myocardial blood flow using PET: joint position paper of the SNMMI Cardiovascular Council and the ASNC. J Nucl Med. 59:273–293. https://doi.org/10.2967/jnumed.117.201368
46. Brown RP, Delp MD, Lindstedt SL, Rhomberg LR, Beliles RP (1997) Physiological parameter values for physiologically based pharmacokinetic models. Toxicol Ind Health. 13:407–484. https://doi.org/10.1177/074823379701300401
47. Chrysanthou-Baustert I, Polycarpou I, Demetriadou O et al (2017) Characterization of attenuation and respiratory motion artifacts and their influence on SPECT MP image evaluation using a dynamic phantom assembly with variable cardiac defects. J Nucl Cardiol. 24:698–707. https://doi.org/10.1007/s12350-015-0378-y
48. Fieseler M, Kugel H, Gigengack F et al (2013) A dynamic thorax phantom for the assessment of cardiac and respiratory motion correction in PET/MRI: A preliminary evaluation. Nucl Instrum Methods Phys Res. 702:59–63. https://doi.org/10.1016/j.nima.2012.09.039
49. Leiva-Salinas C, Hom J, Warach S, Wintermark M (2012) Stroke Imaging Research Roadmap. Neuroimaging Clin N Am. 21:1–9. https://doi.org/10.1016/j.nic.2011.01.009
50. Miles KA, Lee T, Goh V, Klotz E, Cuenod C (2012) Current status and guidelines for the assessment of tumour vascular support with dynamic contrast-enhanced computed tomography. Eur Radiol 22:1430–1441. https://doi.org/10.1007/s00330-012-2379-4
51. Van Meurs WL (2011) Modeling and simulation in biomedical engineering - applications in cardiorespiratory physiology. The McGraw-Hill Companies. https://doi.org/10.1109/MPUL.2013.2289532
52. Sargent RG (2010) Verification and validation of simulation models. Proc 2010 Winter Simul Conf 166–183. https://doi.org/10.1109/WSC.2007.4419595
53. Wang K, Ho C, Zhang C, Wang B (2017) A review on the 3D printing of functional structures for medical phantoms and regenerated tissue and organ applications. Engineering. 3:653–662. https://doi.org/10.1016/J.ENG.2017.05.013
54. Wood RP, Khobragade P, Ying L et al (2015) Initial testing of a 3D printed perfusion phantom using digital subtraction angiography. Proc SPIE 9417, Medical Imaging 2015: Biomedical Applications in Molecular, Structural, and Functional Imaging, 94170V. https://doi.org/10.1117/12.2081471

3

Marije E. Kamphuis
Gijs J. de Vries
Henny Kuipers
Marloes Saaltink
Jacqueline Verschoor
Marcel J. W. Greuter
Riemer H. J. A. Slart
Cornelis H. Slump

Medical & Biological Engineering & Computing
volume 60, pages 1541–1550 (2022)

Development of a dedicated 3D printed myocardial perfusion phantom: proof-of-concept in dynamic SPECT

Abstract

Introduction We aim to facilitate phantom based (ground truth) evaluation of dynamic, quantitative myocardial perfusion imaging (MPI) applications. Current MPI phantoms are static representations or lack clinical hardware and software evaluation capabilities.

Materials and Methods This proof-of-concept study demonstrates the design, realization and testing of a dedicated cardiac flow phantom. The 3D printed phantom mimics flow through a left ventricular cavity (LVC) and three myocardial segments. In the accompanying flow circuit, tap water is pumped through the LVC and thereafter partially directed to the segments using adjustable resistances. Regulation hereof mimics perfusion deficit, whereby flow sensors serve as reference standard. Seven phantom measurements were performed while varying injected activity of [^{99m}Tc]Tc-tetrofosmin (330–550 MBq), cardiac output (1.5–3.0 L/min) and myocardial segmental flows (50–150 mL/min). Image data from dynamic single photon emission computed tomography (SPECT) was analyzed with clinical software.

Results Derived time activity curves were reproducible, showing logical trends regarding selected input variables. A promising correlation was found between software computed myocardial flows and its reference ($\rho = -0.98$; $p = 0.003$).

Conclusion This proof-of-concept paper demonstrates we have successfully measured first-pass LV flow and myocardial perfusion in SPECT-MPI using a novel, dedicated, myocardial perfusion phantom.

Introduction

Absolute quantification in dynamic rest and stress myocardial perfusion imaging (MPI) is becoming more routine in the assessment of myocardial ischemia and the diagnosis of coronary artery disease.[1–3] Patients suffering from balanced ischemia, complicated previous multiple coronary interventions and microvascular dysfunction may especially benefit from measurement of myocardial blood flow (MBF) and flow reserve (MFR).[4,5] This is in addition to visual evaluation or semi-quantitative approaches. Apart from a higher diagnostic accuracy in these particular patient groups, absolute MPI might also facilitate standardised assessment, with the aim of implementing universal cut-off values of flow estimates, e.g., in revascularisation decision-making.[6]

In previous decades, many studies have focused on quantitative MPI with positron emission tomography (PET).[5–7] Currently, quantitative MPI expands to other imaging domains, including computed tomography (CT)[8,9], magnetic resonance imaging (MRI)[10], single photon emission CT (SPECT)[11–13] and ultrasound (US).[14] Validation of MBF and MFR quantification, and underlying variety in blood flow models[15], is important in order to achieve adequate, safe and widespread clinical implementation and interpretation. Moreover, if one indicates and appreciates the possibilities of specific hardware and software, one might learn how to deal with current limitations. Perfusion phantom studies can contribute to this unmet need for robust quality assessment due to the controlled setup and use of flow sensors as reference standard.

Our aim is to contribute to the evaluation of multimodal dynamic MPI applications using perfusion phantom models. Based on a previous literature search[16], current available myocardial perfusion phantoms are predominantly static representations (no flow component) or lack evaluation capabilities regarding clinical software.[16–18] This proof-of-concept paper describes the design and realization of a dedicated 3D printed myocardial perfusion phantom and initial performance testing in dynamic SPECT-MPI.

Materials

The myocardial perfusion phantom

The myocardial perfusion phantom has the shape and size of a normal to hypertrophic male LV at end-diastolic phase. The phantom consists of a modular stationary setup, including a LV base unit and three identical add-on myocardial segments (**Figure 1**). All components are designed for 3D printing (Objet260 Connex3, Stratasys, Israel) enabling rapid prototyping. The base unit contains a connector unit and a LV cavity. To prevent printing of enclosed volumes, the parts are printed separately and assembled afterwards. As can be seen in **Figure 1C**, the main tube enters the

overall cavity at the right-hand side and opens just before the apex (left-hand side) to direct the in- and outgoing flow. The LV cavity is a cylinder that is spherically shaped at the apex. The outgoing fluid within the connector unit flows into the aorta and branches into three myocardial segments (**Figure 1B,D**).

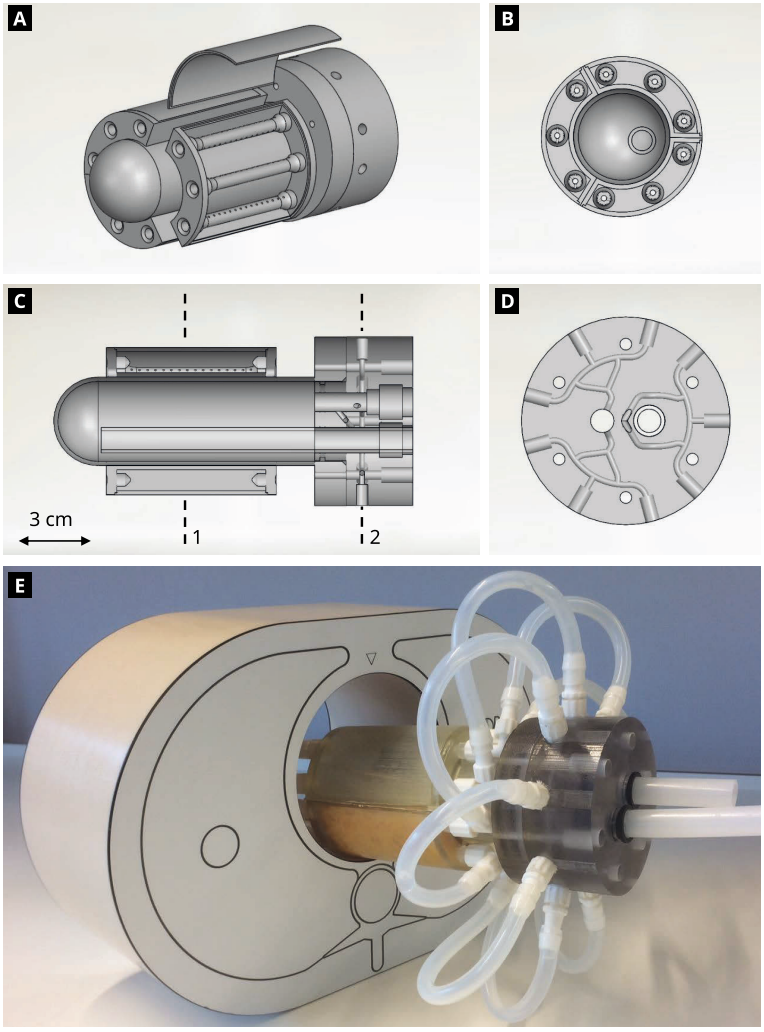

Figure 1 (Schematic) representation of the 3D printed myocardial perfusion phantom. (**A**) The modular phantom design including left ventricular base unit and three add-on myocardial segments. These segments can consist of different inlays. In this example, a second compartment is simulated using three perforated tubes. (**C**) a longitudinal section of the phantom in which dotted lines **1** and **2** visualise the cross-sections as depicted in respectively (**B**) and (**D**). (**E**) The overall cardiac phantom, including connectors and tubing, inserted into a thorax phantom.

The three myocardial segments correspond to the three main coronary territories, i.e., regions supplied by the left anterior descending coronary artery (LAD), right coronary artery (RCA) and the left circumflex coronary artery (LCX). Simulation of the apex was disregarded to facilitate comparability. The myocardial segment inlay can alter per measurement due to its modular add-on design (see Phantom Measurements). The phantom fits in an anthropomorphic thorax phantom (QRM GmbH, Moehrendorf, Germany) to obtain adequate X-ray attenuation profiles. **Figure 1E** shows the 3D printed myocardial perfusion phantom including connectors and tubing.

The flow circuit

The measurement setup generates first-pass flow through the LVC and downstream myocardial segments (**Figure 2**). The thorax phantom, containing the cardiac perfusion phantom, covers the scanner's field of view. Tap water is pumped from a reservoir towards the LVC. Before the water enters the LVC, a radiotracer bolus can be administered to the stream using a clinical contrast media injector. After the injection, the radiotracer bolus flows through the LVC and is increasingly mixed and diluted. The outgoing tube represents the aorta and branches into three parallel-connected coronary arteries. These arteries split further into nine coronary branches of similar length that connect the three surrounding myocardial segments. Each segment ends in three coronary veins that merge into one. The diluted radiotracer concentration, passing through the aorta and three myocardial segments, is collected in two separate reservoirs. Simulation of radiotracer recirculation falls outside the scope of this study. Two sizes of plastic and silicone tubing are used ($\varnothing_{inner}$ = 10 and 5 mm) to differentiate between the aorta and coronary arteries/veins.

Flow sensors measure the flow through the left ventricle (UFo8B, ultrasonic flowmeter, Cynergy 3, UK) and in each myocardial segment (FCH-m-POM-LC, low flow tur-

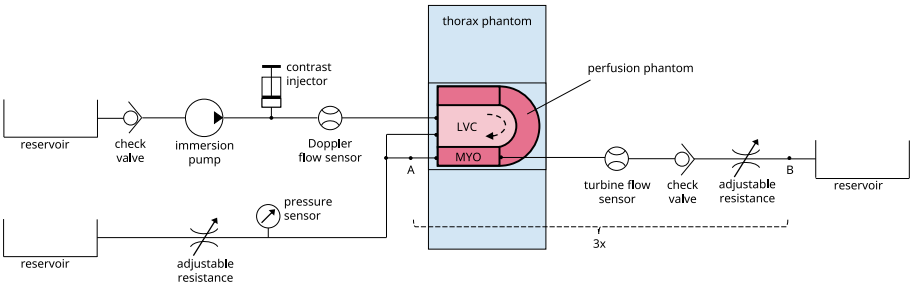

Figure 2 Flow circuit diagram of measurement set-up. The phantom simulates first-pass left ventricular flow and myocardial perfusion. The cardiac phantom is inserted into a thorax phantom, comprising the scanner's field of view. The myocardium (MYO) consists of three segments surrounding the left ventricular cavity (LVC). The components between A and B concern one myocardial segment circuit. In total there are three such circuits connected in parallel. Water flows from top left to bottom left and right.

bine flowmeter, B.I.O-TECH, Germany). Four adjustable resistances are placed in the flow circuit to set the flow ratio between aorta and individual myocardial segments. In this way, it is also possible to simulate global and regional perfusion deficits. An in-house built, digital control system monitors the various flows and controls an immersion pump (Comet immersion pump, OCEAN, Germany) using flow-feedback from the ultrasonic flow sensor. A pressure sensor (40PC series, Honeywell Inc., Freeport, Illinois) keeps the pump operating in the same pressure range.

Methods

In dynamic SPECT-MPI, the distribution of an injected radiotracer bolus is recorded over time and displayed in so-called time activity curves (TACs), including the arterial input function (AIF) and tissue response functions (TRFs). Blood flow models use this information to estimate tissue perfusion levels. At this stage of phantom development and evaluation, we explored the effect of varying cardiac output (CO; L/min), myocardial flow rate (Q_{myo}; mL/min), and injected activity (A_{inj}; MBq) on the resulting AIF, TRF, and computed MBF.

Phantom measurements

Seven flow measurements were executed in two measurement sessions. Pump flow (i.e., CO) was set at 1.5 and 3.0 L/min and the planned activity administration between 350 and 550 MBq to evaluate their effect on AIF measurement. Reproducibility of the AIF curve was measured by fivefold repetition (CO = 1.5 L/min, $A_{inj} \approx 350$ MBq). These five measurements were also used to evaluate TRF simulation in the three myocardial segments, including reproducibility measurements. This resulted in 15 TRFs in total. Each myocardial segment contained a different inlay to investigate which one was most suitable for the measurement of tissue perfusion. The three myocardial segments comprised:

- a basic one-compartment with no inlay (basic 1C),
- a one-compartment with sponge inlay (sponge 1C) and
- a two-compartment created by three perforated tubes (tubes 2C) (see **Figure 1A**).

In the measurements, average flow measured in the myocardial segments (Q_{myo}) served as reference standard and was varied between 50 and 150 mL/min.

Myocardial perfusion imaging

All data were acquired in list mode using a cadmium-zinc-telluride SPECT system (D-SPECT, Spectrum Dynamics, Caesarea, Israel). The standard clinical protocol consisted of 6 min dynamic scanning, starting just before injection of a radiotracer bolus. Two millilitres of 330–550 MBq [^{99m}Tc]Tc-tetrofosmin solution was injected at 1 mL/s, followed by a 20 mL saline flush. Typically, data was re-binned into 32 frames consisting of 21 frames of 3 s; 4 frames of respectively 9, 15, 21 and 27 s; and 7 frames of 30 s.

An OSEM technique was used for reconstruction of dynamic imaging acquisitions, with 4 iterations and 32 subsets.[19]

Data-analysis

Resulting dynamic image datasets were analysed with clinical software (Corridor4DM software, INVIA Medical Imaging Solutions, United States). In this software, myocardial surfaces were algorithmically estimated from summed myocardial images[19], indicating the region of interest (ROI) for TRF measurement. The AIF was derived from a manually selected ROI in the LVC using a default size box placed at the centre of the LVC (see **Figure 3**). The software displayed the AIF, TRFs and computed MBF for different anatomical regions. We selected the display of the three main coronary regions to match the visualised data with the myocardial segments of the phantom.

The blood flow model applied in the clinical MBF analysis software was a net retention model proposed by Leppo et al.[20] and Yoshida et al.[21] The following modified

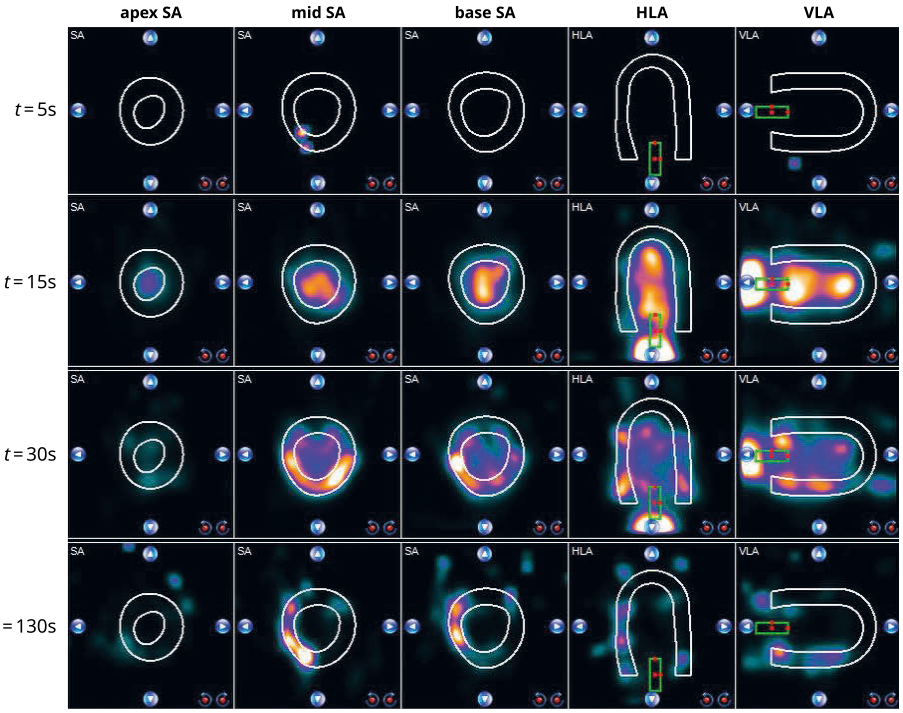

Figure 3 Time lapse of radiotracer distribution in the myocardial perfusion phantom visualized by clinical analysis software. The white contours indicate the myocardial tissue region of interest (ROI) and the green box the arterial ROI. The visualized coronary territories correspond to different myocardial tissue inlays in the phantom. SA = short axis, HLA = horizontal long axis, VLA = vertical long axis.

equation was used to calculate the retention rate (R) of tracer in the myocardium in millilitres/gram/minute at time t. This myocardial uptake can be expressed as the product of the MBF (mL/g/min) and the extraction fraction (E):

$$R = \mathrm{MBF} \times E = \frac{\frac{1}{\mathrm{PV}(t_3 - t_2)} \int_{t_2}^{t_3} \left(P(t) - S_\mathrm{m} C_\mathrm{a}(t)\right) \mathrm{d}t}{\mathrm{CF} \int_0^{t_1} \left(C_\mathrm{a}(t) - S_\mathrm{b} P(t)\right) \mathrm{d}t}$$

In this, $C_a(t)$ and $P(t)$ correspond to the average arterial and tissue tracer concentration over time, the AIF and TRF respectively. Integration limit t_1 denotes the end of the blood pool phase (typically at 1.5 min), whereas t_2 and t_3 denote integration limits of the average tissue activity (typically from 1.5 to 2.5 min). In our measurements, t_2 and t_3 were set to frames 15 and 20 (around 40–60 s), due to the absence of tracer trapping and recirculation in the perfusion phantom model. Several corrections were applied to the data to compute absolute flow. Firstly, the acquired myocardial counts were corrected for partial volume losses using a recovery coefficient for the myocardium (PV). Partial volume effects also occurred in the measurement of blood-pool activity, whereby subsequent decrease in AIF was compensated by a cross-calibration factor (CF). Finally, theoretically computed spill over fractions, S_m and S_b, correct the spill over from the blood pool activity to the myocardium, and vice versa.[15,16,22]

TACs of all phantom measurements were exported to Matlab (2016a; The MathWorks Inc, Natick, Mass) for further data analysis, visualisation and comparison with a patient example.[23] Reproducibility of phantom-based TAC measurement was evaluated by comparing the obtained area under the curve (AUC). The mean AUC and standard deviation were calculated for all 5 AIFs and 9 (3 × 3) TRFs. In this, the injected radiotracer activity was first normalised to 350 MBq. The relation between Q_{myo} and computed MBF was described with Pearson correlation statistics.

Results

Dynamic perfusion images

Figure 3 shows a typical perfusion image time lapse of the radiotracer distribution in the myocardial perfusion phantom along the short, horizontal, and vertical long axes. At t = 15 s, passing of the diluted radiotracer bolus is captured in the LVC. Subsequently, a part of the radiotracer solution flows into the myocardial segments, which is shown at t = 30 s and t = 130 s. The matching dynamic perfusion imaging video can be found in the **Supplement**.

Time activity curve analysis

Resulting TACs of the AIF and TRF are displayed for varying settings (**Figure 4**). As can be seen, injection of larger radiotracer bolus activity corresponds to higher observed peak activity. Moreover, at an increased CO (i.e., set pump flow), the AIF exhib-

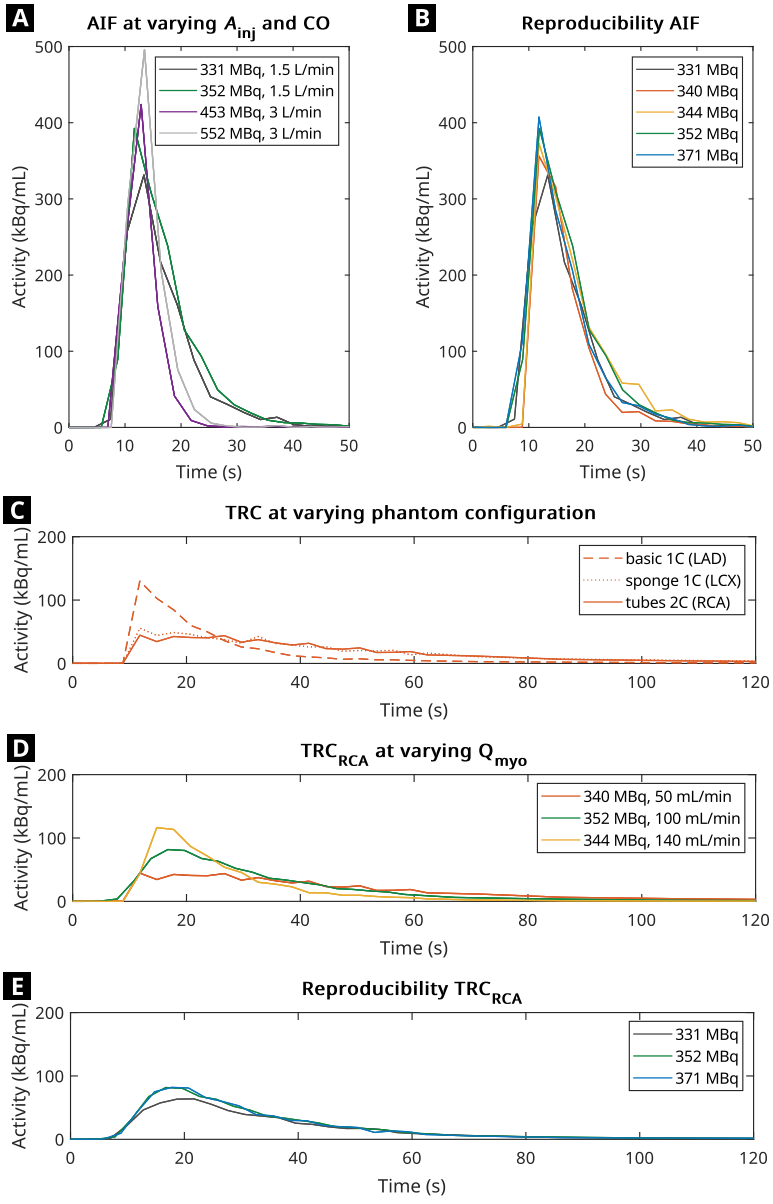

Figure 4 A–E Time activity curves obtained using the myocardial perfusion phantom. Arterial input functions (AIFs) were acquired in the left ventricle at varying injected activity of [^{99m}Tc]Tc-tetrofosmin (A_{inj}) and cardiac output (CO). Resulting tissue response curves (TRCs) in the three myocardial segments were executed at varying myocardial flow rates (Q_{myo}) and tissue inlays (1 or 2 compartments). Each line colour denotes a single flow measurement ($n = 7$). LAD = left anterior descending coronary artery, RCA = right coronary artery, LCX = left circumflex coronary artery.

Table 1 Reproducibility of phantom based time activity curve (TAC) measurements. The mean and standard deviation (SD) were calculated for the areas under the curve (AUCs) of both the arterial input function (AIF) and tissue response functions (TRFs) for *n* measurements. The TRCs correspond with the three coronary regions that have a varying tissue inlay (1 or 2 compartments).

	AUC (MBq mL^{-1} s)	
Normalized TACs	**Mean (SD)**	***n***
Normalized AIF	3.77 (0.33)	5
Normalized TRF		
basic 1C (LAD)	1.34 (0.12)	3
sponge 1C (LCX)	2.40 (0.08)	3
tubes 2C (RCA)	2.33 (0.11)	3

LAD = left anterior descending coronary artery, LCX = left circumflex coronary artery, and RCA = right coronary artery.

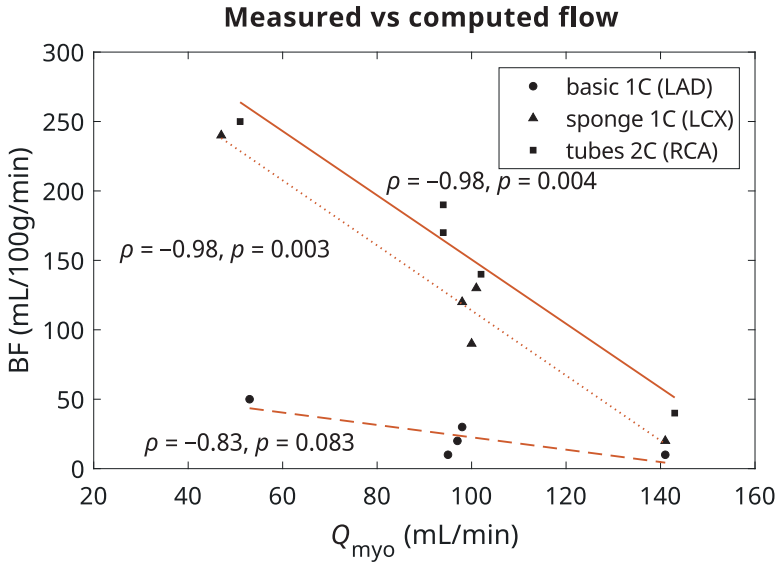

Figure 5 Correlation plot of reference flow (Q_{myo}) and computed myocardial blood flow (MBF) for three different phantom tissue inlays (1 or 2 compartment). *ρ* = Pearson correlation coefficient, LAD = left anterior descending coronary artery, RCA = right coronary artery, LCX = left circumflex coronary artery.

its a shorter retention time. Repeated measurements show good AIF reproducibility (**Figure 4B** and **Table 1**). Measured TRFs generally show a higher peak activity for the basic 1C configuration, though the retention time of the radiotracer is longer for the sponge 1C and tubes 2C (**Figure 4C**). An increased Q_{myo} generally results in higher measured peak activity and shorter retention time. TRF measurements demonstrate good reproducibility as well (**Figure 4E** and **Table 1**). **Figure 5** shows the correlation between measured and computed flow in the three myocardial segments, whereby each segment corresponds to a different tissue inlay. Pearson correlation coefficient ρ is largest for measurements with the sponge 1C and tubes 2C ($\rho = -0.98$).

Patient data comparison

Figures 6 and 7 match phantom data with patient data. The phantom-based AIF closely resembles the shape of the AIF in a patient (**Figure 6A**). The phantom based TRF is comparable to that of a patient, though it has a substantially shorter retention time. **Figure 7** shows an example of a MBF analysis in a patient and a phantom, both indicating a perfusion deficit in the LAD region.

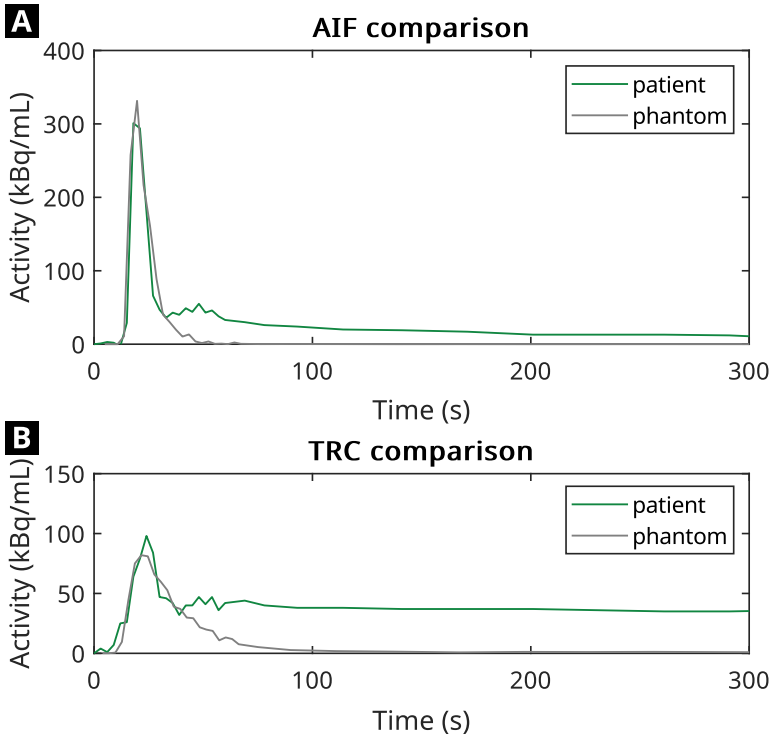

Figure 6 A,B Time activity curves comparing normal patient data with phantom data. The patient example is adapted from 23. AIF = arterial input function, TRC = tissue response curve.

Discussion

To our knowledge, this paper presents the first myocardial perfusion phantom described in literature, dedicated to quantitative evaluation of clinical SPECT-MPI hardware and software. We have successfully measured first-pass LV flow and myocardial perfusion in SPECT-MPI. In addition, we have performed initial reproducibility measurements and initial sensitivity analyses on TAC measurement and MBF computation for the following parameters: CO, Q_{myo} and A_{inj}.

Phantom design, realization, and testing

The phantom resembles the anatomy and (patho-) physiology of LV flow and myocardial perfusion in many respects. Nonetheless, several assumptions and simplifications have been applied in its design and realization. First, we focused on measuring first-pass myocardial perfusion; hence, tracer recirculation and uptake in surrounding tissue were disregarded. Second, we designed a stationary perfusion phantom constructed of rigid plastic, which does not model cardiac contraction, nor has a physiological flow profile. Third, we also excluded simulation of the apex. Last, the current inlays of the myocardial segments only mimic tissue perfusion as a semi-controllable two-compartment representation (i.e., no tracer trapping).

We have carried out multiple measurements to investigate how accurately and reproducibly the phantom resembles myocardial perfusion, given the simplifications that were made. Accordingly, the acquired phantom TAC curves are like those in patients in multiple ways, e.g., the shape of the curves and their activity range. Aside from these promising results, we also noticed some dissimilarities. For example, we

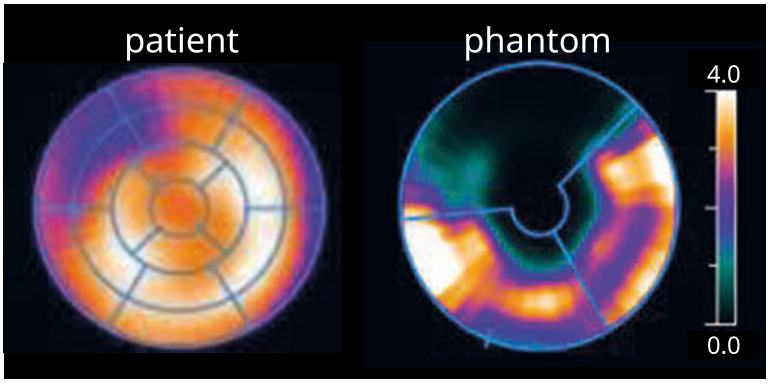

Figure 7 Myocardial blood flow (MBF) bull's eye plot comparison between example patient and phantom data. Both plots indicate a perfusion deficit in the coronary territory supplied by the left anterior descending coronary artery. The patient example is adapted from 23. In the phantom, apex simulation was disregarded. AIF = arterial input function, TRC = tissue response curve.

observe an additional peak in the patient-based AIF around $t = 45$ s (**Figure 6A**). This peak can be explained by (unwanted) spill over activity from the myocardium to the blood pool. By enlarging and narrowing the arterial ROI (green box in **Figure 3**), it becomes possible to create and control similar spill over effects in our phantom setup. Secondly, we observed shorter retention times for the phantom TRFs compared to those obtained in patients (**Figure 6B**). The missing tracer trapping, and recirculation can explain this effect.

In the phantom TAC analysis, the obtained TRFs showed a higher peak activity and shorter retention time at increasing Q_{myo}, which agrees with our expectations and enables the opportunity to measure local and global perfusion deficits. In addition, the phantom comprised of three different myocardial segment inlays to enable investigation of which one is most suitable for measuring tissue perfusion. The basic 1C inlay yielded the shortest retention time and showed an uneven distribution of tracer within the compartment. The other two inlays, i.e. the sponge 1C and tubes 2C, presented more favourable tracer dynamic behaviour, though distribution of tracer within the segment can be further optimised (see **Figure 4**). We expected that a two-compartment inlay ensures an even longer retention time, but due to the low number of perforated tubes, this effect became insignificant. The underlying cause of the observed uneven tracer distribution seems to be jet formation at the three entrance points of each myocardial segment. This might be an oversimplification in mimicking the physiological precapillary network. Its effect is most present in the absence of simulated tissue or capillaries.

Figure 5 visualises the possibility of comparing set Q_{myo} in the phantom setup with computed BF derived from clinical hardware and software. The observed high, linear correlation is physiologically incorrect (at this stage of phantom development) and is comprised of a relatively small dataset. Nevertheless, in this proof-of-concept stage, these measurements confirm what is being simulated and give us a glimpse of future phantom potential. In addition, **Figure 7** exemplifies the possibility to simulate perfusion deficits. Underlying causes of the severe perfusion deficit mimicked in the LAD region are the use of a basic 1C tissue inlay (shortest retention time of tracer) and a low Q_{myo} of 50 mL/min. These settings resulted in a computed MBF of around 50 mL/100 g/min in the LAD region (see **Figure 5**).

The obtained results are comparable to the performance of other perfusion phantoms. Li et al.[24] compared tissue perfusion with a dialysis cartridge to a basic spherical-shaped volume using US imaging. Kim et al.[25] performed a similar analysis in MRI by comparing a dialysis cartridge with a gel bead–filled perfusion phantom. Both studies showed an even distribution of contrast agent with a prolonged retention time using the numerous permeable fibres of the dialysis cartridge. Such dialysis cartridges are therefore frequently used to model tissue perfusion.[16] Nonetheless,

the tracer uptake in myocardial tissue is uncontrolled in these phantom models and simulation of organ anatomy (e.g., heart contours) is being disregarded. In our experimental setup, we observe a promising correlation between reference flow and computed MBF, which is comparable to other perfusion phantom studies.[16]

Phantom validation and application

Justification of the choices made in phantom design and testing depends on the intended phantom application. In our design, most notable choices are the absence of cardiac contraction, tracer trapping and recirculation, together with the relatively low CO that was applied in our measurements. These choices and simplifications are considered acceptable if we are predominantly interested in the evaluation of MPI system responses. In such evaluations, excellent reproducibility of phantom performance is most essential. A more advanced myocardial perfusion phantom may broaden its application domain; however, an increase in complexity is difficult to achieve in terms of controllability and phantom validation. Our initial TAC measurements show good reproducibility, as shown in **Figure 4** and displayed in **Table 1**. **Table 1** demonstrates that the AUCs from the obtained AIFs and TRFs were quite similar for repeated measurements (SD is below 10 % of mean AUC), which can be even further optimised in future work (e.g., by removing the presence of unwanted air bubbles).

In this study, our phantom application domain was restricted to SPECT-MPI. However, the phantom could be applied in other imaging modalities as well. At this moment, phantom-based evaluation of dynamic SPECT-MPI is of major relevance, since recent advances in detector-technology speculates it may become technically feasible to perform quantitative MBF and MFR analysis with SPECT-MPI.[26] We are confident that perfusion phantom studies will make a valuable contribution to this research domain.

Overall, we present a novel myocardial perfusion phantom with add-on myocardial segments that has the possibility to mimic regional and global perfusion deficits and is unique in its compatibility with clinical hardware and software. This combination of features can be of interest in the validation of blood flow models, for example, to evaluate effects of attenuation and spill over on TAC measurement and MBF computation. Other foreseen applications involve intra- and intermodal comparison. Further phantom testing and validation is needed to achieve these goals.

Conclusion

This proof-of-concept paper demonstrates we have successfully measured first-pass LV flow and myocardial perfusion in SPECT-MPI using a novel, dedicated, myocardial perfusion phantom. The resulting AIFs and TRFs show good reproducibility and re-

semble a patient TAC curve on multiple aspects. Other phantom requirements were also met, including the acceptance of phantom contours by commercial MBF analysis software and the simulation of local and global perfusion deficits. Moreover, the phantom's modular and 3D printed design enables rapid prototyping, allowing us to further improve on the measurement and evaluation of radiotracer/contrast kinetics in dynamic, multimodal MPI applications.

Supplement

Dynamic perfusion imaging video

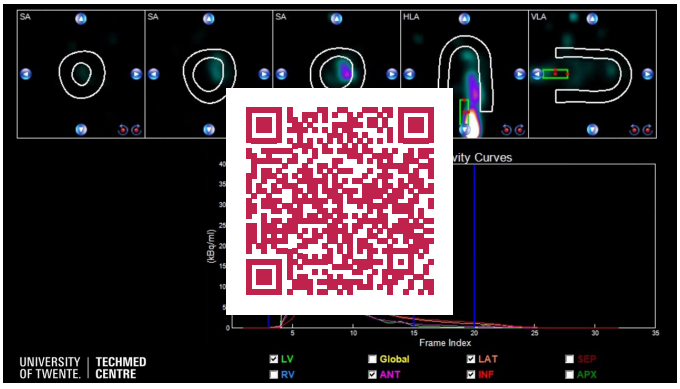

https://link.springer.com/article/10.1007/s11517-021-02490-z#Sec17

References

1. Sciagrà R, Lubberink M, Hyafil F, Saraste A, Slart RHJA, Agostini D, et al. EANM procedural guidelines for PET/CT quantitative myocardial perfusion imaging. Eur J Nucl Med Mol Imaging [Internet]. 2021;48(4):1040–69. Available from: https://doi.org/10.1007/s00259-020-05046-9
2. Berman DS, Kang X, Slomka PJ, Gerlach J, de Yang L, Hayes SW, et al. Underestimation of extent of ischemia by gated SPECT myocardial perfusion imaging in patients with left main coronary artery disease. J Nucl Cardiol. 2007;14(4 SPEC. ISS.):521–8.
3. Waller AH, Blankstein R, Kwong RY, Di Carli MF. Myocardial Blood Flow Quantification for Evaluation of Coronary Artery Disease by Positron Emission Tomography, Cardiac Magnetic Resonance Imaging, and Computed Tomography. Curr Cardiol Rep [Internet]. 2014;16(5):483. Available from: https://doi.org/10.1007/s11886-014-0483-6
4. Gould KL, Johnson NP. Coronary Physiology Beyond Coronary Flow Reserve in Microvascular Angina: JACC State-of-the-Art Review. J Am Coll Cardiol [Internet]. 2018;72(21):2642–62. Available from: https://www.sciencedirect.com/science/article/pii/S0735109718386340
5. Guerraty MA, Rao HS, Anjan VY, Szapary H, Mankoff DA, Pryma DA, et al. The role of resting myocardial blood flow and myocardial blood flow reserve as a predictor of major adverse cardiovascular outcomes. PLoS One [Internet]. 2020 Feb 13;15(2):e0228931. Available from: https://doi.org/10.1371/journal.pone.0228931
6. Knuuti J, Kajander S, Mäki M, Ukkonen H. Quantification of myocardial blood flow will reform the detection of CAD. J Nucl Cardiol [Internet]. 2009;16(4):497–506. Available from: https://doi.org/10.1007/s12350-009-9101-1
7. DeKemp RA, Ruddy TD, Hewitt T, Dalipaj MM, Beanlands RSB. Detection of serial changes in absolute myocardial perfusion with 82Rb PET. J Nucl Med. 2000;41(8):1426–35.
8. Li Y, Dai X, Lu Z, Shen C, Zhang J. Diagnostic performance of quantitative, semi-quantitative, and visual analysis of dynamic CT myocardial perfusion imaging: a validation study with invasive fractional flow reserve. Eur Radiol [Internet]. 2021;31(1):525–34. Available from: https://doi.org/10.1007/s00330-020-07145-5
9. Rossi A, Merkus D, Klotz E, Mollet N, de Feyter PJ, Krestin GP. Stress myocardial perfusion: imaging with multidetector CT. Radiology. 2014;270(1):25–46.
10. Lee DC, Johnson NP. Quantification of Absolute Myocardial Blood Flow by Magnetic Resonance Perfusion Imaging. JACC Cardiovasc Imaging. 2009;2(6):761–70.
11. Agostini D, Roule V, Nganoa C, Roth N, Baavour R, Parienti JJ, et al. First validation of myocardial flow reserve assessed by dynamic 99mTc-sestamibi CZT-SPECT camera: head to head comparison with 15O-water PET and fractional flow reserve in patients with suspected coronary artery disease. The WATERDAY study. Eur J Nucl Med Mol Imaging. 2018;45(7):1079–90.
12. Nkoulou R, Fuchs TA, Pazhenkottil AP, Kuest SM, Ghadri JR, Stehli J, et al. Absolute Myocardial Blood Flow and Flow Reserve Assessed by Gated SPECT with Cadmium–Zinc–Telluride Detectors Using 99mTc-Tetrofosmin: Head-to-Head Comparison with 13N-Ammonia PET. J Nucl Med [Internet]. 2016 Dec 1;57(12):1887 LP – 1892. Available from: http://jnm.snmjournals.org/content/57/12/1887.abstract

13. Otaki Y, Manabe O, Miller RJH, Manrique A, Nganoa C, Roth N, et al. Quantification of myocardial blood flow by CZT-SPECT with motion correction and comparison with 15O-water PET. J Nucl Cardiol [Internet]. 2021;28(4):1477–86. Available from: https://doi.org/10.1007/s12350-019-01854-1
14. Vogel R, Indermühle A, Reinhardt J, Meier P, Siegrist PT, Namdar M, et al. The quantification of absolute myocardial perfusion in humans by contrast echocardiography: Algorithm and validation. J Am Coll Cardiol [Internet]. 2005;45(5):754–62. Available from: https://www.sciencedirect.com/science/article/pii/S0735109704024180
15. Yoshinaga K, Manabe O, Tamaki N. Absolute quantification of myocardial blood flow. J Nucl Cardiol [Internet]. 2018;25(2):635–51. Available from: https://doi.org/10.1007/s12350-016-0591-3
16. Kamphuis ME, Greuter MJW, Slart RHJA, Slump CH. Quantitative imaging: systematic review of perfusion/flow phantoms. Eur Radiol Exp [Internet]. 2020;4(1):15. Available from: https://doi.org/10.1186/s41747-019-0133-2
17. Kok G, Pelevic N, Chiribiri A, Milidonis X, Nazir M, Capstick M, et al. A calibrated physical flow standard for medical perfusion imaging. Flow Meas Instrum [Internet]. 2021;78:101907. Available from: https://www.sciencedirect.com/science/article/pii/S0955598621000224
18. Gabrani-Juma H, Clarkin OJ, Pourmoghaddas A, Driscoll B, Wells RG, deKemp RA, et al. Validation of a Multimodality Flow Phantom and Its Application for Assessment of Dynamic SPECT and PET Technologies. IEEE Trans Med Imaging. 2017;36(1):132–41.
19. Spectrum Dynamic Medical. Calculating Coronary Flow Reserve with CZT SPECT Fundamentals and Applications White Paper. 2017.
20. Leppo JA, Meerdink DJ. Comparison of the myocardial uptake of a technetium-labeled isonitrile analogue and thallium. Circ Res. 1989;65(3):632–9.
21. Yoshida K, Mullani N, Gould KL. Coronary flow and flow reserve by PET simplified for clinical applications using rubidium-82 or nitrogen-13-ammonia. J Nucl Med. 1996;37(10):1701–12.
22. Visser JJN, Busemann Sokole E, Verberne HJ, Habraken JBA, van de Stadt HJF, Jaspers JEN, et al. A realistic 3-D gated cardiac phantom for quality control of gated myocardial perfusion SPET: the Amsterdam gated (AGATE) cardiac phantom. Eur J Nucl Med Mol Imaging [Internet]. 2004;31(2):222–8. Available from: https://doi.org/10.1007/s00259-003-1352-5
23. Spectrum Dynamics Medical. Dynamic SPECT Case Study [Internet]. 2019 [cited 2021 Nov 1]. Available from: https://www.spectrum-dynamics.com/case-studies/dynamic-spect/dynamic-spect-case-study-patient-1/
24. Li P-C, Yeh C-K, Wang S-W. Time-intensity-based volumetric flow measurements: An in vitro study. Ultrasound Med Biol. 2002 Apr 1;28:349–58.
25. Kim E-J, Kim D-H, Lee SH, Huh Y-M, Song H-T, Suh J-S. Simultaneous acquisition of perfusion and permeability from corrected relaxation rates with dynamic susceptibility contrast dual gradient echo. Magn Reson Imaging [Internet]. 2004;22(3):307–14. Available from: https://www.sciencedirect.com/science/article/pii/S0730725X0400030X
26. Slomka PJ, Miller RJH, Hu LH, Germano G, Berman DS. Solid-state detector SPECT myocardial perfusion imaging. J Nucl Med. 2019;60(9):1194–204.

4

Marije E. Kamphuis
Henny Kuipers
Jacqueline Verschoor
Johannes C. G. van Hespen
Marcel J.W. Greuter
Riemer H.J.A. Slart
Cornelis H. Slump

EJNMMI Physics
volume 9, Article number: 31 (2022)

Development of a dynamic myocardial perfusion phantom model for tracer kinetic measurements

Abstract

Background Absolute myocardial perfusion imaging (MPI) is beneficial in the diagnosis and prognosis of patients with suspected or known coronary artery disease. However, validation and standardization of perfusion estimates across centers is needed to ensure safe and adequate integration into the clinical workflow. Physical myocardial perfusion models can contribute to this clinical need as these can provide ground truth validation of perfusion estimates in a simplified, though controlled setup. This work presents the design and realization of such a myocardial perfusion phantom and highlights initial performance testing of the overall phantom setup using dynamic single photon emission computed tomography.

Results Due to anatomical and (patho-)physiological representation in the 3D printed myocardial perfusion phantom we were able to acquire 22 dynamic MPI datasets in which ^{99m}Tc-labeled tracer kinetics was measured and analyzed using clinical MPI software. After phantom setup optimization, time activity curve analysis was executed for measurements with normal myocardial perfusion settings (1.5 mL/g/min) and with settings containing a regional or global perfusion deficit (0.8 mL/g/min). In these measurements, a specific amount of activated carbon was used to adsorb radiotracer in the simulated myocardial tissue. Such mimicking of myocardial tracer uptake and retention over time satisfactorily matched patient tracer kinetics. For normal perfusion levels, the absolute mean error between computed myocardial blood flow and ground truth flow settings ranged between 0.1–0.4 mL/g/min.

Conclusion The presented myocardial perfusion phantom is a first step towards ground truth validation of multimodal, absolute MPI applications in the clinical setting. Its dedicated and 3D printed design enables tracer kinetic measurement, including time activity curve and potentially compartmental myocardial blood flow analysis.

Background

Absolute, multimodal myocardial perfusion imaging (MPI) has become a clinically relevant research topic within the cardiac imaging community.[1,2] Especially for positron emission tomography (PET) the advantages of quantitative assessment in addition to qualitative, visual evaluation have been demonstrated.[3] Quantification of myocardial blood flow (MBF) and myocardial flow reserve provides a substantial advantage for diagnostic and prognostic evaluation of suspected or established coronary artery disease.[1–4] Currently these quantitative approaches are on the verge of being translated into the clinical workflow. In addition, similar approaches are also being explored for other imaging modalities, including computed tomography, magnetic resonance imaging, and single photon emission computed tomography (SPECT). However, further efforts are necessary to standardize measures across clinical centers, radiotracers, equipment, and software.[4]

Our ultimate aim is to realize reference standards for validation and harmonization of absolute, multimodal MPI applications using physical perfusion models, i.e., hardware perfusion phantoms. Even though such models will never fully mimic actual patient anatomy and (patho-)physiology, it allows study of dynamic MPI applications in a simplified, although controlled environment.[5] Several left ventricular phantoms have been described in literature, in which various physiological states of perfusion can be simulated under static conditions without flow.[6,7] In this, we observe an increasing trend in the use of 3D printing technology to obtain comprehensive representations of the heart.[8–10] Also, numerous perfusion phantoms have been proposed to facilitate physical flow standards for multimodal tissue perfusion imaging.[11–14] Nevertheless, current flow phantoms generally require in-house developed software for perfusion analysis. Evaluation of the entire absolute MPI application involves an adequate phantom to mimic flow dynamics on the one hand and to make clinical software believe the phantom resembles a human heart on the other (i.e., including anatomical representation).

This work describes an empirical approach towards the development of a dedicated myocardial perfusion phantom, and initial performance evaluation in dynamic SPECT-MPI. In this paper, we introduce a unique way of mimicking radiotracer uptake and retention in the myocardial tissue. The main design goals are:

1. to make the phantom compatible with clinical perfusion analysis software, and
2. to incorporate mimicking of tracer kinetics (i.e., up to the level of ground truth comparison with software derived MBF estimation).

Materials

The phantom setup has emerged from the redesign of a previously described myocardial perfusion phantom.[15] Phantom redesign concerned a novel way of tissue simulation, integration of coronary branches in the phantom model, and improved sealing to prevent leakage. In addition, an important adjustment is the transition from an open to a closed flow circuit.

Phantom design and realization

Figure 1 and 2 illustrate the designed and realized stationary myocardial perfusion phantom. All components were constructed with and designed for 3D printing (Objet260 Connex3, Stratasys Inc., Rehovot, Israel), enabling rapid prototyping. As visualized in the exploded view of **Figure 1**, the phantom assembly consists of three cylindrical parts made of rigid transparent photopolymer material (VeroClear, Stratasys Inc., Rehovot, Israel). These parts were secured by nylon screws with silicone seals in between for waterproofing. The entire phantom cylinder fits as insert in an anthropomorphic thorax phantom (QRM, PTW company, Freiburg, Germany) for realistic x-ray attenuation during imaging.[16]

The inner part includes the simulated left ventricular cavity (LVC) and surrounding myocardial tissue, while the two outer parts contain the branches to the myocardial tissue and the in- and outlet connections to the flow circuit. The LVC has an inner diameter of 38 mm and a length of 85 mm. The myocardium is mimicked by three identical segments, as depicted in **Figure 2C** and **D** by the three circumferential cutouts (1 cm thick) from base to apex. These segments correspond to the three main coronary territories, i.e., regions supplied by the left anterior descending coronary artery (LAD), right coronary artery (RCA), and the left circumflex coronary artery (LCX). Each myocardial segment has an in- and outlet at the base and apex, respectively.

Tissue mimicking

Distribution and retention of the injected radiotracer within the myocardial tissue is mimicked using sorption technology. Sorption occurs when a substance in a fluid is selectively transferred to insoluble, rigid particles.[17] In this way, the use of an adequate sorbent or mixture of sorbents can in essence mimic all kinds of desired radiotracer/contrast agent distribution and (temporary) trapping in a tissue perfusion phantom (our hypothesis). Commonly known adsorbents, i.e., activated carbon and zeolite, were in different quantities individually or as mixture (~50/50) blended with plastic beads before pouring into the empty myocardial segments. The plastic beads serve as tissue filling material. **Figure 2D** demonstrates the fabrication process of the myocardial tissue inlays. The tissue mimicking material was enclosed by a glass wool layer and 3D printed sieves to prevent the material from being carried into the flow circuit. As part of this study, the composition of the myocardial segments was further

explored empirically aiming to achieve adequate myocardial uptake of ^{99m}Tc-labeled pharmaceuticals for dynamic MPI-SPECT (see phantom measurements).

Phantom flow setup

For several reasons the phantom flow setup consists of a closed loop flow circuit. In this way, water can be circulated with the same flow over time and the circuit will not drain when turning the pump off in between measurements.

Tap water can be pumped at a continuous flow from the reservoir towards the cardiac flow phantom using an external pump (Low voltage impeller pump, Barwig 02, Germany). Next, a radiotracer bolus can be administered via a clinical contrast injector (by Luer Lock connection). After injection, the radiotracer bolus is diluted and flows

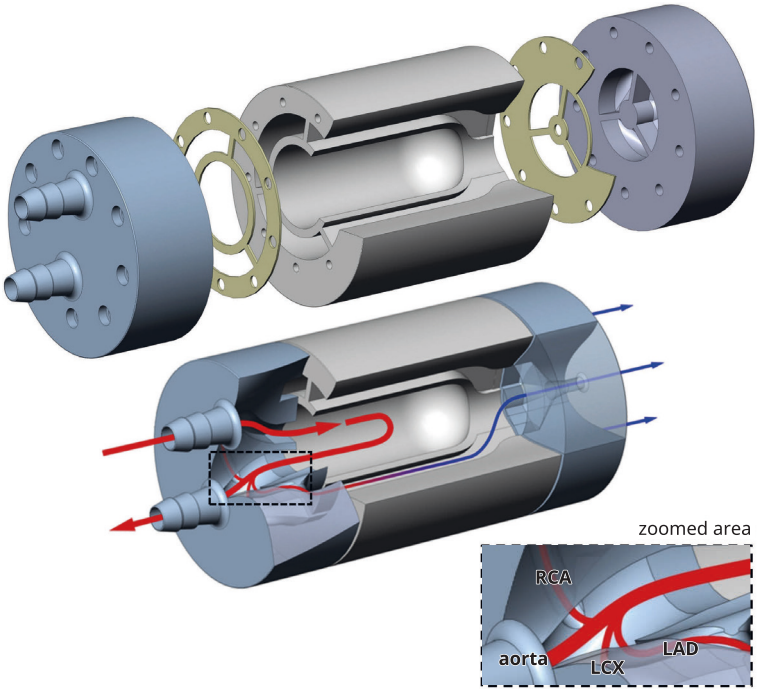

Figure 1 Exploded view (top) of phantom design and tailored cross-section (bottom) to illustrate inner phantom connections. The arrows indicate flow direction and magnitude, and its color differentiates between arterial input (red) and venous output (blue). The middle phantom part comprises the simulated left ventricular cavity and three surrounding myocardial segments. The two outer parts contain the in- and outlet connections to the flow circuit and the internal branches to the segments. These branches correspond to the main coronary arteries, i.e., the left anterior descending coronary artery (LAD), right coronary artery (RCA) and left circumflex coronary artery (LCX). The phantom parts are fastened together with nylon screws whereby silicone seals are placed in between the parts for waterproofing.

through the LVC where it is fully mixed with the water present in the LVC. The LVC outlet connects to the reservoir again but branches first to three myocardial segments. The segment outlets connect separately to the reservoir as well. The inserted flow sensors measure volume flux through the LVC (UFo8B, ultrasonic flowmeter, Cynergy 3, United Kingdom) and myocardial segments (FCH-m-POM-LC, low flow turbine flowmeter, B.I.O-TECH, Germany). Four adjustable resistances can set the flow ratio between the returning parallel circuits. Hence, it becomes feasible to create a perfusion deficit in one or multiple myocardial segments within the phantom by (partially) closing one or multiple tap(s). A pressure sensor (40PC series, Honeywell Inc., Freeport, Illinois) verifies whether the pump is still operating in the desired pressure range (kept below 1.0 bar). Pump steering and real-time sensor readout (sample frequency of 1 Hz) is achieved using in-house built hardware and software.[18] The latter is used to set the resistances accordingly before starting a measurement.

Finally, custom-built filters are positioned in all returning tubing to extract radioactive material from the water before re-entering the reservoir. In this way, controlled first pass radiotracer kinetics is envisaged without the necessity of a rather unpractical open loop circuit design. For example, just a single phantom measurement with an open loop configuration can easily produce tens of litres of radioactive wastewater (given a cardiac output of about 4 L/min), while the current setup reuses a vol-

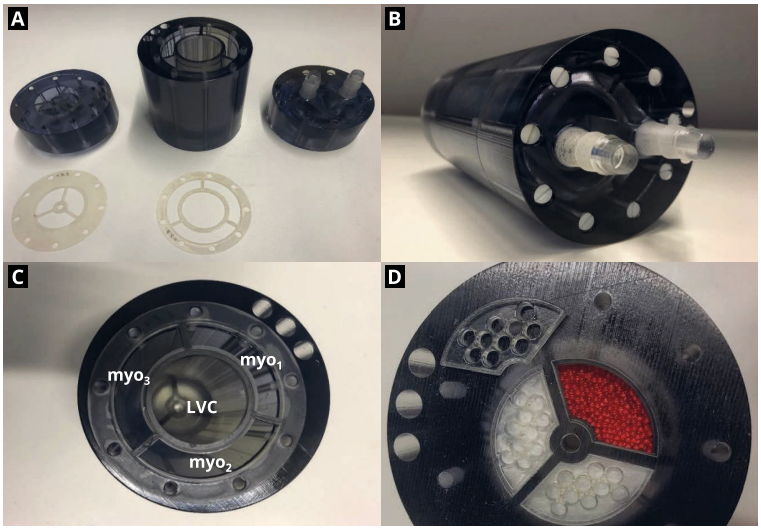

Figure 2 Overview of the realized myocardial perfusion phantom. (**A**) displays the individual 3D printed parts and silicone seals. In (**B**) all pieces are assembled and secured by nylon screws (2 × 9). (**C**) The left ventricular cavity (LVC) and the three myocardial segments (myo1–3) are indicated in this cross-section. (**D**) demonstrates fabrication of the myocardial inlays. The tissue mimicking material was enclosed by a glass wool layer and a 3D printed sieve before assembling all pieces.

Table 1 Measurement variables.

ID	Phantom variables						Flow circuit variables					
	s_{MYO1}	$m_{s,MYO1}$ [g]	s_{MYO2}	$m_{s,MYO2}$ [g]	s_{MYO3}	$m_{s,MYO3}$ [g]	Φ_{AI} [L/min]	Φ_{MYO1} [mL/min]	Φ_{MYO2} [mL/min]	Φ_{MYO3} [mL/min]	P [%]	filters y/n
D1#1	AC + Z	30	AC + Z	15			4.5	100	100	100	6.7	n
D1#2	AC + Z	30	AC + Z	15			4.5	100	100	100	6.7	n
D2#3	AC + Z	30	AC + Z	15			4.0	100	100	100	7.5	y
D2#4	AC + Z	30	AC + Z	15			4.0	100	100	100	7.5	y
D2#5	AC + Z	30	AC + Z	15			4.0	50	100	100	6.3	y
D2#6	AC + Z	30	AC + Z	15			4.0	50	125	125	7.5	y
D3#7	Z	7	Z	7	Z	7	4.0	80	80	80	6.0	y
D3#8	Z	7	Z	7	Z	7	4.0	80	40	80	5.0	y
D3#9	Z	7	Z	7	Z	7	4.0	80	0	80	4.0	y
D3#10	Z	7	Z	7	Z	7	4.0	80	40	80	5.0	y
D4#11	AC + Z	20	AC + Z	20	AC + Z	20	4.0	80	80	80	6.0	y
D4#12	AC + Z	20	AC + Z	20	AC + Z	20	4.0	80	80	80	6.0	y
D4#13	AC + Z	20	AC + Z	20	AC + Z	20	4.0	40	40	40	3.0	y
D4#14	AC + Z	20	AC + Z	20	AC + Z	20	4.0	80	0	80	4.0	y
D5#15	AC	7	AC	7	AC	7	4.0	80	40	80	5.0	y
D5#16	AC	7	AC	7	AC	7	4.0	40	80	40	4.0	y
D5#17	AC	7	AC	7	AC	7	4.0	40	40	40	3.0	y
D5#18	AC	7	AC	7	AC	7	4.0	80	80	80	6.0	y
D6#19	AC	7	AC	7	AC	7	4.0	40	40	40	3.0	y
D6#20	AC	7	AC	7	AC	7	4.0	80	80	80	6.0	y
D6#21	AC	7	AC	7	AC	7	4.0	80	80	80	6.0	y
D6#22	AC	7	AC	7	AC	7	4.0	40	80	80	5.0	y

D = day; *s* = sorbent; *m* = mass; AC = activated carbon; Z = zeolite; MYO = myocardial segment; AI = arterial input; Φ = flow; *P* = perfusion rate.

ume of about 5 L for multiple measurements. Two sizes of silicone tubing ($\varnothing_{inner}$ = 10 and 5 mm) are used to connect the individual components in the setup, distinguishing between higher and lower flow values.

Methods

Phantom measurements

In total, twenty-two phantom measurements were executed spread over six, non-consecutive measurement days. **Table 1** provides an overview of the phantom and flow circuit variables in our measurement protocol. The measurements performed in this

study were aimed for performance evaluation and optimization. As can be seen, the first fourteen measurements were used to optimize the overall setup and the remaining eight measurements were executed using the same phantom configuration. Results from the optimized setup (e.g., comprising an adequate myocardial tissue configuration) were used for further data analysis.

Performance was evaluated regarding to: 1) software compatibility, and 2) mimicking of radiotracer kinetics. Software compatibility was investigated by loading all phantom image data into the clinical software. We have verified whether the software would consider the phantom as a human heart and whether all processing and analysis steps can be performed sufficiently. Mimicking of radiotracer uptake/retention was explored empirically. We have filled the myocardial segments with two types of sorbents, namely activated carbon, and zeolite (SuperFish, biological filter media, Aquadistri, Klundert, The Netherlands), in different compositions (see **Table 1** phantom variables). Regional and global perfusion deficit was mimicked by halving the standard volume flux of 80 mL/min, representing normal perfusion, in one or all three myocardial segments (see **Table 1** flow circuit variables).

Myocardial perfusion imaging

Phantom measurements included dynamic imaging of the flow of a radiotracer bolus through the LVC and myocardial segments over time. **Figure 3B** presents an overview of the experimental setup during performance testing with a clinical cadmium-zinc-telluride SPECT system (D-SPECT, Spectrum Dynamics, Caesarea, Israel). The cardiac flow and thorax phantom were positioned in the scanner's field of view in a standard way. All flow circuit variables were set prior to dynamic MPI acquisition and were kept the same for the entire scanning period. The clinical dynamic MPI acquisition protocol consisted of two 6 min dynamic scans, namely a rest scan followed by a stress scan, respectively. The phantom cannot distinguish between these patient related physiological states, though the additional scan can be used for another purpose. During the rest scan, no radiotracer was administered. This baseline scan was solely used for background subtraction of previously trapped radiotracer. The subsequent dynamic stress scan started just before injection of the radiotracer bolus. 1.5 mL of 500 MBq [^{99m}Tc]Tc-pertechnetate solution was injected by a clinical contrast injector (Mark V Provis, Medrad, Warrendale, United States) at 1.0 mL/s, followed by a 40 mL saline flush.

After scanning, the orientation of the imaged heart contours was manually adjusted using vendor software. We applied the same rotation angles for all scans — i.e., 0° along the sagittal axis (SA) and 90° along the vertical long axis (VLA) — since the phantom was positioned under the scanner in a standard way. The list-mode image data was re-binned into 32 frames consisting of 21 frames of 3 s, 4 frames of 9, 15, 21 and 27 s, and 7 frames of 30 s. An ordered subset expectation maximization tech-

nique was used for reconstruction of the dynamic image acquisitions with 4 iterations and 32 subsets.[19] Detailed information on the clinical workflow with a D-SPECT scanner can be found in published studies.[20,21]

Image processing

Resulting dynamic image datasets were processed and analyzed with clinical software (Corridor4DM software, INVIA Medical Imaging Solutions, United States). These images contained a total number of pixels of 9216 (96 × 96) with a pixel size of

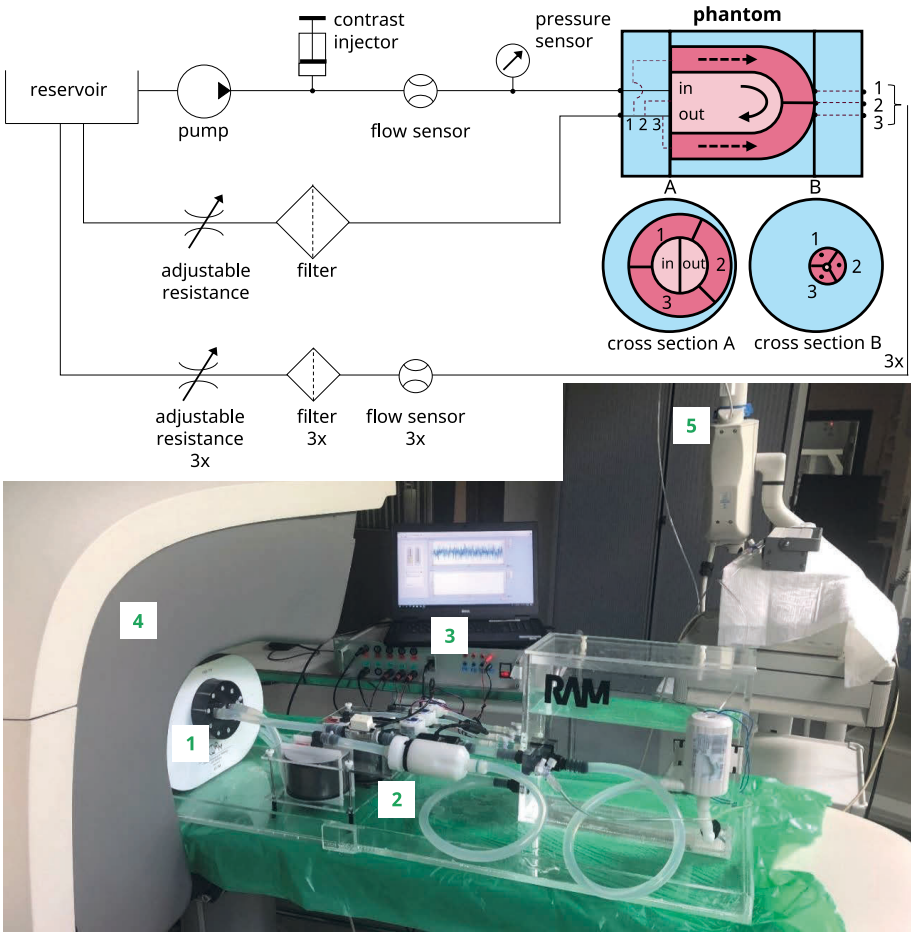

Figure 3 Flow circuit diagram of the myocardial perfusion phantom setup (top) and subsequent experimental setup during performance testing (bottom). The numbers represent the following components: **1.** the myocardial perfusion (and thorax) phantom, **2.** its accompanying flow circuit, **3.** in-house built hardware and software for pump steering and sensor readout **4.** dynamic SPECT scanner, and **5.** the contrast injector.

2.26 mm × 2.26 mm. In this software, myocardial areas were estimated from summed myocardial image cross-sections.[19] We indicated preferred dimensions of the myocardial areas in a way they would match in length and width with all phantom measurements. The software included these dimensions subsequently in its calculation of the myocardial contours. The contoured time-lapse image data was displayed as cross-sections along the short axis (SA) (from base to apex), horizontal longitudinal axis (HLA) and vertical longitudinal axis (VLA). Summed myocardial images were also captured in a polar map.

Based on these contoured images, regions of interest (ROIs) were drawn automatically at the center of the LV base (see default size green box in Fig. 4 example 1) and within the myocardial surfaces. We used the American Heart Association (AHA) 17-segment heart model for standardized segmentation of the myocardial surfaces.[22] In this heart model, segment 1,2,7 and 8 corresponded to the mimicked LAD region, segment 3,4,9 and 10 to the RCA region and 5,6,11, and 12 to the LCX region. When the image data was correctly aligned, these displays matched with the three myocardial segments within the TMP phantom. Segments 14–17 were excluded in this analysis as the phantom does not mimic the apex.

In the vendor software, the average measured activity over time within these ROIs was displayed in time activity curves (TAC). Two arterial input functions (AIFs) and multiple tissue response functions (TRFs) were acquired per phantom measurement since each measurement comprised of two dynamic scans (rest and stress). Background activity, as present in the TACs derived from the rest scans, was then subtracted from the stress scans using a standard tool in the software. The resultant TACs served as input for myocardial blood flow estimation.

Myocardial blood flow estimation

Myocardial perfusion or myocardial blood flow (MBF) is generally expressed as the flow rate normalized by the mass of the tissue volume of interest (in mL/min/g). The blood flow model applied in the clinical MBF analysis software was a net retention model proposed by Leppo et al.[23] and Yoshida et al.[24] The following modified equation was used to calculate the retention rate (R) of tracer in the myocardium in mL/g/min. This myocardial uptake was expressed as the product of the MBF (mL/g/min) and the extraction fraction (E):

$$R = \mathrm{MBF} \times E = \frac{\frac{1}{\mathrm{PV}(t_3 - t_2)} \int_{t_2}^{t_3} \left(P(t) - S_m C_a(t)\right) dt}{\mathrm{CF} \int_0^{t_1} \left(C_a(t) - S_b P(t)\right) dt}$$

In this, $C_a(t)$ and $P(t)$ corresponded to the average arterial and tissue tracer concentration over time, the AIF and TRF respectively. Integration limit t_1 denoted the end of the blood pool phase and was set by default to 60 s. t_2 and t_3 denoted integration

limits of the average tissue activity, which was set to 60 and 120 s, respectively. Several predefined corrections by the software were applied to the data to compute absolute flow. Firstly, the acquired myocardial counts were corrected for partial volume losses using a recovery coefficient (PV) for the myocardium (PV = 0.63). Partial volume effects regarding measurement in the blood pool activity were neglected, therefore the cross-calibration factor (CF) was 1. Finally, theoretically computed spill over fractions S_m and S_b were set at 0.4 and 0. These fractions corrected for spill over from the blood pool activity to the myocardium and vice versa.[25–27]

Data analysis

All visual MPI data was analyzed in the clinical software (see image processing). Derived TACs were exported to Matlab (MathWorks, R2021b) for further analysis. In this, all TACs were first normalized based on their injected activity (ranged between 468–551 MBq, normalized to 500 MBq). Then linear interpolation was performed prior to peak alignment of the AIFs. Peak locations were determined using a spline interpolation technique. The aligned time scale was then also applied to the TRF data. Subsequently, the mean and standard deviation (SD) of corresponding AIFs and TRFs were plotted in combination with the mean and SD of specified area under the curves (AUCs). The AUCs comprised of the integration limits as denoted by the used blood flow model. Myocardial blood flow estimation by the clinical software was compared to ground truth volume flux measurement and visualized in a polar map. In this, the set volume flux of 80 mL/min went through a tissue volume of interest of

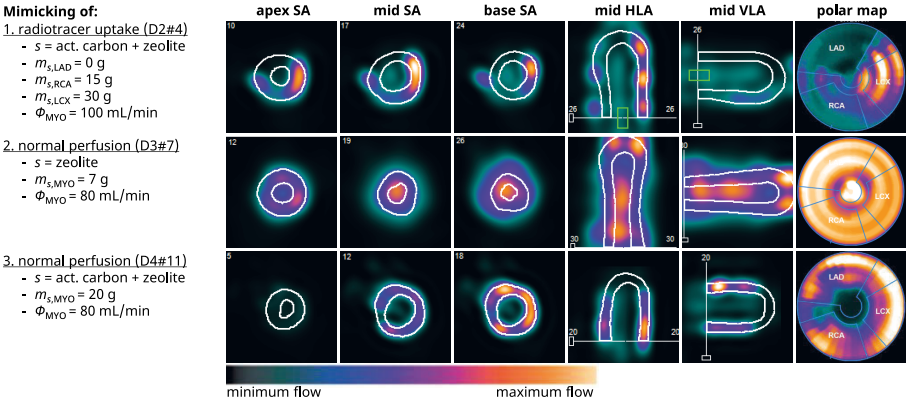

Figure 4 A selection of seven myocardial perfusion imaging series aiming to highlight the overall phantom development and evaluation process. The image cross-sections and polar maps present the accumulated radiotracer distribution inside the phantom, which is a static representation of a dynamic measurement. Note that the relative color scale is determined by default for each individual measurement and is therefore not linked between measurements. In these measurements, mimicking of radiotracer uptake, normal perfusion and perfusion deficit was examined using different parameter settings. *(cont.▶)*

53 ± 2 mL. Assuming a tissue density of 1 g/mL, this resulted in a ground truth, normal myocardial blood flow of 1.5 mL/g/min.

Results

A selection of seven myocardial perfusion image series is displayed in **Figure 4** to highlight the overall phantom development and evaluation process. In 16 out of 22 phantom measurements, a similar orientation and alignment of the phantom based heart contours were obtained. Semi-automatic heart contour recognition failed in the experiments where sorption of radiotracer was lacking. The first example MPI series illustrate that the more sorbent utilized for myocardial segment fabrication, the more radiotracer trapping occurred. In the second example, only zeolite was used as sorbent, which led to less overall accumulated adsorption of radiotracer compared to a similar phantom measurement executed with activated carbon (see example 4–7). After thirteen setup optimization measurements, 7 g of activated carbon was found to be sufficient for the manufacturing of each myocardial segment, which was then applied in further phantom testing and evaluation.

Mimicking of normal perfusion, regional and global perfusion deficit was illustrated in examples 4–7. The clinical software could not detect the heart contours of a simulated global perfusion deficit. A local perfusion deficit was evidently visible in the MPI

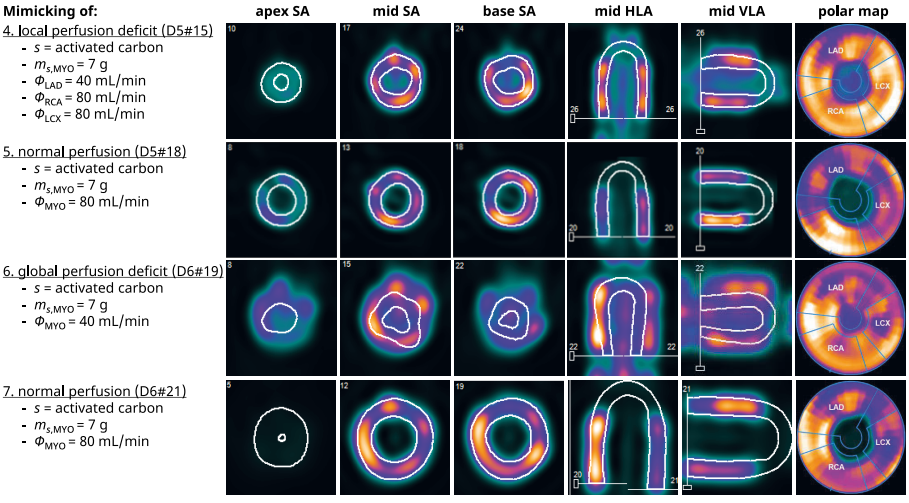

Figure 4 (cont.) Settings include the type and mass of sorbent (*s*) utilized to mimic myocardial tissue, and the amount of volume flux (Φ) directed through the myocardial segments (MYO). D2#4 stands for the measurement day and number, respectively. LAD = left anterior descending coronary artery, RCA = right coronary artery, LCX = left circumflex coronary artery, SA = short axis, HLA = horizontal long axis, and VLA is vertical long axis.

series, especially if it was the first measurement of the day and no radiotracer activity had yet accumulated in the segments of a previous measurement.

TACs derived from these dynamic MPI series are summarized in **Figure 5**. The mean AIF and SD of 22 measurements was plotted, together with its mean AUC and SD. A similar analysis was shown for the TRFs that corresponded to a volume flux of 40 and 80 mL/min. In addition, a noteworthy, increasing tracer activity was visible in the TRFS over time.

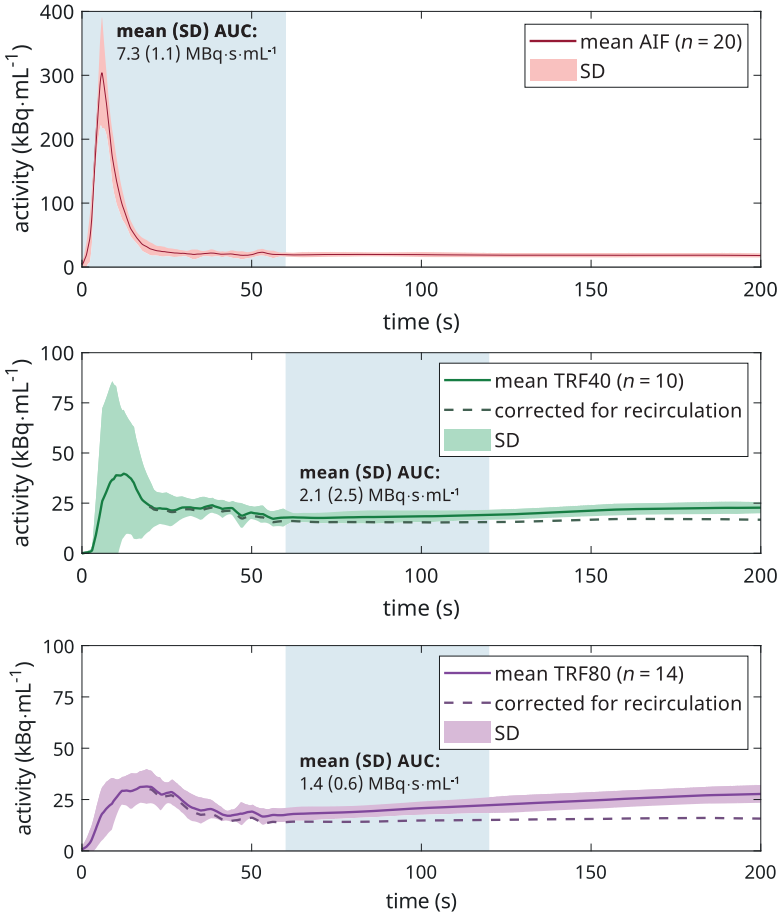

Figure 5 Time activity curves derived from phantom measurements. The mean arterial input function (AIF) and tissue functions (TRFs) of *n* measurements were plotted together with their standard deviation (SD). TRF analysis distinguished between myocardial segment flow settings of 40 and 80 mL/min. The AUCs within the indicated blue regions served as input for myocardial blood flow estimation. The dashed lines in the TRFs suggest how the curves would look when corrected for radiotracer recirculation.

An absolute value for segmental MBF was estimated for phantom measurements with a volume flux of 80 mL/min. These preliminary results are plotted in **Figure 6**. As shown, the mean MBF for the twelve heart segments ranged between 0.7–2.3 mL/g/min. The absolute mean error between the computed MBF and ground truth was 0.4, 0.1 and 0.1 mL/g/min for the overall mimicked LAD, RCA and LCX region, respectively. Video 1 (can be found in the **Supplement**) illustrates the software display containing all analyses for measurement sixteen, including the time-lapse MPI data, TACs, and regional MBF estimates.

Discussion

This experimental work reflects on the design and realization of the TMP phantom, and on initial performance testing in dynamic SPECT-MPI. Performance testing was used to examine whether the set design goals were achieved. The first goal was to develop a phantom that is applicable/compatible with clinical MPI software. The second goal was that within the phantom, tracer kinetics can be mimicked up to the level of ground truth comparison with software derived MBF estimation. Results attained in both areas are now further described.

Software compatibility

Compatibility was verified by going through all processing and analysis steps in the clinical software using the phantom data. It was possible to load all dynamic phantom MPI data into the 4DM program. In sixteen out of 22 measurements (73 %)

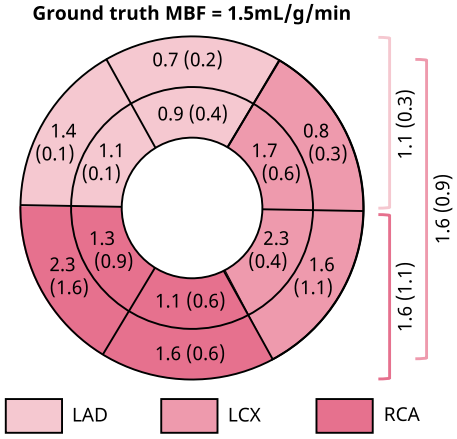

Figure 6 Preliminary results of computed MBF by clinical software (presented in polar map) compared to ground truth phantom flow measurement. The presented mean values and standard deviations (SDs) are in mL/g/min. The inner segments of the plot are left blank as the phantom does not mimic the apex. On the right, the mean MBF estimates and SDs are listed for the mimicked regions supplied by the left anterior descending coronary artery (LAD), the left circumflex coronary artery (LCX) and right coronary artery (RCA).

the myocardial contours were drawn correctly, which also implied that the delineated coronary regions and twelve heart model segments matched with the phantom orientation. Semi-automatic heart contour recognition failed in the measurements where sorption of radiotracer was lacking, hence mistaking accumulated tracer activity in the LVC for myocardial tissue (see example 1, 2 and 6 in Fig. 4). Contour delineation sometimes failed (partially) in cases where local and global perfusion deficits were mimicked. In general, inadequate delineation of poorly perfused tissue is also observed in clinical practice. However, the chosen 40 mL/min indicates a severe perfusion deficit. A global perfusion limitation of this magnitude is not patient realistic and was therefore not adequately analyzed by the software.

Hereafter, TAC analysis took place. A background subtraction is necessary to correct for already present radiotracer activity from previous measurement(s). A one-day clinical protocol for dynamic rest and stress MPI also requires this software feature for the same reason.[28] Unfortunately, the usefulness of this clinical feature could not be further examined because of a small remaining percentage of recirculating tracer over time. The mean TRFs in **Figure 5** highlight this effect, whereby a suggestion has been made on the expected course in the absence of tracer recirculation (assuming a linear increase starting from ~20 s). This is also a partial explanation for the relatively high SD observed in similar / reproducible TACs. The highest SDs were observed in the first 60 s of the mean TRF40 (Fig. 4). This variation is the result of misalignment of the heart contours, hence mistaking accumulated tracer activity from the AIF for myocardial tracer activity.

Despite of the recirculation drawback, we continued our analysis and showed how ground truth comparison between measured volume flux of normal perfusion (flow sensor readout) and software derived MBF estimation could be envisioned using the phantom setup (**Figure 6**). Yet, before such data can be interpreted, the measurement setup must be further optimized first.

Overall, compatibility with other commercial MPI analysis software is expected as well, as the phantom resembles a human heart sufficiently. However, the results in MBF quantification may differ.[29] This is one of the reasons why it is important to include various software packages in future research, for example to define similarities, differences, and boundary conditions (e.g., by exposing the software to phantom measurements covering the full range of myocardial perfusion levels).

Mimicking tracer kinetics

Now we have shown that the clinical software can be successfully applied for evaluation purposes of the phantom setup, the next step is to evaluate the extent to which the TMP phantom can mimic the desired tracer kinetics. This study makes use of sorbents, whose mode of action is very similar to the physiological processes of

(temporary) tracer retention in the myocardial tissue. The first pass extraction fraction of ^{99m}Tc-labeled MPI tracers is around 55–65 % of the total injected dose, and for a small fraction (1–5 %) irreversibly trapped in myocardial tissue.[30] As shown in example 1 in **Figure 5**, the degree of simulated radiotracer trapping depends on the type and amount of sorbent used. Activated carbon seems to be a suitable sorbent for this tracer application, as it also shows irreversible trapping. When using zeolite, we have observed reversible trapping, which may indicate that the zeolite acts as an ion exchanger instead of an adsorbent. Remarkably, there is no homogeneous distribution of accumulated tracer within the myocardial segments. This may be because the sorbents used are granulates with dimensions up to ~5 mm diameter. The empirically determined sorbent composition for adequate myocardial uptake simulation (7 g of activated carbon) covered only a small part of the total segment filling and was supplemented with plastic beads. We aim to achieve a better distribution of sorbent within the myocardial segments in future phantom research.

To our knowledge, this tracer specific way of tissue mimicking has not been described before in the literature. Most perfusion phantoms (commercial and research oriented) use aligned porous fibers or 3D printed capillaries instead.[11,14,31,32] In terms of transport characteristics, these fiber phantoms are solely based on convection and diffusion processes. Porous, capillary media can slow down processes like tracer retention but cannot realize actual trapping. This phantom has the potential to exert more influence on mimicking perfusion characteristics as described in single- and multi-tissue compartment models. In line with this, we have observed satisfying similarities when comparing our phantom data with patient data (see **Figure 7**). The visible differences come from spillover effects in the patient data (in the AIF at $t \approx 30$ s and in the TRF at $t \approx 15$ s) and the previously discussed tracer recirculation in the phantom TRFs. The latter results in a slightly rising phantom TRF over time, instead of a flattened line as observed in the patient example. The observed stronger increase in measured tracer activity in the patient TRF, including a higher peak activity, might also occur due to a higher flow. Extensive comparison with patient data was beyond the scope of this study but is an important component for future validation of the TMP phantom.

Study limitations

The main limitation of this study was that the recirculation filters did not yet result in total extraction of tracer from the fluid circuit before recirculation. In first tests, the filters worked properly, thus we no longer changed this for follow-up measurements. Afterwards it turned out to be somewhat insufficient, which had consequences on the reliability and reproducibility of the results. A new filter design will be incorporated in future phantom measurements. A second limitation of this study is that we used [^{99m}Tc]Tc-pertechnetate (easy accessibility), while in patient MPI studies radio-

active technetium is labeled with tetrofosmin or sestamibi. A different molecule implies different sorption characteristics. Prior to these phantom measurements, we studied the effect-size of this in adsorption column experiments. The differences seem small, though for future phantom validation purposes we intend to utilize the clinically used radiotracers. Of note, perfusion deficits simulating ischemia or infarction were not implemented in the current phantom set-up. This issue needs to be addressed in a next phantom iteration. Finally, it could be mentioned why we started phantom evaluation using SPECT, while PET-MPI is considered the clinical standard. This was due to easy accessibility.

Towards phantom application

Now that the possibilities of this phantom in simulating tracer kinetics have been explored, and initial phantom measurements have been successfully executed in dynamic SPECT-MPI, a logical next step is to optimize and validate the setup for radiotracer specific MBF estimation. In addition, the phantom setup can be extended and tested for multimodal, absolute MPI applications. In phantom validation it is important to verify whether choices and simplifications made in the phantom design are justified for the intended application. For example, the decision was made to first realize a stationary flow phantom. It can be argued that current phantom design is overly simplified due to missing cardiac contraction and respiratory motion dynamics. However, an outstanding measurement reproducibility is preferred over the degree of realism, especially since it concerns early-stage development of a validation phantom. This simplification could have presented misleading results in terms of an underestimated quantification accuracy. A possible solution is to include a motion inaccuracy factor (to be determined from literature) during future phantom application. Moreover, even without these motion dynamics incorporated, the phantom has relevant application domains, e.g., in studying the effect of patient size on MBF computation independently from motion influences. Another simplification

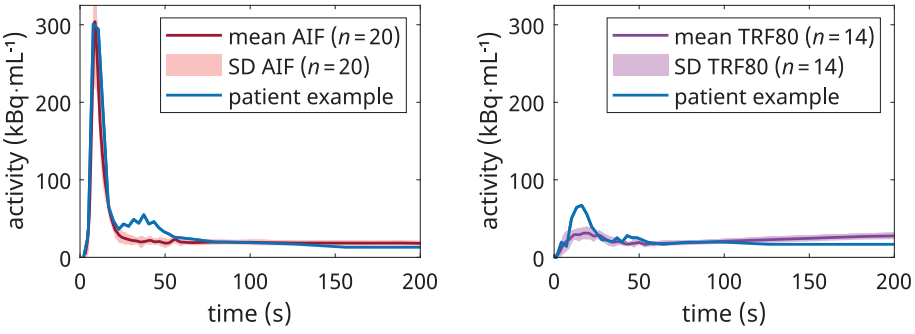

Figure 7 Time activity curve comparison of average phantom data (±SD) with patient example (derived from 33). AIF = arterial input function, TRF80 = tissue response function at a volume flux of 80 mL/min.

concerns that we excluded mimicking of the left ventricular apex. Phantom design incorporates three identical myocardial regions to have similar flow dynamics and tracer kinetics present in all three regions. This appearance mismatches clinical delineation of coronary regions and heart segments, as the apex falls entirely within the LAD region. We performed only TAC and MBF analysis in the more basal heart segments, and disregarded apex simulation, to prevent misleading data analysis. In future research we do strive for phantom redesign in which the apex is incorporated.

As a final remark, large SDs were observed for the mean TACs, mean AUCs and mean MBFs. On the one hand, we expect to be able to maximize measurement accuracy and precision by further optimizing the phantom setup (based on the findings obtained in this study). On the other hand, it may also be the case that part of these obtained deviations fall within the uncertainty of the measurement technique used. Whether absolute SPECT-MPI is accurate and precise enough is a prime example of what we can study further in such controlled phantom environment.

Conclusion

The presented myocardial perfusion phantom is a first step towards ground truth validation of and harmonization between multimodal, absolute MPI applications in the clinical setting. The set phantom design goals have been largely achieved. Due to its dedicated and 3D printed design we have facilitated tracer kinetic phantom measurements, including TAC and potentially compartmental MBF analysis using commercially available software.

Supplement

Video: Software display containing all analyses for measurement sixteen, including the time-lapse MPI data, TACs, and regional MBF estimates.

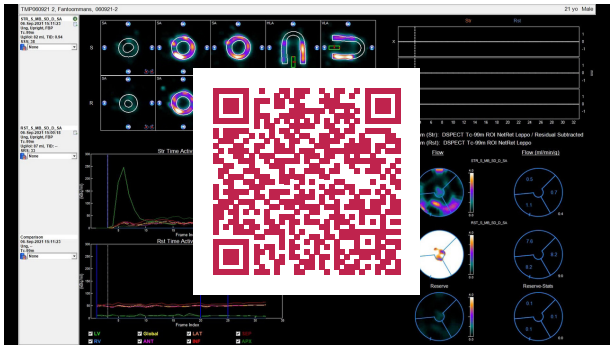

https://ejnmmiphys.springeropen.com/articles/10.1186/s40658-022-00458-y#Sec19

References

1 Dewey M, Siebes M, Kachelrieß M, Kofoed KF, Maurovich-Horvat P, Nikolaou K, et al. Clinical quantitative cardiac imaging for the assessment of myocardial ischaemia. Nat Rev Cardiol [Internet]. 2020;17(7):427–50. Available from: http://dx.doi.org/10.1038/s41569-020-0341-8

2 Sciagrà R, Lubberink M, Hyafil F, Saraste A, Slart RHJA, Agostini D, et al. EANM procedural guidelines for PET/CT quantitative myocardial perfusion imaging. Eur J Nucl Med Mol Imaging. 2021;48(4):1040–69.

3 Cho SG, Lee SJ, Na MH, Choi YY, Bom HHS. Comparison of diagnostic accuracy of PET-derived myocardial blood flow parameters: A meta-analysis. J Nucl Cardiol [Internet]. 2020;27(6):1955–66. Available from: https://doi.org/10.1007/s12350-018-01476-z

4 Murthy VL, Bateman TM, Beanlands RS, Berman DS, Borges-Neto S, Chareonthaitawee P, et al. Clinical quantification of myocardial blood flow using PET: Joint position paper of the SNMMI cardiovascular council and the ASNC. J Nucl Med. 2018;59(2):273–93.

5 Van Meurs W. Modeling and simulation in biomedical engineering - Applications in cardiorespiratory physiology. Penn M, Mulcahy M, Fogarty DE, McLaughlin D, editors. The McGraw-Hill Companies; 2011. ix–193.

6 Visser JJN, Sokole EB, Verberne HJ, Habraken JBA, Van De Stadt HJF, Jaspers JEN, et al. A realistic 3-D gated cardiac phantom for quality control of gated myocardial perfusion SPET: The Amsterdam gated (AGATE) cardiac phantom. Eur J Nucl Med Mol Imaging. 2004;31(2):222–8.

7 Data Spectrum Corporation. Cardiac Insert [Internet]. Product catablogues. 2001 [cited 2021 Oct 28]. p. 1–40. Available from: http://www.orion-france.com/pdf/catalogues/Orion_Data_Spectrum.pdf

8 Grice J, Green S, Yuhas A. An Improved 3D Printed Cardiac Phantom. J Nucl Med [Internet]. 2020 May 1;61(supplement 1):391 LP – 391. Available from: http://jnm.snmjournals.org/content/61/supplement_1/391.abstract

9 Abdullah K, McEntee M, Reed W, Kench P. Development of an organ-specific insert phantom generated using a 3D printer for investigations of cardiac computed tomography protocols. J Med Radiat Sci. 2018 Apr 30;65.

10 Jin Z, Li Y, Yu K, Liu L, Fu J, Yao X, et al. 3D Printing of Physical Organ Models: Recent Developments and Challenges. Adv Sci [Internet]. 2021 Sep 1;8(17):2101394. Available from: https://doi.org/10.1002/advs.202101394

11 Kok G, Pelevic N, Chiribiri A, Milidonis X, Nazir M, Capstick M, et al. A calibrated physical flow standard for medical perfusion imaging. Flow Meas Instrum. 2021;78(February):0–5.

12 Sun Nuclear Corporation. CT Perfusion Phantom [Internet]. 2021 [cited 2021 Oct 28]. Available from: https://www.sunnuclear.com/products/ct-perfusion-phantom

13 Driscoll B, Keller H, Jaffray D, Coolens C. Development of a dynamic quality assurance testing protocol for multisite clinical trial DCE-CT accreditation. Med Phys [Internet]. 2013;40(8):081906. Available from: http://www.ncbi.nlm.nih.gov/pubmed/23927320

14 Kamphuis ME, Greuter MJW, Slart RHJA, SLump CH. Quantitative imaging: systematic review of perfusion/flow phantoms. Eur Radiol Exp.

15 Kamphuis ME, de Vries GJ, Verschoor J, Slump CH. Development of a dedicated 3D printed myocardial perfusion phantom: Proof-of-concept in dynamic SPECT. Med Biol Eng Comput.

16 QRM GmbH. Anthropomorphic Thorax Phantom [Internet]. [cited 2021 Oct 28]. Available from: https://www.qrm.de/en/products/thorax-phantom/?type=3451&downloadfile=1720&cHash=27fd6589a8800d48c23d0653841d8d7a

17 Seader JD, Henley EJ, Roper DK, editors. Adsorption, Ion Exchange, Chromatography, and Electrophoresis. In: Separation Process Principles: Chemical and Biochemical Operations. 3rd ed. John Wiley & Sons; 2010.

18 de Vries GJ. Development of a myocardial perfusion phantom [Internet]. Enschede; 2019. Available from: https://essay.utwente.nl/78887/1/deVries_MA_EEMCS.pdf

19 Spectrum Dynamic Medical. Calculating Coronary Flow Reserve with CZT SPECT Fundamentals and Applications White Paper. 2017.

20 Johnson RD, Bath NK, Rinker J, Fong S, St James S, Pampaloni MH, et al. Introduction to the D-SPECT for Technologists: Workflow Using a Dedicated Digital Cardiac Camera. J Nucl Med Technol. 2020;48(4):297–303.

21 Hyafil F, Gimelli A, Slart RHJA, Georgoulias P, Rischpler C, Lubberink M, et al. EANM procedural guidelines for myocardial perfusion scintigraphy using cardiac-centered gamma cameras. Eur J Hybrid Imaging. 2019;3(1).

22 Cerqueira MD, Weissman NJ, Dilsizian V, Jacobs AK, Kaul S, Laskey WK, et al. Standardized myocardial segmentation and nomenclature for tomographic imaging of the heart. J Cardiovasc Magn Reson. 2002;4(2):203–10.

23 Leppo JA, Meerdink DJ. Comparison of the myocardial uptake of a technetium-labeled isonitrile analogue and thallium. Circ Res. 1989;65(3):632–9.

24 Yoshida K, Mullani N, Gould KL. Coronary flow and flow reserve by PET simplified for clinical applications using rubidium-82 or nitrogen-13-ammonia. J Nucl Med. 1996;37(10):1701–12.

25 Hutchins GD, Caraher JM, Raylman R. Strategy for Minimizing Resolution Distortions in Quantitative MyocardialPET Studies. J Nucl Med. 1992;33(6):1243–50.

26 Renaud JM, Dasilva JN, Beanlands RSB, Dekemp RA. Characterizing the normal range of myocardial blood flow with 82rubidium and 13N-ammonia PET imaging. J Nucl Cardiol. 2013;20(4):578–91.

27 Tsuchida T, Yonekura Y, Takahashi N, Nakano A, Lee JD, Sadato N, et al. A trial for the quantification of regional myocardial blood flow with continuous infusion of Tc-99m MIBI and dynamic SPECT. Ann Nucl Med. 1999;13(1):61–4.

28 Santos A, Lemos Pereira E. SPECT and SPECT/CT Protocols and New Imaging Equipment. In: Ryder H, Testanera G, Veloso Jeronimo V, Vidovic B, editors. Myocardial perfusion imaging, a technologist's guide. EANM; 2014. p. 54–61.

29 Monroy-Gonzalez AG, Juarez-Orozco LE, Han C, Vedder IR, García DV, Borra R, et al. Software reproducibility of myocardial blood flow and flow reserve quantification in ischemic heart disease: A 13N-ammonia PET study. J Nucl Cardiol. 2020;27(4):1225–33.

30 Ballinger JR, Koziorowski J. Advances in Radiopharmaceuticals for Myocardial Perfusion Imaging. In: Ryder H, Testanera G, Veloso Jerónimo V, Vidovič B, editors. Myocardial Perfusion Imaging: a technologist's guide. EANM; 2014. p. 42–53.

31 Chiribiri A, Schuster A, Ishida M, Hautvast G, Zarinabad N, Morton G, et al. Perfusion Phantom : An Efficient and Reproducible Method to Simulate Myocardial First-Pass Perfusion Measurements with Cardiovascular Magnetic Resonance. Magn Reson Med. 2013;69:698–707.

32 Driscoll B, Keller H, Coolens C. Development of a dynamic flow imaging phantom for dynamic contrast-enhanced CT. Med Phys. 2011;38(8):4866–80.

33 Spectrum Dynamics Medical. Dynamic SPECT Case Study [Internet]. 2019 [cited 2021 Nov 1]. Available from: https://www.spectrum-dynamics.com/case-studies/dynamic-spect/dynamic-spect-case-study-patient-1/

5

Marije E. Kamphuis
Marcel J. W. Greuter
Riemer H. J. A. Slart
Cornelis H. Slump

SPIE Medical Imaging Conference Proceeding
volume 12036, Proceeding number: 1203626 (2022)

Evaluation of a cardiac flow phantom for absolute myocardial perfusion SPECT measurements

Abstract

Introduction Absolute myocardial perfusion imaging (MPI) can be beneficial in the diagnosis and prognosis of patients with coronary artery disease. However, validation and standardization of perfusion estimates across centers is needed to ensure safe and adequate integration into clinical routine. MPI phantoms can contribute to this clinical need as these models can provide ground truth evaluation of absolute MPI in a controlled setup.

Phantom verification This work presents verification of phantom design choices, including the justification for using sorbents in mimicking contrast kinetics (i.e., tracer uptake and retention). Moreover, we compare preliminary phantom results obtained with SPECT-MPI with patient data. Finally, we applied a general two-tissue compartment model to describe the obtained phantom time activity curve data.

Conclusion These evaluation steps support shaping of a suitable verification and validation strategy for multi-modality myocardial perfusion phantom design and realization.

Introduction

Myocardial perfusion imaging

Myocardial perfusion imaging (MPI) is a functional imaging technique to confirm the diagnosis and assess the prognosis of coronary artery disease.[1] MPI is mostly performed with single photon emitting computed tomography (SPECT) and positron emission tomography (PET) imaging. This imaging method aims to identify areas of the left ventricular myocardium with reduced perfusion by comparing a static perfusion scan in rest with a static perfusion scan in stress (i.e., exercise). During the MPI procedure, a radiolabeled tracer is administered intravenously. Common MPI tracers are [^{99m}Tc]Tc-sestamibi and [^{99m}Tc]Tc-tetrofosmin in SPECT and ^{82}Rb and [^{13}N]NH_3 and H_2[^{15}O]O in PET. A region in the perfusion scan with less than the average number of detected photons can indicate a local perfusion deficit, possibly as a result of a significant stenosis upstream. By performing both a scan in rest and in stress, one can differentiate between a reversible or irreversible perfusion deficit, implying ischemia or infarction, respectively.[1–3]

Absolute, multimodal MPI has become a clinically relevant research topic within the cardiac imaging community.[4,5] Especially for PET the advantages of quantitative assessment in addition to qualitative visual evaluation have been demonstrated.[6] Quantification of myocardial blood flow (MBF) and myocardial flow reserve provide a substantial advantage for diagnostic and prognostic evaluation of suspected or established coronary artery disease.[4–7] Currently these quantitative PET perfusion approaches are being translated into clinical workflows. In addition, similar approaches are explored for other imaging modalities, including computed tomography (CT), magnetic resonance imaging (MRI), and SPECT. However, further efforts are necessary for on-site validation and to standardize measures across clinical centers, radiotracers, equipment, and software.[7]

Myocardial perfusion phantoms

Myocardial perfusion phantom studies can contribute to this unmet need for robust and on-site quality assessment due to their controlled setup and use of flow sensors providing a reference standard. Several left ventricular phantoms have been described in literature, in which various physiological states of perfusion can be simulated under static conditions, without flow.[8,9] In this, an increasing trend is observed in the use of 3D printing technology to obtain comprehensive representations of the heart.[10–12] Also, numerous perfusion phantoms have been proposed to facilitate physical flow standards for multimodal tissue perfusion imaging.[13–15] Nevertheless, current myocardial perfusion phantoms generally require in-house developed software for perfusion analysis. Evaluation of the entire absolute MPI application, i.e., both clinical hardware and software, involves an adequate phantom to mimic flow

dynamics on the one hand and to make clinical software accept the phantom data as a human heart on the other.

Research goal

Our main research goal encompasses the development of a myocardial perfusion phantom model to study MPI systems, and validate quantitative, multimodal MPI applications in a controlled setup (with reference flow measures). At this point, several steps have already been taken in our iterative phantom development process. We have started with designing, realizing, and testing of a proof-of-concept 3D printed left ventricular flow phantom that showed good compatibility with both clinical MPI hardware and software.[16] As a next step, we have incorporated in the following phantom iteration a novel concept for mimicking tracer kinetics[17], and performed initial tests with the phantom setup with SPECT-MPI. The phantom evaluation as presented in this work builds on the previously developed phantom prototype and focuses on:

- Verifying the phantom design choices, including justification for a novel concept in mimicking tracer kinetics.
- Preliminary verification of initial phantom results in dynamic SPECT, involving comparison with a general two-tissue compartment model.

We aim to take these insights into account in the development of the next, multimodal phantom prototype. Moreover, these steps in phantom evaluation support shaping of a suitable verification and validation strategy for multimodal myocardial perfusion phantom design and realization.

Phantom design verification

Requirements

Phantom design starts with drawing up the set of requirements. In this, we have aimed to minimize phantom complexity in order to maximize the reproducibility of phantom measurements. Henceforth, the main requirements for the myocardial perfusion phantom comprise:

1. Sufficient mimicking of the physical appearance of the heart, mainly the left ventricle, to enable phantom compatibility with dynamic, multimodal MPI hardware and software.
2. Adequate mimicking of the left ventricular flow to facilitate dynamic contrast measurement and derivation of arterial input functions (AIFs) that fall within a standardized normal and pathological patient range.
3. Advanced mimicking of myocardial perfusion to facilitate dynamic contrast measurement and derivation of tissue response functions (TRFs) that fall within a standardized normal and pathological patient range. This patient range entails a distinction between mimicking normal myocardial perfusion levels and grada-

Table 1 Phantom specifications.

Properties	Specifications	Symbol	Level or range	Unit
Physical appearance	1 Stationary cardiac insert for commercial thorax phantom			
	2 Basic left ventricular shape of an average patient, comprising: – a left ventricular cavity – a flow inlet and outlet with branches to three identical, surrounding myocardial regions			
	3 Made of adequate materials for proper x-ray attenuation			
Functioning	4 Tunable fluid flow through the left ventricular cavity, specified by: – a continuous flow of tap water with administered (radiolabeled) contrast kinetics – the first pass of (radiolabeled) contrast kinetics – accurate measurement of reference fluid flow	$\Phi_{ai}(t)$	4.0	L/min
	5 Tunable fluid flow through the myocardial regions, specified by: – a continuous, unidirectional fluid flow – the first pass of (radiolabeled) contrast kinetics – tunable myocardial uptake and retention – accurate measurement of reference fluid flow	$\Phi_{myo1-3}(t)$	[0.04 - 0.08]	L/min per myocardial region

tions of regional perfusion deficits.

Design specifications

At this stage we have dedicated phantom development and evaluation to SPECT-MPI. Several phantom design specifications have evolved from the set of requirements (see **Table 1**), which are particularly focused on simulating a flow and perfusion component in such a way that it could be used for ground truth validation of clinical, quantitative MPI applications.

These design specifications can be divided in elements of physical appearance and functioning. In terms of physical appearance, the myocardial perfusion phantom is intended as a stationary cardiac insert for a commercial anthropomorphic thorax phantom. The insert ought to be made of materials that attain x-ray attenuation profiles in accordance with soft tissue. The cardiac insert is designed for 3D printing and consists of three cylindrical pieces (see **Figure 1**). The center part comprises a basic

left ventricular cavity with an outlet that branches to three surrounding myocardial volumes. These identical volumes can be filled with tissue mimicking materials.

Phantom functioning is characterized by the incorporated flow dynamics in phantom and associated flow setup design. The overall setup (see **Figure 2**) comprises a closed loop flow circuit in which a fluid is circulated from the reservoir towards the phantom and back. The different components in the setup are connected with tubes. In this way, a (radiolabeled) contrast medium can be administered via a clinical contrast injector before entering the phantom. The phantom itself has a left ventricular cavity inlet and outlet, of which the outgoing flow is branched internally to the three myocardial volumes. These regions have individual outlets back to the reservoir. The flow can be regulated and measured in all parallel circuits using flow sensors and adjustable resistances. This setup primarily focuses on controlled mimicry of first-pass contrast kinetics by having a custom-built filter placed in the circuit that aims to prevent recirculation of contrast.

We have applied a black box approach to obtain adequate, flow dependent time activity curve (TAC) outputs from phantom measurements with preset reference flows

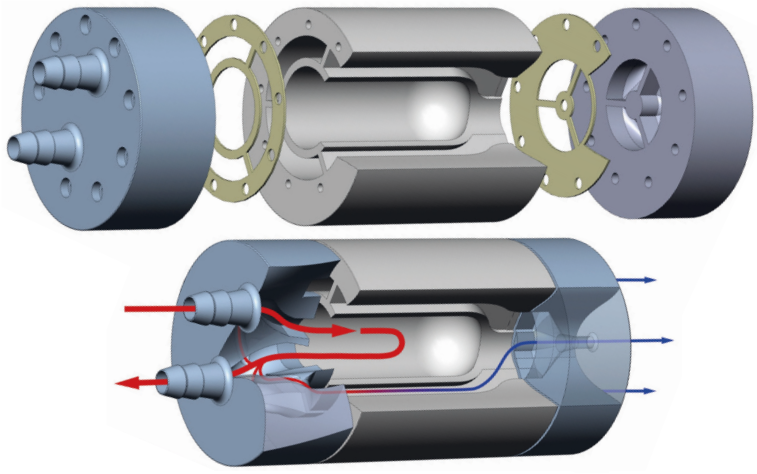

Figure 1 Myocardial perfusion phantom design. The exploded view (top) illustrates individual phantom parts. The three 3D printed pieces are fastened together with nylon screws with sealing in between for water proofing. The tailored cross section (bottom) visualizes inner phantom flow connections. The arrows indicate flow direction and magnitude, and its color differentiates between arterial input (red) and venous output (blue). The center phantom piece comprises the simulated left ventricular cavity and three surrounding myocardial volumes. These volumes are filled with tissue mimicking material during phantom fabrication. The two outer phantom pieces contain the inlet and outlet connection to the flow circuit and the internal branches to the myocardial volumes. The total phantom cylinder is designed to fit as cardiac insert in an anthropomorphic thorax phantom.

in the setup as inputs. This approach implies that we are not interested in the exact configuration of the myocardial tissue inlays, only in its input and output relation, which is refined empirically. Largely because of this black box approach, several simplifications have been made to functional phantom design in terms of simulating:

- flow dynamics,
- cardiac contraction dynamics, and
- tissue mimicking properties.

Regarding flow dynamics, we choose to generate a continuous instead of a physiological flow profile. In support of this simplification, patient TACs do not show fluctuations of a physiological flow profile either. An underlying cause is that TACs are based on average measured activities in a region of interest, which balances out fluctuations. In addition, measurement of the AIF concerns relatively fast kinetics of a respective small contrast volume (~2 mL) in order to capture the contrast bolus within a single heartbeat. That is also why tap water is considered a sufficient blood mimicking fluid for current application with SPECT as the administration of a small radiotracer volume mixes well with the passing water. Another reason to simplify the phantom flow profiles is that the human coronary circulation has several mechanisms to facilitate a rather constant blood flow rate to the cells. This also reduces the presence of blood flow fluctuations in measured TRFs.

In the current phantom design, the coronary circulation is simplified into three 'coronary arteries' that open into three volumes and converge thereafter in three 'cardiac veins'. Unidirectional flow through these volumes represents both microcirculation and tissue perfusion. This generalization is based on how the relevant outputs

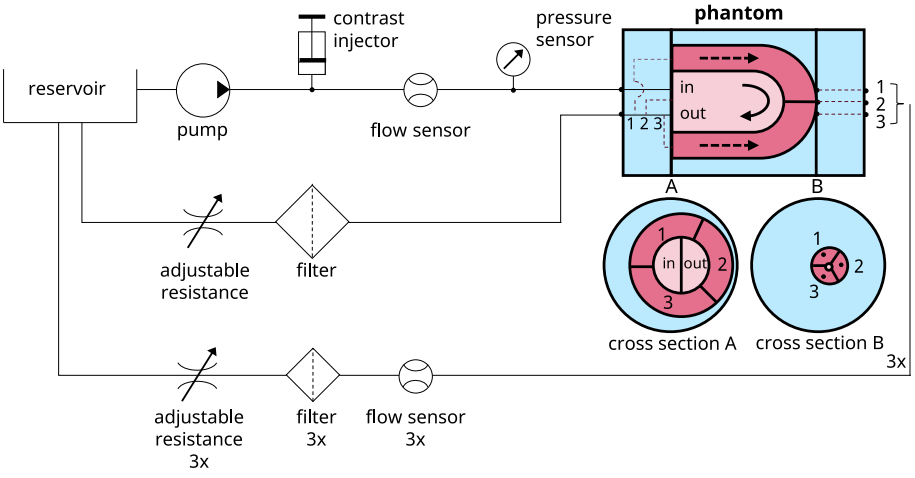

Figure 2 Phantom flow setup design.

are evaluated in clinical practice. Commonly, patient TRFs are assessed regionally and not locally. Moreover, these curves are composed of tracer kinetic measurement in the combined (micro)vascular and tissue component. Ensuing MBF computation usually arises from compartment modeling. In this type of tracer kinetic modeling one of the main assumptions is that the concentration of tracer is equally distributed within the entire compartment.[18] In this, a correction factor is typically applied for the proportion of arterial tracer concentration in the measured TRF.[19,20] These arguments substantiate why a black box approach seems to suffice, provided that the measured tracer activity over time within the myocardial phantom region of interest corresponds to standardized patient tracer kinetics. Hence, a greater level of detail of the coronary circulation seems unnecessary to incorporate in phantom design.

A possible disadvantage of this black box approach can be that the simplified microcirculation and tissue mimicking properties are fine-tuned for a certain flow setting and may therefore show a different flow dependence than observed in patients. From that point of view it was decided to opt for standard flow settings within the phantom, hence also in mimicking normal perfusion and perfusion deficits. Normal reference flow is considered a cardiac output of 4.0 L/min and a flow through each myocardial phantom volume of 80 mL/min. This equates to a coronary flow of 6 % of total cardiac output. A perfusion deficit is simulated by a reduced flow through one or multiple myocardial phantom regions by tuning the adjustable resistances. These settings comprise also a cardiac output of 4.0 L/min, and myocardial flows through each phantom myocardial volume of 40–80 mL/min (see **Table 1**). It is of importance to verify during phantom testing and evaluation whether the regulation and measurement of these flows are within the desired accuracy and reproducibility range. This was tested and considered sufficiently (kept within 5 % of flow sensor readout), though it took considerable time to set the flows correctly for each phantom measurement by manually adjusting the resistances.

It has been decided to build a stationary flow phantom, thereby excluding cardiac contraction dynamics in current phantom design. Although incorporation of cardiac contraction dynamics (and respiratory motion) will result in a more realistic phantom, it also entails great complexity in phantom realization. This will most likely go hand in hand with a decreased measurement reproducibility. It can be argued that the latter is also apparent in the in-vivo situation and can therefore not be neglected. However, at this stage, a high measurement reproducibility is preferred over the degree of representativeness when it comes to developing a perfusion validation phantom.

In this phantom design we can alter the tissue mimicking properties by modifying the inlay of the myocardial volumes. Previous research by Kamphuis et al.[17] has demonstrated that sorbents can be used to fill the phantom tissue volumes in order to mimic tracer specific uptake and retention kinetics in the myocardium. This con-

cept, as illustrated in **Figure 3**, can be approached with compartment modeling as well. Sorption is a physical and chemical process in which one substance, in our case the (radiolabeled) contrast medium, becomes (temporarily) attached to a selected sorbent or sorbent mixture.[21] In this, ion exchange and adsorption processes are of particular interest, as these can essentially mimic freely diffusible contrast kinetics in tissue, reversible binding of contrast media, and irreversible binding of contrast media to cells. As shown in **Figure 3**, the rate constants that describe contrast kinetics for a general two-tissue compartment model are comparable to the sorption and desorption rate constants that describe our physical phantom perfusion model. There is a small difference between the physiological and phantom model in how the tissue compartments are represented, namely as a series or parallel connection between unbound and bound tissue compartments. This results in a distinctive set of tissue

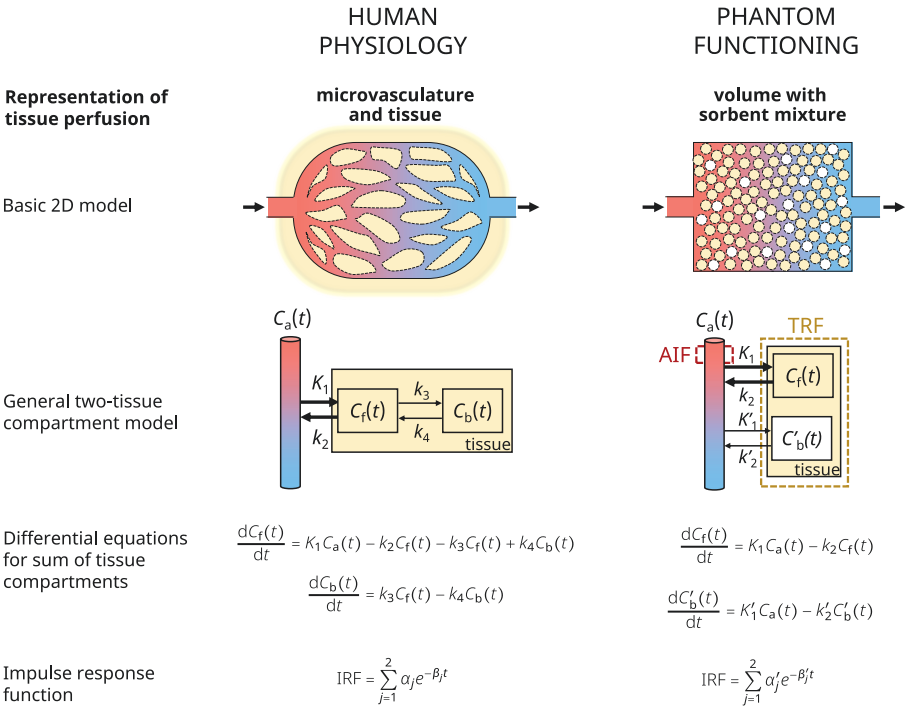

Figure 3 Schematic overview to illustrate a novel concept in mimicking contrast kinetics related to tissue perfusion in a physical phantom model. $C_a(t)$, $C_f(t)$, and $C_b(t)$ correspond to the contrast concentration measured / imaged over time in arterial blood, and free or bound in tissue, respectively. The illustrated phantom concept describes a similar relation between these measured concentrations using sorbents as tissue mimicking material. The rate constants that describe inter-compartmental contrast exchange rates are similar of nature for the physiological and phantom model, as can be seen by tissue derived differential equations and resulting impulse response function (see **Equation 1**).

compartmental differential equations. Nonetheless, the slightly altered tissue-mimicking phantom design can be justified because in both models (physiological and patient) the image derived contrast kinetic measurement in tissues always comprises the sum of both tissue compartments. Hence, when solving the differential equations, the general analytical solutions of both sets of differential equations encompass a similar type of impulse response function (IRF)[22], as displayed in **Figure 3**. In this, $\alpha \neq \alpha'$ and $\beta \neq \beta'$.

In the case of tracer kinetic phantom measurement with ^{99m}Tc labeled MPI tracers it is known that the first pass extraction fraction is around 55–65 % of the total injected dose and is for a small fraction (1–5 %) irreversibly trapped in myocardial tissue[23], hence $k_3 = 0.01–0.05$ min^{-1} and $k_4 = 0$ min^{-1}. Subsequently, the differential equations posed by this general two-tissue compartment model can be solved analytically using the Blomqvist approach.[22] This approach results in the following equation:

$$C_t = C_f + C_b = \frac{K_1}{k_2 + k_3}\left(k_2 e^{-(k_2+k_3)t} + k_3\right) \otimes C_a \qquad \text{[Eq. 1]}$$

In this, C_t comprises the tracer concentration in tissue over time, which is the sum of the tracer concentration freely diffused in tissue (C_f) and bound to cells (C_b). In general, the tissue concentration equals the convolution of the tracer concentration in the arterial blood component C_a with its impulse response function (IRF). In our SPECT phantom measurements, we obtain an image derived and sampled tracer concentration time measurement from a region of interest in the LVC, i.e., the AIF (corresponding to $C_a(t)$), and in the myocardial phantom volumes. i.e., the TRFs (corresponding to $C_t(t)$). During phantom evaluation, we have assessed how changes in flow and tissue mimicking material compositions correlate with these theoretical model descriptions.

Initial verification of phantom results

Phantom measurements

Figure 4 shows an overview of the overall phantom setup during initial phantom testing in SPECT-MPI. In total, twenty-two phantom measurements were executed in dynamic SPECT-MPI spread over six, non-consecutive measurement days. In these measurements, the clinical protocol was followed completely, from dynamic image acquisition, tracer injection, image data reconstruction, to perfusion image visualization and quantitative perfusion analysis. Around 500 MBq of [^{99m}Tc]Tc-pertechnetate tracer dissolved in 1.5 mL saline was injected at 1.0 mL/s just after initiating a standard 6 min dynamic scan. **Figure 5** shows two examples of obtained phantom perfusion images, in which we varied myocardial flow and tissue mimicking properties. The methods used and results obtained with these phantom measurements are

described in related work.[17] This work extends our current analysis by comparing the obtained AIF and TRFs with a patient example in combination with a general two-tissue compartment model.

Comparison with patient data

Figure 5 displays the mean AIF and TRF for similar phantom measurements compared to a patient example. The phantom measurements are very similar to the patient example. One of the observations was that a small percentage of tracer passed the filters in the flow setup and got recirculated into the phantom, as can be seen by the gradually upward trend in the average phantom TRF over time. The visible differences come from spillover effects in the patient data (in the AIF at $t \approx 30$ s and in the TRF at $t \approx 15$ s) and by a small fraction of recirculating tracer. This effect can be observed by a slightly increasing TRF over time, instead of the flattened line as observed in the patient example. The observed stronger increase in measured tracer activity in the patient TRF, including a higher peak activity, might also occur due to a higher flow.

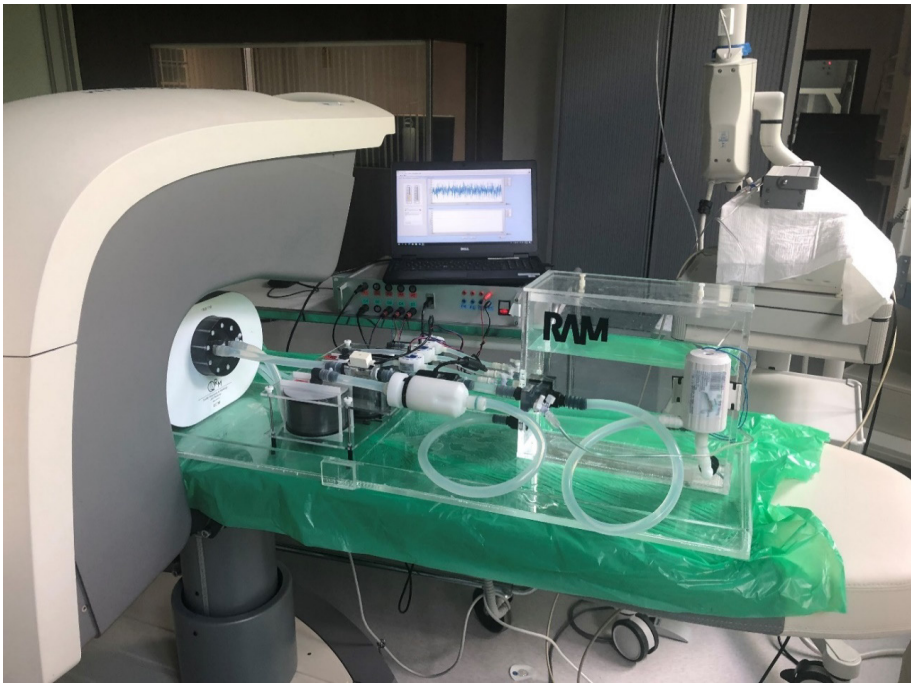

Figure 4 Overview of the phantom flow setup during initial phantom testing on a clinical SPECT system.

Comparison with general two-tissue compartment model

We verified our phantom observations by fitting the analytical solution as proposed by Eq. 1 to our phantom data. As a starting point, we introduced a Gaussian AIF with characteristics similar to the AIFs observed in **Figure 6**, i.e., a peak maximum of 300 kBq/mL at $t = 15$ s and a full-with at half maximum of 15 s. We have also incorporated a simplified scenario of tracer recirculation by introducing contrast recirculation in the simulated AIF building up to a continuous recirculation level of 10 kBq/mL from $t = 15$ s. For subsequent parameter estimation we used values from literature for k_3 and experimentally altered K_1 and k_2 to manually fit the data. **Figure 7** visualizes the simulated AIF and TRF for different values for K_1 since this rate constant is most closely related to MBF. It should be noted that this model has been simplified in such a way that only K_1 is varied, while in reality this is an interplay between all rate constants. However, for the purpose of initial phantom verification it was considered to be sufficient.

When comparing the model data with phantom data we can indeed relate the upward trend in the phantom TRFs to the small extent of tracer recirculation. In addition, K_1 (and presumably MBF) does affect the presence and height of the TRF peak around $t = 20$ s. In our current phantom setup, we observed a less dominant TRF peak, which may indicate a lower flow rate compared to the patient example and to our modeling results.

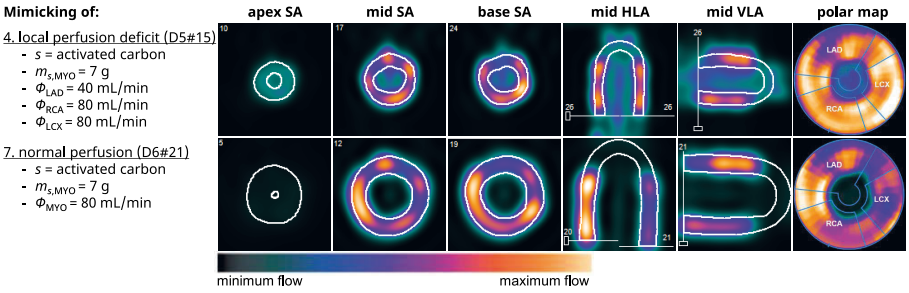

Figure 5 Two examples of myocardial perfusion imaging series aiming to highlight the overall phantom development and evaluation process. The image cross-sections and polar maps present the accumulated radiotracer distribution inside the phantom, which is a static representation of a dynamic time measurement. Note that the relative color scale is determined by default for each individual measurement and is therefore not linked between measurements. In these measurements, mimicking of radiotracer uptake, normal perfusion and perfusion deficit was examined using different parameter settings. Settings include the type and mass of sorbent (*s*) utilized to mimic myocardial tissue, and the amount of volume flux (Φ) directed through the myocardial segments (MYO). D5#15 stands for the measurement day and number, respectively. LAD = left anterior descending coronary artery, RCA = right coronary artery, LCX = left circumflex coronary artery, SA = short axis, HLA = horizontal long axis, and VLA is vertical long axis.

Verification of the obtained phantom data is still a work in progress. We also want to look at the different sorbent compositions that we used to empirically match the phantom TRFs with patient data and try to verify how these changes affect the rate constants.

Conclusion

With this work we have presented a start of phantom evaluation. This concerned verification of the phantom design choices and initial verification of phantom results in SPECT by comparing the obtained tracer kinetic results with a patient example and a tracer kinetic model. We have demonstrated that the rate constants that describe contrast kinetics for a general two-tissue compartment model are comparable

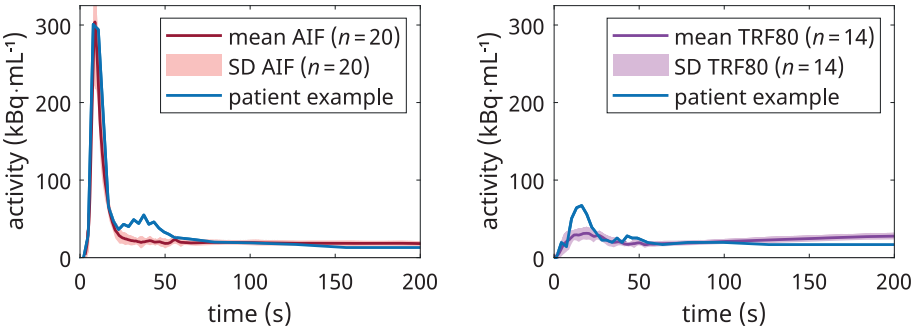

Figure 6 Time activity curve comparison between phantom data and a patient example. For the phantom data, the mean and standard deviation of the derived arterial input functions (AIFs) and tissue response functions (TRFs) at a flow of 80 mL/min were plotted.

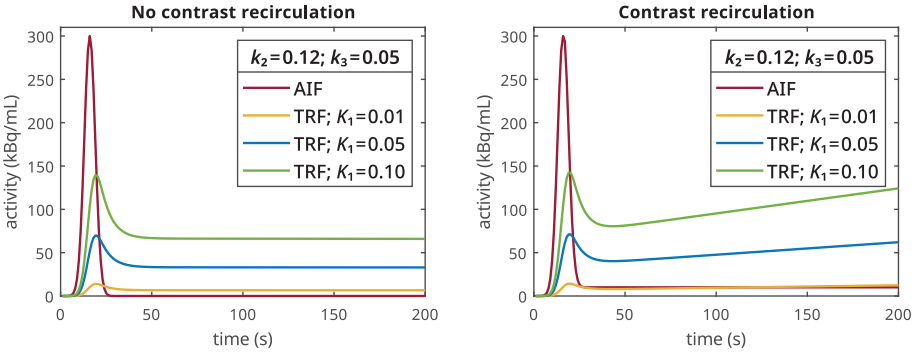

Figure 7 A two-compartment model comparison indicating the effect of contrast recirculation (in phantom measurements) on time activity curve derivation for different values of K_1. K_1, k_2, and k_3 are transfer rate constants. AIF = arterial input function, TRF = tissue response function.

to the sorption and desorption rate constants in the phantom. Moreover, we were able to verify observations in phantom TRF data with preliminary simulation results. This part of our phantom evaluation is still work in progress and underpins certain aspects of multimodal phantom redesign, but also supports shaping of a suitable verification and validation strategy for a multimodal myocardial perfusion phantom.

References

1 Hesse B, Tägil K, Cuocolo A, et al. EANM/ESC procedural guidelines for myocardial perfusion imaging in nuclear cardiology. Eur J Nucl Med Mol Imaging. 2005;32(7):855-897. doi:10.1007/s00259-005-1779-y

2 Verberne HJ, Acampa W, Anagnostopoulos C, et al. EANM Procedural Guidelines for Radionuclide Myocardial Perfusion Imaging with SPECT and SPECT / CT Chair of Writing Committee (Responsible for the Coordination of the Overall Process): Hein J . Verberne and Birger Hesse Authors : Correspondence to : H .; 2015.

3 Hyafil F, Gimelli A, Slart RHJA, et al. EANM procedural guidelines for myocardial perfusion scintigraphy using cardiac-centered gamma cameras. Eur J Hybrid Imaging. 2019;3(1). doi:10.1186/s41824-019-0058-2

4 Dewey M, Siebes M, Kachelrieß M, et al. Clinical quantitative cardiac imaging for the assessment of myocardial ischaemia. Nat Rev Cardiol. 2020;17(7):427-450. doi:10.1038/s41569-020-0341-8

5 Sciagrà R, Lubberink M, Hyafil F, et al. EANM procedural guidelines for PET/CT quantitative myocardial perfusion imaging. Eur J Nucl Med Mol Imaging. 2021;48(4):1040-1069. doi:10.1007/s00259-020-05046-9

6 Cho SG, Lee SJ, Na MH, Choi YY, Bom HHS. Comparison of diagnostic accuracy of PET-derived myocardial blood flow parameters: A meta-analysis. J Nucl Cardiol. 2020;27(6):1955-1966. doi:10.1007/s12350-018-01476-z

7 Murthy VL, Bateman TM, Beanlands RS, et al. Clinical quantification of myocardial blood flow using PET: Joint position paper of the SNMMI cardiovascular council and the ASNC. J Nucl Med. 2018;59(2):273-293. doi:10.2967/jnumed.117.201368

8 Visser JJN, Sokole EB, Verberne HJ, et al. A realistic 3-D gated cardiac phantom for quality control of gated myocardial perfusion SPET: The Amsterdam gated (AGATE) cardiac phantom. Eur J Nucl Med Mol Imaging. 2004;31(2):222-228. doi:10.1007/s00259-003-1352-5

9 Data Spectrum Corporation. Cardiac Insert. Product catablogues. http://www.orion-france.com/pdf/catalogues/Orion_Data_Spectrum.pdf. Published 2001. Accessed October 28, 2021.

10 Grice J, Green S, Yuhas A. An Improved 3D Printed Cardiac Phantom. J Nucl Med. 2020;61(supplement 1):391 LP - 391. http://jnm.snmjournals.org/content/61/supplement_1/391.abstract.

11 Abdullah K, McEntee M, Reed W, Kench P. Development of an organ-specific insert phantom generated using a 3D printer for investigations of cardiac computed tomography protocols. J Med Radiat Sci. 2018;65. doi:10.1002/jmrs.279

12 Jin Z, Li Y, Yu K, et al. 3D Printing of Physical Organ Models: Recent Developments and Challenges. Adv Sci. 2021;8(17):2101394. doi:https://doi.org/10.1002/advs.202101394

13 Kok G, Pelevic N, Chiribiri A, et al. A calibrated physical flow standard for medical perfusion imaging. Flow Meas Instrum. 2021;78(February):0-5. doi:10.1016/j.flowmeasinst.2021.101907

14 Sun Nuclear Corporation. CT Perfusion Phantom. https://www.sunnuclear.com/products/ct-perfusion-phantom. Published 2021. Accessed October 28, 2021.

15 Driscoll B, Keller H, Jaffray D, Coolens C. Development of a dynamic quality assurance testing protocol for multisite clinical trial DCE-CT accreditation. Med Phys. 2013;40(8):081906. doi:10.1118/1.4812429

16 Kamphuis ME, de Vries GJ, Verschoor J, Slump CH. Development of a dedicated 3D printed myocardial perfusion phantom: Proof-of-concept in dynamic SPECT. Med Biol Eng Comput.

17 Kamphuis ME, Kuipers H, Verschoor J, et al. Development of a dynamic myocardial perfusion phantom model for tracer kinetic measurement. under Rev.

18 Carson RE. Tracer kinetic modeling in PET. In: Positron Emission Tomography. Springer; 2005:127-159.

19 Leppo JA, Meerdink DJ. Comparison of the myocardial uptake of a technetium-labeled isonitrile analogue and thallium. Circ Res. 1989;65(3):632-639. doi:10.1161/01.RES.65.3.632

20 Yoshida K, Mullani N, Gould KL. Coronary flow and flow reserve by PET simplified for clinical applications using rubidium-82 or nitrogen-13-ammonia. J Nucl Med. 1996;37(10):1701-1712.

21 Seader JD, Henley EJ, Roper DK, eds. Adsorption, Ion Exchange, Chromatography, and Electrophoresis. In: Separation Process Principles: Chemical and Biochemical Operations. 3rd ed. John Wiley & Sons; 2010.

22 Blomqvist G, Pauli S, Farde L, Eriksson L, Persson A, Halldin C. Maps of receptor binding parameters in the human brain — a kinetic analysis of PET measurements. Eur J Nucl Med. 1990;16(4):257-265. doi:10.1007/BF00842777

23 Ballinger JR, Koziorowski J. Advances in Radiopharmaceuticals for Myocardial Perfusion Imaging. In: Ryder H, Testanera G, Veloso Jerónimo V, Vidovič B, eds. Myocardial Perfusion Imaging: A Technologist's Guide. EANM; 2014:42-53. doi:10.1046/j.1617-0830.2003.70206.x

6

Marije E Kamphuis
Henny Kuipers
H Remco Liefers
Jan van Es
Frank FJ Simonis
Marcel JW Greuter
Cornelis H Slump
Riemer HJA Slart

Submitted (2022)

A multimodality myocardial perfusion phantom: initial quantitative imaging results

Abstract

Objectives This study explores multimodal application of a dedicated cardiac flow phantom for ground truth contrast measurements in dynamic myocardial perfusion imaging with CT, PET/CT, and MRI.

Materials and Methods The phantom setup comprises a 3D printed cardiac flow phantom and flow circuit. The stationary phantom mimics the shape of a basic, left ventricular cavity (LVC) and three surrounding myocardial regions. The regions are filled with tissue mimicking materials, including sorbents and sponge material. The flow circuit regulates and measures water flow (with injected contrast media) through the LVC and myocardial regions. In this way, normal tissue perfusion and regional or global perfusion deficits can be simulated. We performed 9 phantom measurements (3 in PET/CT, 3 in CT, and 3 in MRI) and evaluated how well the phantom mimics the results of an average patient with clinically used hardware and software. The reference arterial input flow was set to 4.0 L/min and the flow in the three myocardial regions to 80 mL/min. This setting corresponded to a myocardial blood flow (MBF) of 1.6 mL/g/min.

Results The phantom results demonstrated successful completion of all the processes involved in these quantitative, multimodal MPI applications. Contrast kinetics as displayed in the time intensity / activity curves were in line with expectations, e.g., in MRI measurements a prolonged time to peak was detected in the myocardial region with a mimicked perfusion deficit (38 s vs 32 s in normal tissue). Derived MBF values in PET/CT and CT led to an under- and overestimation of the reference flow with 0.9 mL/g/min and 4.5 mL/g/min, respectively. A simulated perfusion deficit (0.8 mL/g/min) in CT resulted in an MBF of 2.8 mL/g/min.

Conclusions We have successfully performed initial, quantitative perfusion measurements with our dedicated phantom setup utilizing clinical hardware and software. These results showcase multimodal phantom potential. An important next step is to further optimize and validate the mimicking of the respective (radiolabeled) contrast kinetics for each imaging modality.

Background

Myocardial perfusion imaging (MPI) in rest and stress is a functional imaging method widely used to assess ischemia and confirm the diagnosis of coronary artery disease.[1,2] This imaging approach is pre-eminently performed and validated using single photon emission computed tomography (SPECT)[3] and to an increasing extent by positron emission tomography (PET).[4] Dynamic image acquisition of contrast media kinetics, including radiolabeled pharmaceuticals, can improve standard, relative perfusion evaluation. Herewith, numerous mathematical blood flow models have been developed to estimate local perfusion values from the imaged contrast properties over time.[5–7] Other quantitative measures indicating perfusion deficit, including a prolonged time to peak, can be derived from subsequent time intensity or time activity curves (TICs/TACs) as well. At the moment, the added value of (absolute) perfusion quantification in addition to standard relative assessment has been carefully investigated merely using PET imaging.[8] From these studies we can conclude that estimation of myocardial blood flow (MBF) and especially myocardial flow reserve (MFR) can lead to improved diagnostic accuracy in certain patient groups and result in better and standardized evaluation capabilities.[9] However, caution is exercised when it comes to embedding absolute perfusion measures into clinical routine. Validation and harmonization hereof is essential before these measurements can optimize revascularization decision making.[10] Next to PET, absolute MPI is also emerging with other imaging modalities, such as SPECT[11,12], computed tomography (CT)[13], magnetic resonance imaging (MRI)[14,15], and ultrasound.[16,17] Due to this diversity in the clinical setting, it is warranted to investigate perfusion measurement (in)accuracy in a controlled environment to work towards a validated standard for quantitative, multimodal MPI.

It is relevant to study clinical applications of quantitative MPI in a simplified and controlled environment. In previous work[18], we have presented a dedicated left ventricular flow phantom in which we have introduced the use of sorbents to mimic radiolabeled contrast media uptake and retention in the simulated myocardium. We have performed several ground truth tracer kinetic phantom measurements in dynamic SPECT and obtained promising, patient realistic TACs (i.e., comprising arterial input functions (AIFs) and tissue response functions (TRFs)) of normal perfusion levels and regional or global perfusion deficits. One of the next steps in phantom development is to expand the current application domain to multiple imaging modalities including associated contrast kinetics. Hence, the two main goals of this explorative study are: 1) to gain insight into the overall functionality of the phantom in quantitative MPI applications with PET/CT, CT, and MRI, and 2) to identify possible improvements in phantom design.

Materials and Methods

Phantom setup

The standard phantom setup comprises 3 elements:

1. a previously adapted myocardial perfusion phantom (cylindrical cardiac insert),
2. a commercial anthropomorphic thorax phantom, and
3. an in-house built flow circuit.

Detailed information on the phantom setup can be found in previous work by Kamphuis et al.[18] In summary, the stationary, 3D printed myocardial perfusion phantom represents the basic shape of a left ventricle. As visualized in **Figure 1**, the phantom assembly consists of three individual parts. The phantom has one inlet to the mimicked left ventricular cavity (LVC) and one main outlet representing the aorta. The aorta branches to three mimicked coronary arteries, namely the left anterior descending coronary artery (LAD), the right coronary artery (RCA) and left circumflex coronary artery (LCA). These branches connect to three identical, surrounding myocardial volumes. Each volume has an individual outlet. The tissue mimicking material used to fill these volumes is linked to the intended contrast/tracer kinetics to be simulated.

The closed loop flow circuit connects to all phantom inlets and outlets (see **Figure 2**). Using this flow circuit, we can generate, regulate, and measure water flow (with injected contrast agent or radiotracer) through the LVC and individual myocardial regions. Tuning of the resistances/taps in the flow circuit enables simulation of normal tissue perfusion and regional or global perfusion deficits. Standard flow settings were 4.0 L/min as cardiac output and 80 mL/min within each myocardial region. The latter corresponds to a myocardial blood flow of 1.6 mL/g/min (normalized by tissue weight, with an assumed tissue density of 1.0 g/mL and a volume of 50 mL per myocardial region).

In all phantom measurements we aimed to image first pass, patient realistic contrast kinetics through the mimicked LVC and myocardial regions over time. The same basic measurement setup, as illustrated in **Figure 3**, was used for all phantom measurements. The following modality specific adjustments have been made regarding the flow circuit and the used tissue mimicking material.

Flow circuit adjustments

The described flow circuit was designed for use with [^{99m}Tc]Tc-pertechnetate and SPECT imaging.[18] In this setup, a closed loop configuration was preferred in order to avoid large amounts of radio-active wastewater. Use of a custom-built filter (adsorbing passing radiotracer) prevents recirculation of radiotracer, hence aims for the intended measurement of first pass tracer kinetics. No adjustments to the flow circuit seemed necessary for phantom measurements with PET/CT imaging as we assumed

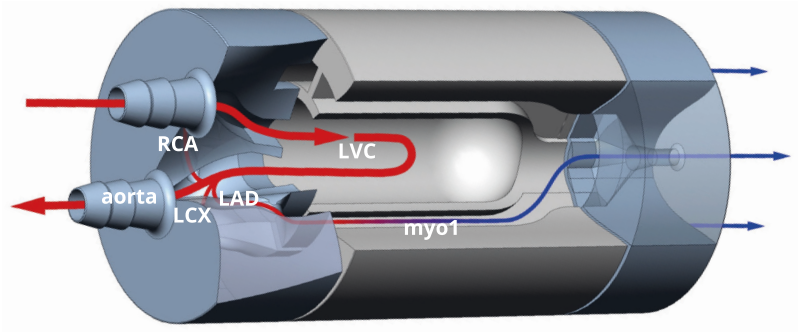

Figure 1 Tailored cross-section of the myocardial perfusion phantom design, consisting of three cylindrical parts fastened together with nylon screws. The middle phantom part comprises the simulated left ventricular cavity (LVC) and three surrounding myocardial regions (myo1–3). The two outer parts contain the in- and outlet connections to the flow circuit and the internal branches from the simulated aorta to myo1–3 (only myo1 is visible in this view). The branches correspond to the main coronary arteries, i.e., the left anterior descending coronary artery (LAD), right coronary artery (RCA) and left circumflex coronary artery (LCX). The arrows indicate flow direction and magnitude, and its color differentiates between arterial input (red) and venous output (blue). Adapted from Kamphuis et al.[18]

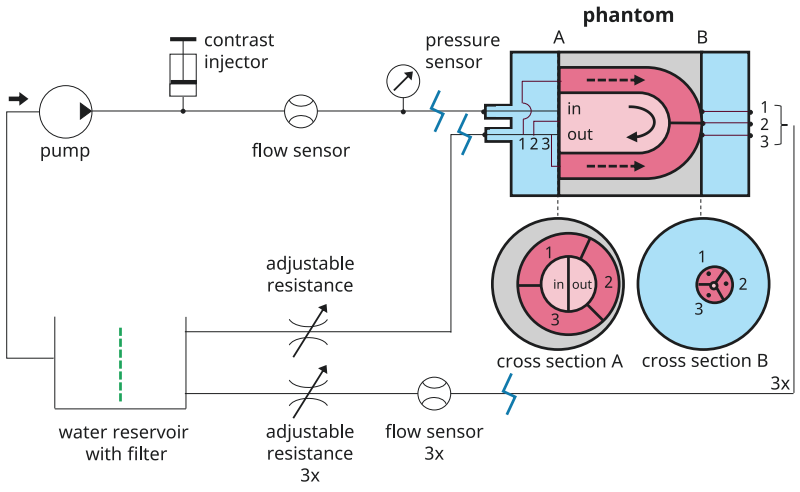

Figure 2 Flow circuit design of the standard phantom setup. The 3D printed phantom cylinder has one inlet to the simulated left ventricular cavity. Its main outlet (mimicking the aorta) branches to three identical surrounding myocardial regions (1–3). Each region has an individual outlet. All flow circuit components are connected by silicon tubing. Modality specific adjustments incorporate a custom-built filter in the water reservoir to adsorb recirculating radiotracer during SPECT and PET measurements (dashed green line) and additional tubing of 8 m was built in at the in blue marked positions for MRI measurements. The arrow in the left top indicates flow direction.

the existing recirculation filter applied in SPECT would be sufficient for PET/CT as well.[19] The filter comprised of 1 kilogram of aquarium filter material, which is a mixture of zeolite (~50%) and activated carbon (~50%) (Superfish Crystal Clear Media, AquaDistri, Klundert, The Netherlands). Previous experiments have shown adsorption of passing [^{99m}Tc]Tc-pertechnetate using activated carbon[18] and it was hypothesized that zeolite would adsorb passing [^{13}N]NH_3 satisfactorily[19], provided that a sufficient amount of filter material was used. Small adjustments to the closed loop flow circuit were necessary for phantom measurements with CT, because no adsorption of an iodine-containing contrast medium was attained in the lab using current filter design. These adjustments included: 1) enlargement of the water reservoir (5 L in total) such that recirculation of contrast falls outside the 30 s scanning time, and 2) replacement of the iodine containing water with fresh tap water in between phantom measurements (i.e., strong dilution) to prevent increasing contrast concentrations being imaged over time. For MR measurements, the setup was placed outside the Faraday cage. Only the phantom itself was positioned on the scanning table by means of 5 silicone tubes of 8 meters (see **Figure 2 and 3**). The phantom cylinder was placed in a water container. For the same reason as with the CT measurements, the contrast containing water was replaced by fresh tap water in between measurements.

Tissue mimicking adjustments

Ideally, a dedicated myocardial perfusion phantom can mimic a standard course of a specific (radiolabeled) contrast medium. Previous phantom measurements with SPECT have shown that the concept of using sorbents as tissue mimicking material offers novel possibilities to mimic contrast specific kinetics.[18] We demonstrated with SPECT-MPI that a certain amount of activated carbon, placed in the myocardial tissue volumes of the phantom, can provide standardized myocardial uptake of [^{99m}Tc]Tc-pertechnetate in accordance with normal perfusion levels. In principle the same can be accomplished with other contrast media and for other imaging modalities. For phantom measurements with PET/CT, we poured different amounts of zeolite, supplemented with activated carbon or silica granulates, into three myocar-

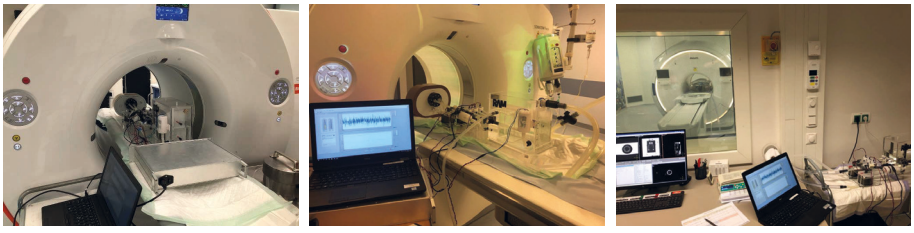

Figure 3 Examples of the overall phantom measurement setup in PET/CT (left), CT (middle) and MRI (right).

dial tissue volumes. This proof-of-concept was done to explore whether trapping of [^{13}N]NH_3 can be attained and modified accordingly. For CT measurements, we used sponge as tissue mimicking material.[20–23] Iodine based contrast media hardly leave the microvasculature and therefore no trapping has to be simulated. For MRI measurements there were no specific requirements set for tissue mimicking properties yet, hence we used a mixture of activated carbon and silica granulate for this feasibility experiment.

Phantom measurements

Initial measurements were aimed at describing to what extent the current phantom setup can be used for multimodal, quantitative MPI evaluation. In this, we went through all steps along the dynamic MPI procedure: from patient/phantom preparation, image acquisition and reconstruction to perfusion analysis, and reporting on the feasibility per modality. A total of nine phantom measurements were performed on three different scanners (3 in PET/CT, 3 in CT, and 3 in MRI) following clinical MPI protocols where possible. An overview of the study variables is listed in **Table 1**. At the start, the phantom setup was built up on the scanning table in a standard manner. Then the flow circuit was filled with tap water and vented, connected to the clinical contrast injector, and set to standard flow settings (4.0 L/min through LVC and 3 × 80 mL/min through the myocardial regions). Hereafter the clinical scanning procedure could be started.

Dynamic myocardial perfusion imaging

PET/CT imaging

The phantom study was performed on a digital PET/CT scanner (Vision Biograph PET/CT 128-Multislice Scanner; Siemens Healthineers, Erlangen Germany). Myocardial perfusion was assessed three times with a dose of 400 MBq [^{13}N]NH_3 injection. CT based transmission scans (120 kVp; 20–30 mA; pitch 1.5) were obtained prior to the first perfusion study to determine the field of view (FOV) and evaluate the presence of unwanted air bubbles, followed by venting efforts until this was resolved satisfactorily. It should be noted that for PET/CT measurements, an unforeseen resistance in one phantom region resulted in a set flow of 40, 80, and 80 mL/min in myocardial region 1–3, respectively. Then, dynamic perfusion imaging data were obtained for 8.5 min and visualized in 25 frames (1 × 7.5 s, 11 × 5 s, 1 × 7.5 s, 1 × 10 s, 1 × 20 s, 6 × 30 s, 1 × 45 s, 1 × 60 s, and 1 × 120 s). A standard reconstruction (2D attenuation-weighted OSEM) was used with 3 iterations, 14 subsets, and 3D post-filtering with a 5 mm Gaussian filter kernel. Transverse data were reformatted to a 168 × 168 × 47 matrix with 2 mm pixels for each dynamic frame.

CT imaging

Dynamic CT perfusion scans were performed at a third-generation dual source CT scanner (SOMATOM Force, Siemens Healthineers, Forchheim, Germany). The FOV

Table 1 Overview of study variables

study variables	PET/CT	CT	MR
imaging settings			
scan duration	8.5 min	30 s	60 s
(radiolabeled) contrast medium	400 MBq [^{13}N]NH_3	12.6 g iomeprol	7.5 mmol gadolinium
V_{tracer} / $V_{contrast}$ (mL)	10	60	15
v_{tracer} / $v_{contrast}$ (mL/s)	1.0	6.0	3.0
$V_{endflush}$ (mL)	30	32	20
$v_{endflush}$ (mL/s)	5.0	6.0	3.0
phantom settings			
tissue mimicking material			
myo1	29.0 g zeolite	sponge	7.0 g activated carbon 14.0 g silica granulates
myo2	14.5 g zeolite 13.7 g silica granulates	sponge	7.0 g activated carbon 14.0 g silica granulates
myo3	7.3 g zeolite 12.8 g activated carbon	sponge	7.0 g activated carbon 14.0 g silica granulates
Φ_{LVC} (L/min)	4.0	4.0	4.0
Φ_{myo1-3} (mL/min)	[40 80]	[40 80 120]	[60 80]

V = volume; v = injection rate; myo1–3 = myocardial tissue regions; LVC = left ventricular cavity; Φ = volume flux

was determined based on frontal and lateral scout images and covered the anthropomorphic thorax phantom with myocardial perfusion phantom insert. Dynamic scans were started nine seconds prior to contrast bolus injection into the flow circuit. 60 mL of 350 mg/mL iomeprol solution (Iomeron350, Bracco, Milan, Italy) was injected at an injection rate of 6.0 mL/s. Contrast injection was followed by a 32 mL saline flush also at 6.0 mL/s. Based on preliminary phantom measurements we slightly altered the standard contrast protocol (40 % dilution with saline) to obtain patient realistic AIFs (i.e., a peak intensity of around 800 HU). Dynamic CT perfusion scans of 30 s were performed in shuttle mode during end-systole (mimicked by a simulated 60 bpm ECG trigger pulse), providing one full heart coverage scan with a z-range of 102 mm per two seconds. Other acquisition parameters included a tube voltage of 70 kVp, a tube current time product of 280 mAs, and a gantry rotation time of 0.6 s. Dynamic CT perfusion data were reconstructed with 3.0 mm slice thickness and 1.5 mm increment. Traditional filtered back projection was used with a B23f kernel.

MR imaging

Dynamic image acquisition was performed using a 1.5 T clinical MRI scanner (Ambition X, Philips, The Netherlands) whereby the same anterior and posterior receive

coils were used as clinically used for patient scanning. In this, the predetermined FOV (210 mm × 252 mm) covered the water tank in which the phantom was positioned. Then, a clinical Balanced Turbo Field Echo sequence was performed. According to clinical protocol, 7.5 mmol of gadolinium (Dotarem, Guerbet, Roissy, Cedex, France) was dissolved in 15 mL saline and injected simultaneously with the start of the sequence at a flow rate of 3.0 mL/s, followed by a saline end flush of 20 mL, injected at the same speed. Dynamic perfusion image series of 1 frame/s were acquired for a scan duration of 60 s in four manually selected image planes. These image planes included three short axis planes from heart base to apex and one of the 4-chamber plane. The image data has a voxel size of 2.02 mm by 2.23 mm (matrix of 104 × 113 voxels) and a slice thickness of 10 mm.

Perfusion analysis

PET/CT analysis

All PET/CT images were processed with SyngoMBF VB14 (Siemens Healthineers, Forchheim, Germany). Dynamic datasets were automatically loaded, centered, and oriented, followed by manual corrections for adjustment of centering and reorientation of axial limits only when needed. The two-tissue compartment model developed by Hutchins et al.[24] was fitted to measure the TACs in order to calculate segmental MBF (presented in polar maps). In this, the arterial input function was derived by an automatically drawn region of interest at the base of the delineated LV. TRFs were extracted from standard delineated myocardial segments according to the America Heart Association's 17 segment model.[25] In this, segment 7, 9, and 11 corresponded to the center of the three phantom tissue regions. For the second and third scan measured background activity in the myocardial regions were subtracted using a standard tool in the clinical software. In this, the activity measured in the last frame of the previous study was subtracted from all frames in the following study. Multimodality TIC/TAC data was exported to Matlab2021 (MathWorks, Inc., Natick, Massachusetts, United States) for visualization purposes.

CT analysis

CT images were processed with Syngo.via Enterprise Browser VB40 HF20 (Siemens Healthineers, Forchheim, Germany). The dynamic datasets were automatically loaded, centered, and oriented. As a next step, an intensity threshold was placed to differentiate arterial input flow data from surrounding tissue. Then two regions of interest (ROIs) were manually drawn in two image slices (comprising both shuttle modes) to derive an average AIF from the ROIs in the LVC. Next, three similar tissue volumes of interest (VOIs) were delineated in different image slices corresponding to the three myocardial regions, after which the software automatically contoured the entire VOIs. Based on the intensity profiles within the VOIs, i.e., the TRFs, the software automatically calculated local and regional MBF values using a maximum slope

method. Such method is derived from the Fick principle and calculates MBF by dividing the maximum gradient of the TRF by the peak of the AIF.[26,27]

MR analysis

The acquired images were analyzed using Intellispace software (Philips Healthcare, the Netherlands). The endocardial and epicardial contours were manually drawn in a single basal, mid ventricle, and apical slice. These were then automatically propagated to all dynamic phases. As a next step, a ROI was automatically drawn in the center of the endocardial contour to generate an AIF. Subsequently, a 6-tissue segment model was superimposed over the image slices in the short axis views, to generate segmental TRFs. The orientation of this segment model was manually oriented to match with the myocardial regions in the phantom.

Results

Figure 4 illustrates clinical analysis of two dynamic PET-MPI data sets. The use of different tissue mimicking material compositions resulted in varying tracer uptake as shown in the uptake polar maps. The tissue region depicted by heart segment 9 showed the highest tracer uptake level, corresponding to myo2 in the phantom. Tracer uptake was almost absent in segment 11, which matched myo3. The second row in **Figure 1** plots a repeated phantom measurement with background subtraction of previously accumulated radiotracer. Scan 1 and 2 showed a similar relative tracer uptake distribution across the mimicked myocardial tissue, though deviated from each other in terms of absolute computed MBF values. **Figure 5** demonstrates myocardial perfusion image visualization and analysis in CT. The top row illustrates a phantom image time-lapse across the short axis showing contrast arrival and distribution within the LVC and myocardial regions. A perfusion deficit was simulated in the rightmost tissue region. The figure displays typical MBF analysis of a VOI in consecutive image slices. An example dynamic phantom image series obtained with MRI is visualized in the top row of **Figure 6**. Underneath a typical (partial) software display is presented for subsequent perfusion analysis.

Multimodal TACs/TICs are displayed in **Figure 7**, highlighting contrast media distribution over time within the mimicked LVC and myocardial tissue regions/segments. **Table 2** provides an impression of software derived MBF values (from a single scan) compared to the set reference flow in the phantom setup.

Discussion

This explorative study had two main goals; at first to study overall functionality of our dedicated myocardial perfusion phantom for multimodal use and second to identify possible improvements in phantom setup design. The phantom results obtained

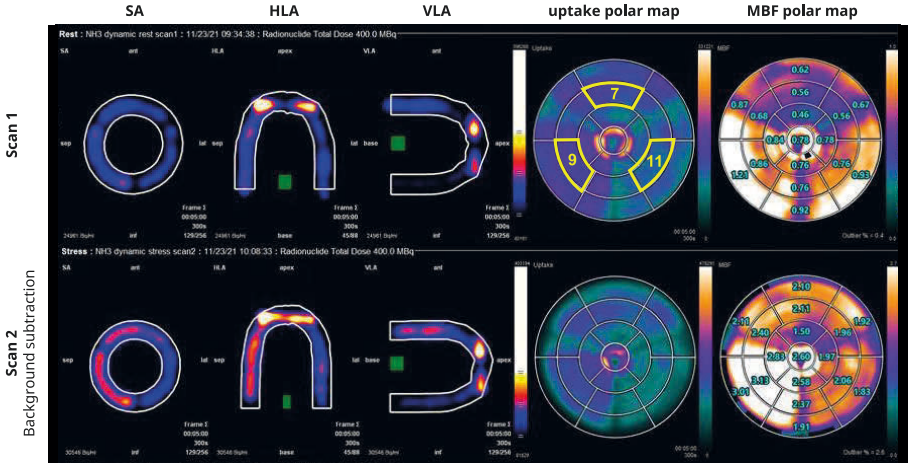

Figure 4 Two PET-CT myocardial perfusion imaging scans. The cross-sections along the sagittal axis (SA), horizontal longitudinal axis (HLA) and vertical longitudinal axis (VLA) display accumulated radiotracer activity. The green boxes indicate the regions of interest that were used to calculate the arterial input function. The polar plots show myocardial tracer uptake (left) and computed myocardial blood flow (MBF)(right). The three depicted heart segments (circled in yellow in the top uptake polar map) represent the center of the three phantom tissue regions (myo1–3) and were used for further tissue response function and MBF analysis.

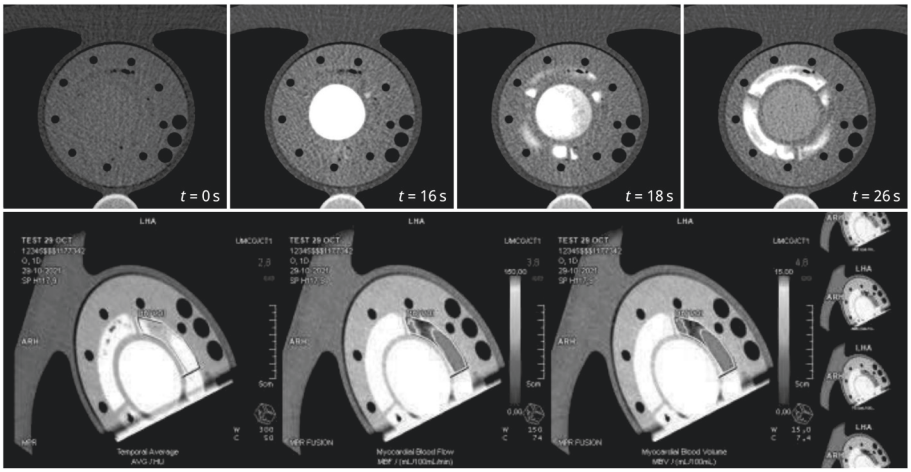

Figure 5 Example of CT myocardial perfusion image analysis. Top: visualizes a time-lapse across a short axis plane of the phantom showing contrast arrival and distribution in the mimicked left ventricular cavity (center) and three surrounding myocardial regions. The rightmost tissue region simulates a perfusion deficit (flow of 40 mL/min instead of 80 mL/min). Bottom: shows a typical software display of CT myocardial perfusion image analysis in consecutive image slices. The level of estimated myocardial blood flow within the manually delineated volume of interest is visualized by the added color, and ranges from 0 (purple) to 150 mL/100 mL/min (red).

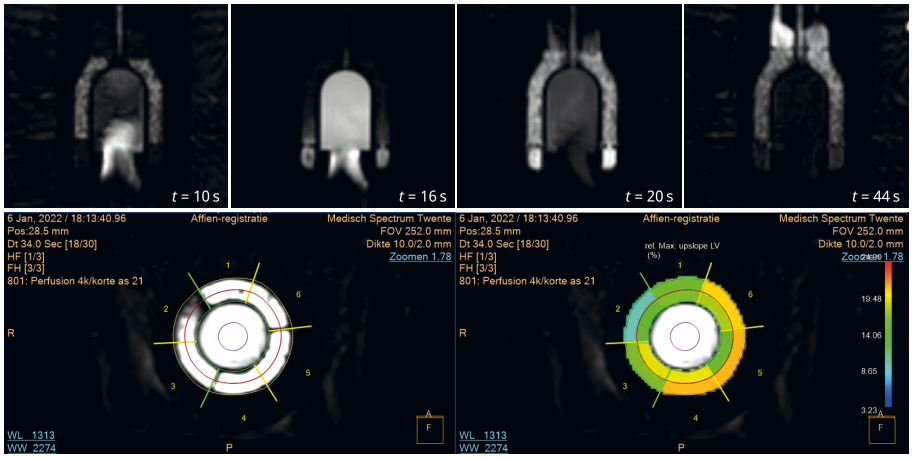

Figure 6 Example of MR myocardial perfusion image analysis. Top: visualizes a time-lapse across a longitudinal heart axis plane showing contrast arrival and distribution in the mimicked left ventricular cavity (center) and three surrounding myocardial regions. Bottom: clinical software display of segmental myocardial perfusion analysis. In this, segment 2 depicts a simulated perfusion deficit. The colors indicate the relative maximum upslope of the tissue region as a ratio of the maximum upslope in the left ventricular cavity, scaled from 3.23 to 24.90 %.

with PET/CT, CT, and MRI demonstrated successful completion of all the steps involved in these quantitative MPI applications: from dynamic image acquisition of contrast kinetics to subsequent perfusion analysis (multimodal software displays are provided in the **Supplement**). We will now further elaborate on the executed steps per imaging modality.

With the PET/CT phantom measurements, we wanted to verify whether it is possible to mimic myocardial uptake of $[^{13}N]NH_3$ using sorption technology. And if so, whether the subsequent accumulated detection of tracer activity in the phantom leads to recognition and mapping of patient realistic heart contours by clinical analysis software. These initial results show that zeolite indeed provides a certain amount of $[^{13}N]NH_3$ trapping, which appears to be controllable by using different tissue mimicking material compositions (**Figure 4 and 7**). As a result, the phantom heart contours were well recognized by the software, as with previous SPECT measurements.[18,28] No activity can occur at the location of the partitions in the myocardial tissue volumes of the phantom. We have used these markings in the polar maps to facilitate standardized orientation and evaluation. Manual adjustments in phantom orientation could be easily applied in the software. As a result, heart segment 7, 9 and 11 could be selected for further TAC and MBF analysis. These segments occupied the center of the myocardial volumes in the phantom. As can be seen in **Figure 7**, the TRF of heart seg-

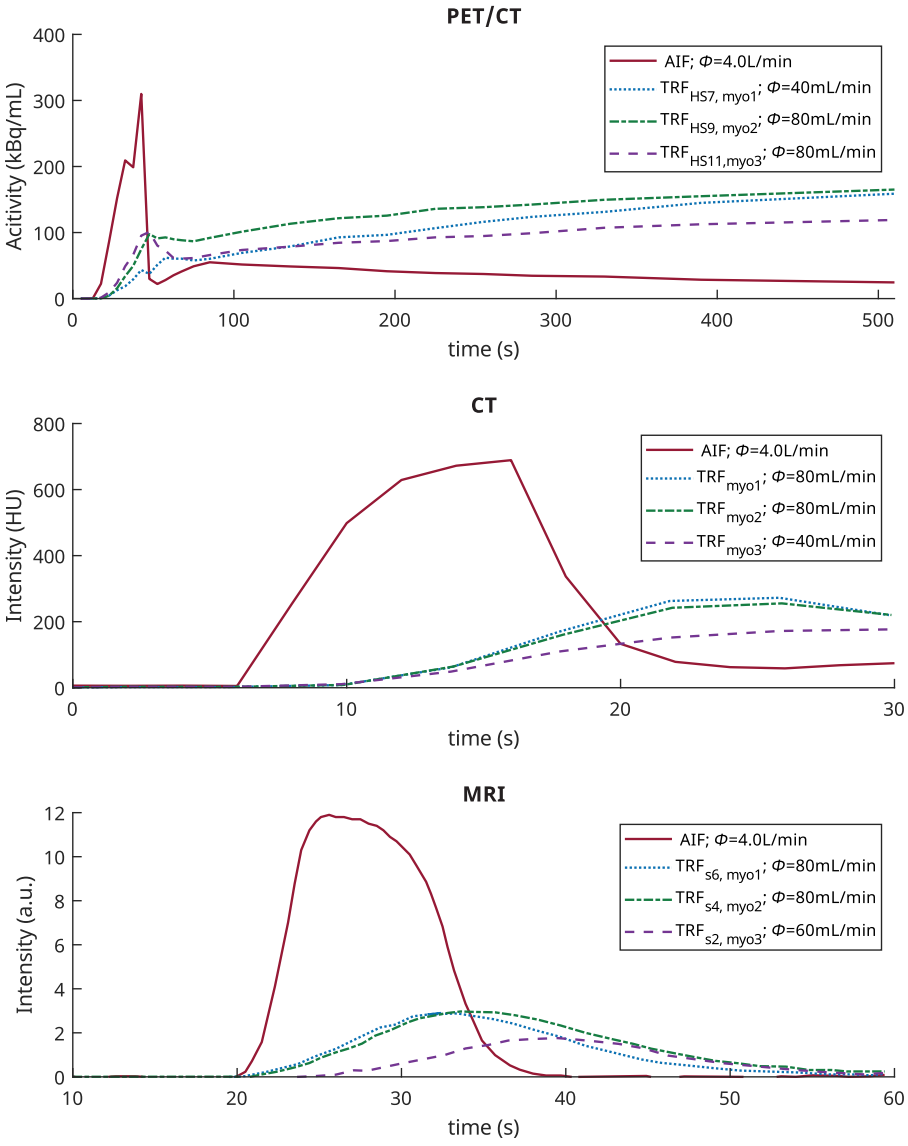

Figure 7 Example time activity / intensity curves for PET/CT, CT, and MRI phantom measurements displaying the arterial input function (AIF) and regional tissue response functions (TRFs). For PET/CT these regions comprised heart segment (HS) 7, 9 and 11, which matched the center of the three phantom myocardial regions (myo1–3). For CT these regions comprised myo1–3 in its total (manually delineated) and for MRI the segments (s) comprised parts of myo1–3. Note: the x-axes have different time scales.

Table 2 Impression of software derived myocardial blood flow (MBF) or other perfusion measures from a reference phantom measurement in PET/CT, CT, and MR.

Imaging modality	Myocardial region	Φ (mL/g/min)	MBF (mL/g/min)	TTP (s)
PET/CT	myo1	0.8	0.6	-
	myo2	1.6	0.9	-
	myo3	1.6	0.8	-
CT	myo1	1.6	4.5	-
	myo2	0.8	2.8	-
	myo3	1.6	4.3	-
MR	myo1	1.6	-	32.0
	myo2	1.6	-	32.0
	myo3	0.8	-	38.0

Φ = volume flux (reference flow); TTP = time to peak

ment 7 had a somewhat delayed uptake of radiotracer due to the lower flow setting. The stronger increase of this curve compared to the other TRFs can be explained by the larger amount of adsorption material present in this segment. Overall, the phantom TACs showed good resemblance with patient TACs.[29] Further research in finding the adequate tissue mimicking material composition and standardized fabrication hereof, may further enhance tracer kinetic phantom measurement of $[^{13}N]NH_3$ up to the level of two-compartmental blood flow analysis. Furthermore, we minimized adjustments to the closed flow circuit and used the same recirculation filter as applied in previous measurements with SPECT. However, we can derive from the slightly increasing TACs in **Figure 7** that using this setup a small amount of $[^{13}N]NH_3$ recirculated throughout the scan time at $t > 50$ s. An improved filter design should encounter for measurement and analysis of more controlled, first pass tracer kinetics. In line with this, we can also argue that current background subtraction method (provided by the analysis software) seems insufficient to correct for residual tracer activity in successive phantom measurements. In general, subtraction of TACs entails a certain measurement inaccuracy, which seems undesirable for the development of a validation phantom and hampers current MBF computation and phantom reproducibility.

The used phantom setup was not dedicated for measurements with CT; hence we performed a measurement series upfront for optimization purposes. With minimal adjustments to phantom and flow circuit design, it became possible to perform dynamic perfusion image acquisition using a slightly modified clinical protocol (see Video, Supplemental Digital Content 2). We performed initial perfusion analyses using associated clinical software. Remarkably, the mapped intensity profiles within the mimicked myocardium were higher compared to patient data.[30] This may be due to the made simplifications in phantom design in mimicking the pericardium and

myocardium as one. In future research more suitable tissue mimicking materials will be explored. Possibly this simplified anatomical representation also limits automatic delineation of the heart contours. Fortunately, we could manually delineate VOIs instead, though this type of evaluation is less easy to standardize for future research purposes and therefore less desirable for phantom validation purposes. MBF was subsequently calculated based on the average TICs within these VOIs. These values do not yet correspond to the reference values (**Table 2**) but do demonstrate the potential of future phantom application.

Minor adjustments to the phantom setup allowed us to obtain dynamic MR perfusion images according to clinical protocol. The obtained dynamic TIC signals in the LVC and myocardial regions were comparable to those in patients.[31] In this, a simulated perfusion deficit led to a delayed time to peak and a decreased maximum peak intensity compared to surrounding normal perfused tissue (see **Figure 7** and **Table 2**). It should be noted that the perfusion deficit as indicated in segment 2 of **Figure 6** and its associated TIC in **Figure 7** comprises only half the myocardial phantom region in which the deficit was located. A comprehensive analysis hereof is presented in the software display presented in Supplemental Digital Content 1. These quantitative perfusion measures are still relative and can therefore underdiagnose patients with balanced ischemia or microvascular dysfunction. The utilized MR imaging technique can be further improved, though is considered sufficient for this proof-of-concept phantom experiment. Within the cardiac MRI field, there are several dynamic imaging methods to look at myocardial perfusion, including calculating MBF. The latter can be done, for example, with arterial spin labeling.[32] In this technique no contrast agent is used, which greatly reduces the signal to noise ratio, but leads to a less robust application. At the moment this application is still in its infancy. Further development of this application can certainly benefit from the dedicated validation phantom as presented in this study.

This study has a few limitations. Only a limited number of measurements have been performed per imaging modality ($n = 3$), which is sufficient for a first feasibility check, though requires more extensive research to draw up an adequate set of requirements for multimodal phantom (re)design. In line with this, for a complete multimodal phantom design it is also important to consider the differences between scanner types and manufacturers, as well as clinical perfusion analysis software packages. In addition, better venting capabilities should be incorporated in the phantom design to diminish the presence of air bubbles. For example, small air bubbles were present during phantom measurements in CT, as depicted in the top myocardial region of the image time-lapse in **Figure 5**. Finally, this phantom feasibility study does not yet include quantitative MPI with contrast enhanced echocardiography. The materials used in current phantom model are not suited for use with ultrasound.

In conclusion, this phantom feasibility study in PET/CT, CT and MRI has shown that our adapted myocardial perfusion phantom setup offers the potential for multimodal functionality. With the current setup, we were able to successfully perform quantitative perfusion measurements using clinical applications and compare the results to a reference flow measure (indicative, not validated). From these initial phantom measurements, we have gained valuable insights to improve our multimodal phantom design. A next step is to further optimize and validate the mimicking of the respective (radiolabeled) contrast kinetics for each imaging modality.

Supplement

Multimodal perfusion analysis displays using clinical software.

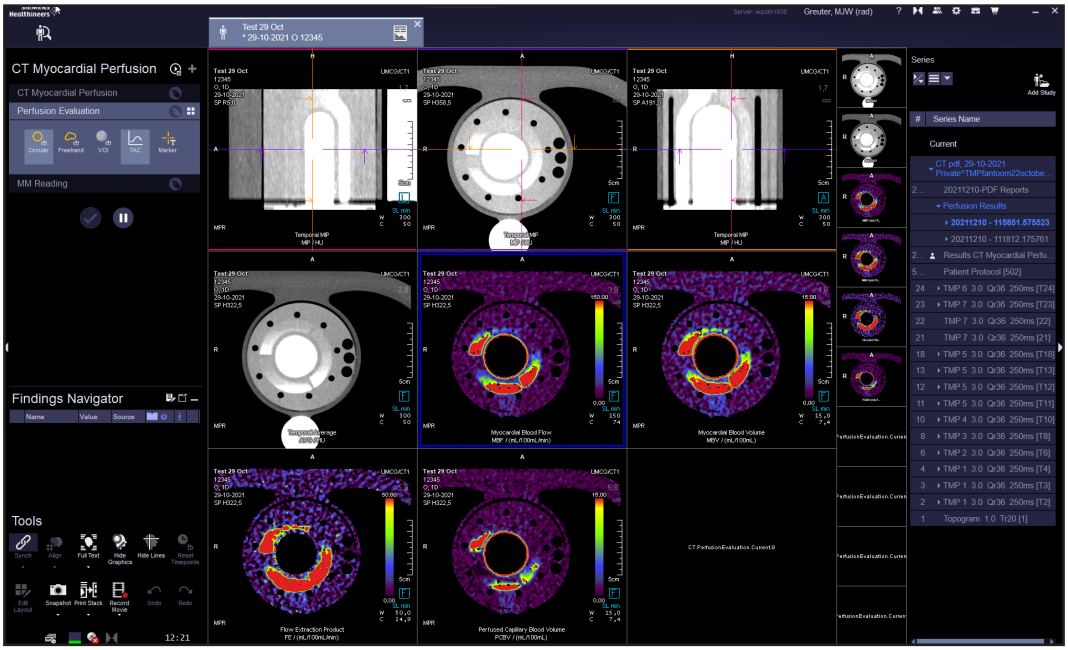

▲ ▼ CT perfusion analysis display using Syngo.via Enterprise Browser VB40 HF20 (Siemens Healthineers, Forchheim, Germany).

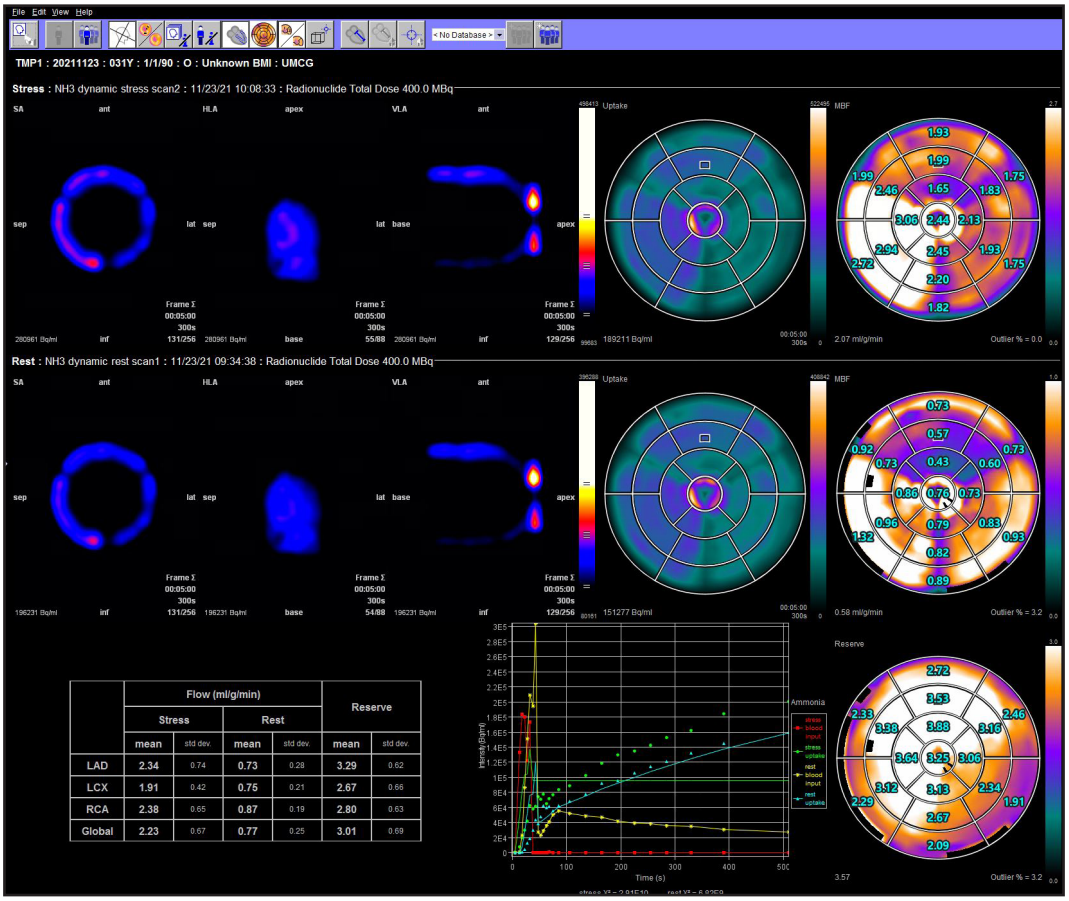

	Flow (ml/g/min)				Reserve	
	Stress		Rest			
	mean	std dev.	mean	std dev.	mean	std dev.
LAD	2.34	0.74	0.73	0.28	3.29	0.62
LCX	1.91	0.42	0.75	0.21	2.67	0.66
RCA	2.38	0.65	0.87	0.19	2.80	0.63
Global	2.23	0.67	0.77	0.25	3.01	0.69

▲ PET/CT perfusion analysis display using SyngoMBF VB14 (Siemens Healthineers, Forchheim, Germany).

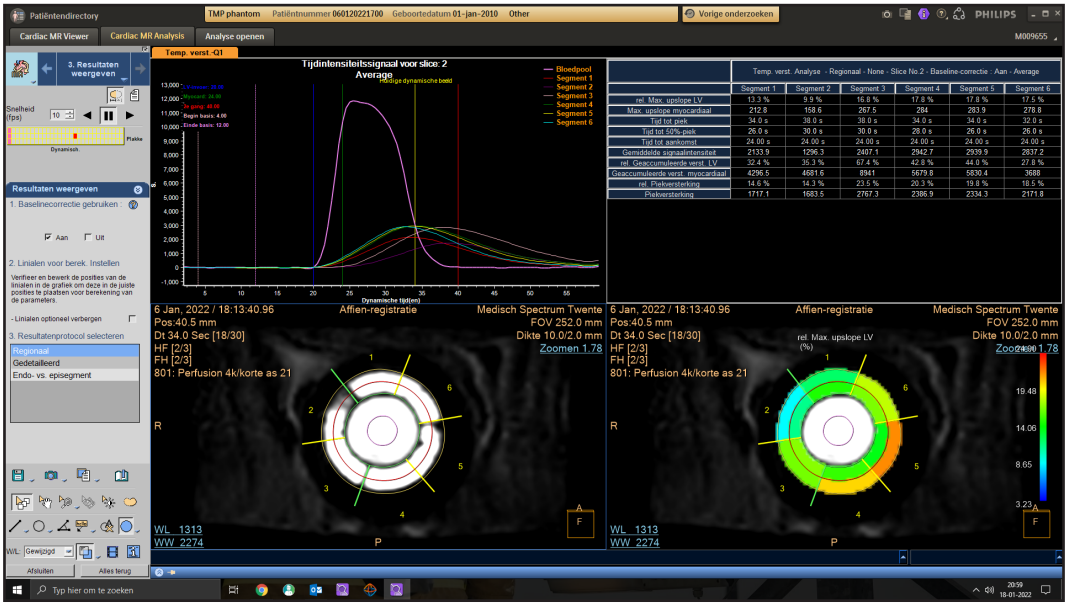

▲ MRI perfusion analysis display using Intellispace software (Philips Healthcare, the Netherlands).

References

1 Dewey M, Siebes M, Kachelrieß M, et al. Clinical quantitative cardiac imaging for the assessment of myocardial ischaemia. Nat Rev Cardiol. 2020;17(7):427-450. doi:10.1038/s41569-020-0341-8

2 Montalescot G, Sechtem U, Achenbach S, et al. 2013 ESC Guidelines on the Management of Stable Coronary Artery Disease. Vol 34.; 2013. doi:10.1093/eurheartj/eht296

3 Hyafil F, Gimelli A, Slart RHJA, et al. EANM procedural guidelines for myocardial perfusion scintigraphy using cardiac-centered gamma cameras. Eur J Hybrid Imaging. 2019;3(1). doi:10.1186/s41824-019-0058-2

4 Sciagrà R, Lubberink M, Hyafil F, et al. EANM procedural guidelines for PET/CT quantitative myocardial perfusion imaging. Eur J Nucl Med Mol Imaging. 2021;48(4):1040-1069. doi:10.1007/s00259-020-05046-9

5 Bindschadler M, Modgil D, Branch KR, La Riviere PJ, Alessio AM. Comparison of blood flow models and acquisitions for quantitative myocardial perfusion estimation from dynamic CT. Phys Med Biol. 2014;59(7):1533-1556. doi:10.1088/0031-9155/59/7/1533

6 Pelgrim GJ, Handayani A, Dijkstra H, et al. Quantitative Myocardial Perfusion with Dynamic Contrast-Enhanced Imaging in MRI and CT: Theoretical Models and Current Implementation. Kelle S, ed. Biomed Res Int. 2016;2016:1734190. doi:10.1155/2016/1734190

7 Carson RE. Tracer kinetic modeling in PET. In: Positron Emission Tomography. Springer; 2005:127-159.

8 Juárez-Orozco LE, Tio RA, Alexanderson E, et al. Quantitative myocardial perfusion evaluation with positron emission tomography and the risk of cardiovascular events in patients with coronary artery disease: A systematic review of prognostic studies. Eur Heart J Cardiovasc Imaging. 2018;19(10):1179-1187. doi:10.1093/ehjci/jex331

9 Ziadi MC. Myocardial flow reserve (MFR) with positron emission tomography (PET)/computed tomography (CT): Clinical impact in diagnosis and prognosis. Cardiovasc Diagn Ther. 2017;7(2):206-218. doi:10.21037/cdt.2017.04.10

10 Murthy VL, Bateman TM, Beanlands RS, et al. Clinical quantification of myocardial blood flow using PET: Joint position paper of the SNMMI cardiovascular council and the ASNC. J Nucl Med. 2018;59(2):273-293. doi:10.2967/jnumed.117.201368

11 Piekarski E, Manrique A, Rouzet F, Le Guludec D. Current Status of Myocardial Perfusion Imaging With New SPECT/CT Cameras. Semin Nucl Med. 2020;50(3):219-226. doi:10.1053/j.semnuclmed.2020.02.009

12 Slomka PJ, Miller RJH, Hu LH, Germano G, Berman DS. Solid-state detector SPECT myocardial perfusion imaging. J Nucl Med. 2019;60(9):1194-1204. doi:10.2967/jnumed.118.220657

13 Nieman K, Balla S. Dynamic CT myocardial perfusion imaging. J Cardiovasc Comput Tomogr. 2020;14(4):303-306. doi:10.1016/j.jcct.2019.09.003

14 Jerosch-Herold M, Seethamraju RT, Swingen CM, Wilke NM, Stillman AE. Analysis of myocardial perfusion MRI. J Magn Reson Imaging. 2004;19(6):758-770. doi:10.1002/jmri.20065

15 Everaars H, van Diemen PA, Bom MJ, et al. Comparison between quantitative cardiac magnetic resonance perfusion imaging and [15O]H2O positron emission tomography. Eur J Nucl Med Mol Imaging. 2020;47(7):1688-1697. doi:10.1007/s00259-019-04641-9

16 Vogel R, Indermühle A, Reinhardt J, et al. The quantification of absolute myocardial perfusion in humans by contrast echocardiography: Algorithm and validation. In: Journal of the American College of Cardiology. Vol 45. ; 2005:754-762. doi:10.1016/j.jacc.2004.11.044

17 Bulte CSE, Slikkerveer J, Meijer RI, et al. Contrast-enhanced ultrasound for myocardial perfusion imaging. In: Anesthesia and Analgesia. Vol 114. ; 2012:938-945. doi:10.1213/ANE.0b013e318248e261

18 Kamphuis ME, Kuipers H, Verschoor J, et al. Development of a dynamic myocardial perfusion phantom model for tracer kinetic measurement.

19 Zito F, De Bernardi E, Soffientini C, et al. The use of zeolites to generate PET phantoms for the validation of quantification strategies in oncology. Med Phys. 2012;39(9):5353-5361. doi:10.1118/1.4736812

20 Chai JW, Chen JH, Kao YH, et al. Spoiled gradient-echo as an arterial spin tagging technique for quick evaluation of local perfusion. J Magn Reson Imaging. 2002;16(1):51-59. doi:10.1002/jmri.10128

21 Potdevin TC, Fowlkes JB, Moskalik AP, Carson PL. Analysis of refill curve shape in ultrasound contrast agent studies. Med Phys. 2004;31(3):623-632. doi:10.1118/1.1649534

22 Ohno N, Miyati T, Chigusa T, et al. Technical note: Development of a cranial phantom for assessing perfusion, diffusion, and biomechanics. Med Phys. 2017;44(5):1646-1654.

23 Cho GY, Kim S, Jensen JH, Storey P, Sodickson DK, Sigmund EE. A versatile flow phantom for intravoxel incoherent motion MRI. Magn Reson Med. 2012;67(6):1710-1720. doi:10.1002/mrm.23193

24 D.Hutchins G, Schwaiger M, Rosenspire KC, Krivokapich J, Schelbert H, Kuhl DE. Noninvasive quantification of regional blood flow in the human heart using N-13 ammonia and dynamic positron emission tomographic imaging. J Am Coll Cardiol. 1990;15(5). doi:https://doi.org/10.1016/0735-1097(90)90237-J

25 Cerqueira MD, Weissman NJ, Dilsizian V, et al. Standardized myocardial segmentation and nomenclature for tomographic imaging of the heart. J Cardiovasc Magn Reson. 2002;4(2):203-210. doi:10.1081/JCMR-120003946

26 Rienmüller R, Baumgartner C, Kern R, et al. Quantitative Bestimmung der linksventrikulären Myokardperfusion mittels EBCT. Herz. 1997;22(2):63-71. doi:10.1007/BF03044305

27 Groves AM, Goh V, Rajasekharan S, et al. CT coronary angiography: Quantitative assessment of myocardial perfusion using test bolus data–initial experience. Eur Radiol. 2008;18(10):2155. doi:10.1007/s00330-008-0987-9

28 Kamphuis ME, de Vries GJ, Verschoor J, Slump CH. Development of a dedicated 3D printed myocardial perfusion phantom: Proof-of-concept in dynamic SPECT. Med Biol Eng Comput.

29 Mabrouk R, Dubeau D, Bentabet L. Dynamic Cardiac PET Imaging: Extraction of Time-Activity Curves Using ICA and a Generalized Gaussian Distribution Model. IEEE Trans Biomed Eng. 2013;60(1):63-71. doi:10.1109/TBME.2012.2221463

30 Yang D, Kim Y-H. CT myocardial perfusion imaging: current status and future perspectives. Int J Cardiovasc Imaging. 2017;33. doi:10.1007/s10554-017-1102-6

31 Coelho-Filho OR, Rickers C, Kwong RY, Jerosch-Herold M. MR Myocardial Perfusion Imaging. Radiology. 2013;266(3):701-715. doi:10.1148/radiol.12110918

32 Aramendía-Vidaurreta V, Echeverría-Chasco R, Vidorreta M, Bastarrika G, Fernández-Seara M. Quantification of Myocardial Perfusion With Vasodilation Using Arterial Spin Labeling at 1.5T. J Magn Reson Imaging. 2021;53(3). doi:10.1002/jmri.27396

7

General discussion

The aim of this thesis is to improve current CAD diagnostics by contributing to on-site validation and standardization of quantitative, multimodal MPI. The research objectives are:

1. Investigating the usability of contemporary flow phantom models for ground truth perfusion measurement in quantitative, multimodal MPI,
2. Defining multimodal phantom requirements for studying dynamic and quantitative MPI procedures, and
3. Developing a dedicated, multimodality myocardial perfusion phantom.

In this thesis, the reader is taken along in the empirical and iterative development process, which describes the need for and the realization of this dedicated myocardial perfusion phantom. Distinctive knowledge, insights and skills have been obtained along the way. Here we will reflect on to what extent the research objectives have been achieved and highlight some of the important lessons learned.

The first research objective has been accomplished. **Chapter 2** provides a systematic review of existing perfusion phantom setups for quantitative imaging. We have attempted to get a grasp on the diverse phantom approaches by presenting an overview of seemingly relevant aspects, including a cautious impression of contemporary phantom performance. The perspective from, and the purpose of looking at these data strongly affect its interpretation. With our phantom purpose in mind, the results presented in the review show that many phantom setups seem to focus on validating imaging technology and often use custom-built analysis software to assess and evaluate perfusion measurements. The review also shows that perfusion mimicking phantoms are usually represented by one physical compartment or at most a two-compartment representation. In the latter case, the fluid exchange between the 'blood' compartment and 'single-tissue' compartment is constructed via one or multiple aligned permeable membrane(s). Yet control over these mimicked myocardial contrast uptake and retention rates, as denoted by the transfer rate constants (e.g., K_1 and k_2), is restricted. In this, higher order contrast kinetic models are fully disregarded. The restricted control over contrast uptake and retention characteris-

tics narrows the possibilities for multimodality phantom application. Striking was that only one of these phantoms is commercially available. Based on these findings we can conclude that current phantom models are insufficient for ground truth perfusion measurement in quantitative, multimodal MPI. Nonetheless we did gain useful insight in possible phantom design, fabrication, and evaluation methods for the development of our own dedicated myocardial perfusion phantom.

Research objective 2 has been achieved as well. The work as presented in **Chapter 3–6** contributed to the establishment, evaluation, and refinement of multimodal phantom requirements. As mentioned, we have observed that contemporary MPI phantoms are mainly focused on validation of novelty in MPI imaging technology. In this thesis, we opt for a reversed approach by developing a functional imaging phantom with the initial purpose to answer clinical questions related to clinical workflows. This functional, multimodality imaging phantom requires: i) sufficient mimicking of the physical appearance of the heart, mainly the left ventricle, to enable phantom compatibility with MPI hardware and software, ii) adequate mimicking of arterial input flow to facilitate dynamic contrast measurement and derivation of arterial input functions that fall within a standardized normal and pathological patient range, iii) advanced mimicking of myocardial perfusion to facilitate dynamic contrast measurement and derivation of tissue response functions that fall within a standardized normal and pathological patient range.

The third and final research objective has been largely achieved. During the iterative phantom development process, the set phantom requirements were translated into a proof-of-concept phantom design, after which this design was realized, tested, and evaluated with dynamic SPECT-MPI (**Chapter 3**). In **Chapter 4** and **Chapter 5** we have refined the phantom model, followed by additional testing and evaluation, again with dynamic SPECT-MPI. **Chapter 6** concluded with initial phantom testing of an extended phantom setup in multiple imaging modalities, including PET, CT, and MRI. Below a brief overview is stated on gained insights, and progress regarding the presented phantom development process. Recommended next steps in phantom development are discussed as part of the outlook.

In our experience, it is most effective and efficient to divide ultimate phantom goal(s) into manageable subgoals and work towards consecutive phantom iterations, preferably using modular building blocks. At the very beginning of this work, an attempt was made to create a fully dynamic and multimodal myocardial perfusion phantom from scratch. It soon became clear that the desired phantom setup was incredibly complicated to realize, control, let alone validate. It makes more sense to build up expertise from a simplified, controllable basis and then proceed with manageable steps towards model refinement and extension to meet the stated (sub)goals. This thesis has focused therefore on a stationary left ventricular flow phantom design,

keeping in mind the ultimate goal of incorporating motion dynamics as well. In addition, a large part of the presented work (**Chapter 3–5**) has been dedicated to phantom measurements in dynamic SPECT-MPI. The main reason for this has been the local accessibility and expertise regarding this clinical workflow. In **Chapter 6**, we then tested the refined phantom model on multimodal MPI workflows and obtained promising first results. The use of modular building blocks supports phantom iteration and is therefore recommended in addition to the advice to build from a simple phantom to the desired phantom complexity. An example hereof is that the various flow circuit components, such as the contrast inlet module, can be designed for multi-purpose (re)use. Another example is that the custom-built control unit can steer multiple pumps and can read and display multiple analog and digital signals (e.g., pressure and flow sensor outputs) simultaneously, which makes it widely applicable. A general advantage of this modular approach is that optimization efforts can easily run in parallel.

To underpin phantom realization, we utilized expertise from various disciplines in addition to biological and medical imaging expertise. In line with this, we believe that the use of 3D printing technology in combination with membrane and sorption technology are key in achieving our phantom requirements. The 3D printing technology has been used to construct a phantom with the physical and functional appearance of a general left ventricle. In **Chapter 3** the created prototype consisted of separate, 3D printed parts that were connected by additional connectors and silicone tubes. This somewhat cumbersome method sufficed in achieving our proof-of-concept goal. We achieved a phantom compatibility with a clinical MPI scanner and software package because of the incorporated left ventricular phantom shape. Our next phantom prototype, as described in **Chapter 4**, was specifically designed for manufacturing with 3D printing. This resulted in a leak-free, cardiac flow phantom containing internal left ventricular structures and connected volumes. In general, 3D printing technology is vastly suitable for fabrication of such complex 3D anatomical structures and volumes at a detailed level. An additional advantage of 3D printing comprises the ability for rapid prototyping, which is also apparent from the fact that more models have been printed than described in this thesis. Printed phantoms can consist of patient-specific or more general models and can vary in complexity depending on the intended goals. Partly because of these described advantages we observe a shift towards additional use of 3D printing technology in the development of diverse (cardiac) imaging phantoms.[1–4] There are many further possibilities to explore in this field.[5,6] For example, it might be interesting to study 3D printing of other materials or combinations of materials (e.g., in terms of stiffness).

The added value of using membrane and sorption technology in phantom development concerns the mimicking of contrast kinetics in tissue. Contemporary perfusion

phantoms are limited in mimicking advanced and tracer specific kinetic behavior, as is also the case in our proof-of-concept phantom in **Chapter 3**. The TAC results obtained with this phantom showed a restricted comparability with patient TRFs (absence of tracer trapping, $k_3 = 0$). These limitations in tissue mimicking properties also resulted in an inverse relationship between phantom setup flow and estimated MBF, making the phantom unsuitable for ground truth evaluation of quantitative MPI. For these reasons, we have introduced a novel concept to mimic compartmental contrast kinetics in **Chapter 4**. This concept was demonstrated by filling the myocardial compartments in the phantom with various sorbent material compositions. Subsequent phantom measurements in dynamic SPECT-MPI showed that the type and amount of sorbent poured into the phantom compartment affected the kinetics of the passing contrast medium within this compartment. These results implicate that we can potentially mimic patient representative (temporary) trapping of a specific contrast agent locally. In this, sorption processes, including ion exchange and adsorption, are of particular interest. These can essentially mimic freely diffusible contrast kinetics in tissue, reversible binding of contrast media, and irreversible binding of contrast media to cells. In **Chapter 5** we have shown that this sorption-based concept is, in a way, similar to (higher order) tracer kinetic modelling approaches. Subsequently we showed in **Chapter 6** that detailed tracer uptake and retention characteristics can be pursued for dynamic PET-MPI as well. A different tissue-mimicking approach might be desirable for other types of contrast media. This might be the case for iodine containing CT contrast media, as these media hardly leave the microcirculation. We believe that the combination of membrane and sorption technology could further improve the mimicking of myocardial perfusion dynamics in phantoms, potentially up to the level of ground truth MBF assessment in multimodal MPI. With the current setup the absolute mean error between phantom reference flow (1.5 mL/g/min) and software derived MBF was 0.4, 0.1 and 0.1 mL/g/min for the LAD, RCA, and LCX region, respectively. Further research into the presented tissue mimicking concept, together with phantom setup optimization and validation, could potentially mimic such myocardial perfusion dynamics up to the level of ground truth MBF assessment in multimodal MPI.

Outlook

The long-term aim of this line of research is to enable ground truth flow and perfusion measurement in quantitative, multimodal MPI. Below we describe some necessary follow-up steps in phantom development to achieve this overall aim. In addition, we describe a few examples of foreseen phantom applications. The outlook concludes with a future perspective for functional imaging phantoms in general.

Next steps in phantom development

Based on the insights gained in this thesis we can make several recommendations for next steps in phantom development. Some of these recommendations, as illustrated in **Figure 1**, will be now explained in more detail.

1. Phantom optimization

It seems a logical next step to adapt the current phantom design to an easily interchangeable module. In current prototype the trapping of tracer in the mimicked tissue causes undesirable buildup of background activity upon successive phantom measurements. These effects hamper reliable perfusion analysis and can be avoided in a next phantom-design iteration by replacing the tissue module (or entire phantom) in between measurements. In addition, we recommend altering the current myocardial tissue model into a physical 17 heart segment tissue model.[7] This does not necessarily have to comprise the full 17 segments, but a few segments or merging of some segments. We foresee significant benefits in standardized perfusion analysis with such model. Moreover, the flow supply to these 17 phantom segments will be more challenging to control (compared to three parallel flows in the current phantom) but will also be a more accurate and desirable representation of the coronary territories. It could for instance facilitate adequate flow measurement in the apex region. Lastly, this modular, heart segment approach enables research onto the control over (radiolabeled) contrast kinetics in an isolated, well defined, small-scale environment, i.e., in one single segment. Various combinations of membrane

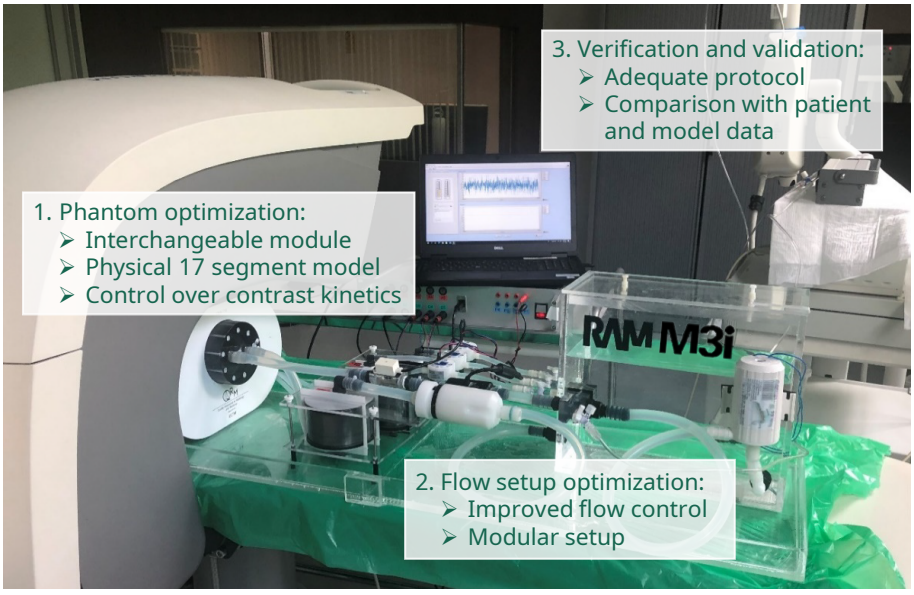

Figure 1 Next steps in phantom development.

and (ad)sorption technology can be applied and studied within this standard module in order to achieve the desired contrast specific kinetics. By doing this on a relatively small scale, it becomes more practical to test and refine these tissue-mimicking modules in preclinical imaging systems. When satisfied, we can incorporate these tissue modules in overall cardiac phantom design and execute phantom testing and validation in the multimodal clinical setting.

2. Flow setup optimization

In the current setup, the flow is regulated by tuning the pumping speed and manual adjustment of resistances (taps). However, flow sensors combined with a measurement system are required to regulate the desired flow settings on site. Once the resistances have been set, the flow sensors and flow sensor readouts become redundant as the settings remain constant during the phantom measurement and scan duration. It would therefore be more convenient to incorporate a number of pre-calibrated flow resistors (apertures) in a standardized setup. The aim hereof is to simplify the current setup, make it more user-friendly and reproducible to regulate flows. Such a setup is also easier to make MRI compatible, without the need for extended tubes. The required electronics then only concern the pump itself and these are available in MRI compatible types. In addition, a modular approach is key for realization of this multi-deployable flow setup. An example hereof comprises the recirculation filters, which need further design optimization as well. The purpose of such filter is to extract passing contrast media in order to prevent undesired recirculation of contrast in the phantom (thereby enabling measurement of first-pass contrast kinetics). An adequate filter design is closely related to the molecular structure of the respective contrast medium that needs to be filtered out. Hence the filter should be easily exchangeable depending on the phantom application.

3. Verification and validation

Initial verification steps were taken in **Chapter 5**. Due to this preliminary analysis, we realized even more how important it is to validate phantom results with representative patient data and physiological model data. We recommend using Sargent's theory on model verification and validation[8] in determining an adequate phantom verification and validation strategy. Van Meurs' interpretation of this theory, including a practical checklist, is also applicable to physical, biomedical models (in adjusted form).[9] Moreover, it is advised to start already collecting relevant patient and model data for validation purposes in parallel to further expedite phantom development.

Expected phantom applications

With this functional imaging phantom, we aim to realize ground truth myocardial perfusion assessment for dynamic, quantitative MPI. Such phantom model allows broadening of our understanding on aspects influencing perfusion measurement in

current and future clinical workflows. Some specific examples of foreseen phantom applications are listed below, thereby aiming to give an idea of its potential value.

Example 1. Clinical implementation of multimodal, quantitative MPI procedures varies widely.[10,11] For example, centers can choose between a one-day stress and rest protocol, or a two-day stress and rest protocol. In a two-day SPECT-MPI protocol, the accumulated radiotracer in the body has decayed substantially before the second scan is started. With a one-day protocol, the consecutive scan is started while residual radiotracer activity is still present in the myocardium. The amount of residual activity at the start of the second scan is reflected by the amount of administered radiotracer activity, the half-life time of the particular radiotracer used, and the time interval between both scans. Often the choice is made to administer a higher radioactive dosage for the second scan in a single-day MPI protocol. This in order to maintain a good SNR for further perfusion analysis. Using our phantom setup, it becomes feasible to study the effects of radiotracer protocol and scan interval on MBF measurement accuracy and precision via comparison with a ground truth. In this way, clinical workflow validation and optimization can be studied, also in terms of dose reduction and logistic efficiency.

Example 2. Another effect that is interesting to mimic in a controlled and representative environment is that of patient size on multimodality MBF measurement accuracy and precision. For example, for dynamic MPI with PET and SPECT it could be interesting to research the possibilities for patient specific dose protocols. The decreasing image quality in patients with a high body mass index can be compensated by administration of a relatively higher patient-specific dose, as has already been proposed for static MPI workflows.[12,13]

Example 3. A third example is to study the direct comparability between different scanner types and between different imaging modalities, since there are manufacturer-specific variations in imaging detector technology, and dynamic imaging and reconstruction protocols. Via phantom studies one can study the similarities and dissimilarities between these scanner hardware and software, which is a key aspect in harmonization.

A future phantom perspective

This phantom has many possible uses that merit further exploration. In our opinion, the application of functional imaging phantoms in general deserves further exploration as well. Our conventional view of imaging phantoms might come across as a technology driven domain, with a strong focus on imaging technology validation and system quality assurance and control. Simply put, those imaging phantoms are physical models that are commonly used by (medical) physicists, engineers, and imaging technologists to verify, validate and/or guarantee image quality in today's and to-

morrow's imaging systems. Clinicians understand the importance of such phantom research but are not likely to regard it as their own field of work, where the patient is central. The use of model and system thinking (as common in more fundamental sciences and engineering), on the other hand, is an elegant way to gain insight in and understanding of complex processes. By considering imaging phantoms more as physical models of comprehensive patient functioning, its extended application domain might become interesting for professionals with both a technical and medical background. After all, both parties have a common main objective: to get a better understanding and grip on how we can translate (innovation in) medical imaging diagnostics into added value for the individual patient in daily clinical practice. By broadening both disciplinary frameworks on validation, we can together strive for embedded phantom usage as part of clinical guidelines and in that way ensure the quality of entire imaging procedures. Perhaps these clinically dedicated models may be even characterized as next generation imaging phantoms because of their envisioned added value in connecting technical and medical disciplines more effectively, thereby enriching the evolving medical imaging domain through synergy.

Concluding remarks

In conclusion it is important to not lose sight of our overall research aim. Ultimately, patients with (suspected) CAD deserve to undergo the most adequate treatment based on the best possible personalized disease diagnostics. We aim to contribute to this endeavor by supporting on-site validation and harmonization of multimodal, quantitative MPI, which is essential in CAD diagnostics. In this thesis, the foundation has been laid for the development of a multimodality validation phantom for dynamic and quantitative MPI procedures. Broad application of these functional imaging phantoms could provide valuable insight into (and hopefully some grip onto) the evolving MPI field in a controlled, clinical, and patient representative environment.

Our final remark concerns something obvious that in our view is still worth mentioning and should not be underestimated. Namely, a fully accomplished validation phantom, like this one in development, owes its successful implementation to a multidisciplinary team effort. Many different students and experts in the field(s) have contributed to the realization of this functional imaging phantom. These inspiring people include clinicians, technical physicians, engineers (e.g., biomedical, mechanical, and electrical), imaging technologists, technicians, chemists, and medical physicists. Along the way we have seen unique opportunities arising from combining these different areas of expertise and consider it indispensable.

References

1 J. Grice, S. Green, and A. Yuhas, "An Improved 3D Printed Cardiac Phantom," J. Nucl. Med., vol. 61, no. supplement 1, pp. 391 LP – 391, May 2020.

2 K. Abdullah, M. McEntee, W. Reed, and P. Kench, "Development of an organ-specific insert phantom generated using a 3D printer for investigations of cardiac computed tomography protocols," J. Med. Radiat. Sci., vol. 65, Apr. 2018.

3 Z. Jin et al., "3D Printing of Physical Organ Models: Recent Developments and Challenges," Adv. Sci., vol. 8, no. 17, p. 2101394, Sep. 2021.

4 S. Wang et al., "Development and Testing of an Ultrasound-Compatible Cardiac Phantom for Interventional Procedure Simulation Using Direct Three-Dimensional Printing," 3D Print. Addit. Manuf., vol. 7, no. 6, pp. 269–278, Sep. 2020.

5 E. M. Lindquist et al., "3D printing in cardiology: A review of applications and roles for advanced cardiac imaging," Ann. 3D Print. Med., vol. 4, p. 100034, 2021.

6 S. Zabala-Travers, "Biomodeling and 3D printing: A novel radiology subspecialty," Ann. 3D Print. Med., vol. 4, p. 100038, 2021.

7 M. D. Cerqueira et al., "Standardized myocardial segmentation and nomenclature for tomographic imaging of the heart," J. Cardiovasc. Magn. Reson., vol. 4, no. 2, pp. 203–210, 2002.

8 R. G. Sargent, "Verification and validation of simulation models," in 2007 Winter Simulation Conference, 2007, pp. 124–137.

9 W. Van Meurs, Modeling and simulation in biomedical engineering - Applications in cardiorespiratory physiology. The McGraw-Hill Companies, 2011.

10 R. Sciagrà et al., "EANM procedural guidelines for PET/CT quantitative myocardial perfusion imaging," Eur. J. Nucl. Med. Mol. Imaging, vol. 48, no. 4, pp. 1040–1069, 2021.

11 B. Hesse et al., "EANM/ESC procedural guidelines for myocardial perfusion imaging in nuclear cardiology," Eur. J. Nucl. Med. Mol. Imaging, vol. 32, no. 7, pp. 855–897, 2005.

12 J. D. van Dijk et al., "Development and validation of a patient-tailored dose regime in myocardial perfusion imaging using conventional SPECT," J. Nucl. Cardiol., vol. 23, no. 1, pp. 134–142, Feb. 2016.

13 J. D. van Dijk et al., "Development and validation of a patient-tailored dose regime in myocardial perfusion imaging using CZT-SPECT," J. Nucl. Cardiol., vol. 21, no. 6, pp. 1158–1167, 2014.

Summary

This thesis aims to improve current coronary artery disease diagnostics by contributing to on-site validation and standardization of quantitative, multimodality myocardial perfusion imaging (MPI). For quantitative MPI it is necessary to record the kinetics of the administered (radiolabeled) contrast medium over time. The resulting dynamic image series allow for perfusion analysis by contrast kinetic modelling. Using these models, estimation of myocardial blood flow and myocardial flow reserve can improve assessment of myocardial ischemia in addition to visual evaluation. It can thereby improve diagnostics particular in patients with balanced ischemia and microvascular dysfunction.

Nonetheless such innovations also come with challenges that need to be addressed to ensure safe and adequate embedding in clinical practice. Before a clinician can rely on quantitative (or even absolute) perfusion values, the measurement technique ought to be reliable and robust. Due to differences in MPI scanner and software technologies, it is challenging to realize validation and standardization by patient studies alone. The use of functional imaging phantoms could contribute to this clinical need. Even though such phantom models will never fully mimic a patient's relevant anatomy and (patho-)physiology, it may facilitate ground truth flow/perfusion measurement for quantitative MPI in a controlled and representative environment. By obtaining a better understanding and control of the similarities and dissimilarities in the broad spectrum of quantitative MPI, the implementation of harmonized cut-off values for treatment decision making comes within reach.

Our first research objective involved studying the usability of contemporary flow phantom models for ground truth perfusion measurement in quantitative MPI. Therefore, a systematic review on existing perfusion phantom setups for quantitative imaging is provided in **Chapter 2**. Results hereof show that phantom endeavors mainly focus on validating imaging technology and often involve custom-built analysis software to evaluate perfusion measurements. The review also indicates that perfusion mimicking phantoms are represented by one or two physical compartment(s). Higher order models are absent. Control over the contrast uptake and retention

rates in tissue mimicking is restricted, narrowing phantom application possibilities. Based on these findings we can conclude that current phantoms are inadequate for ground truth perfusion measurement in quantitative, multimodal MPI. Nonetheless the review helped to gain insight in possible phantom design, fabrication, and evaluation methods for developing a dedicated myocardial perfusion phantom.

Research objective 2 is achieved as well, which comprised defining the set of requirements. This functional, multimodality imaging phantom requires: i) sufficient mimicking of the physical appearance of the heart, mainly the left ventricle, to enable phantom compatibility with MPI hardware and software, ii) adequate mimicking of arterial input flow to facilitate dynamic contrast measurement and derivation of arterial input functions that fall within a standardized normal and pathological patient range, iii) advanced mimicking of myocardial perfusion to facilitate dynamic contrast measurement and derivation of tissue response functions that fall within a standardized normal and pathological patient range.

The final research objective, comprising multimodality phantom development, has been largely achieved. During this empirical and iterative phantom development process, the phantom requirements were translated into a proof-of-concept phantom design, after which this design was realized, tested, and evaluated with dynamic SPECT-MPI (**Chapter 3**). Thereafter, we have refined the phantom model, followed by additional testing and evaluation (**Chapter 4**). This phantom design utilizes the benefits of 3D printing technology by incorporating the 3D physical and functional appearance of a generic left ventricle. Phantom results showed good compatibility with clinical MPI hardware and software because of this patient representative design. In addition, we introduced a novel concept to mimic compartmental contrast kinetics. The concept was demonstrated by filling the myocardial compartments in the phantom with various sorbent material compositions. Subsequent phantom measurements in dynamic SPECT-MPI showed that the type and amount of sorbent used, affected the kinetics of the passing contrast medium within this phantom compartment. Resulting time activity curves were in good agreement with patient data. These findings implicate that we can potentially mimic patient representative (temporary) trapping of a specific contrast agent locally. Sorption processes, including ion exchange and adsorption, are of particular interest as these can essentially mimic freely diffusible contrast kinetics in tissue, reversible binding of contrast media, and irreversible binding of contrast media to cells. In **Chapter 5** it is shown that this sorption-based concept is similar to (higher order) tracer kinetic modelling approaches. The thesis concludes with a feasibility study of the extended phantom setup for multimodal use, including PET, CT, and MRI (**Chapter 6**). The results showed compatibility with these scanners and software packages, and highlighted possibilities for multimodal phantom use. We foresee that the combination of membrane and sorp-

tion technology can further enhance the mimicking of tissue perfusion dynamics in multimodality perfusion phantoms, in MPI potentially up to the level of ground truth myocardial blood flow assessment. Currently, we have achieved an absolute mean error between ground truth phantom flow (1.5 mL/g/min) and software derived MBF of 0.4, 0.1 and 0.1 mL/g/min for the LAD, RCA and LCX region, respectively. This novel tissue-mimicking approach needs to be further researched and validated for different contrast media. In addition, several recommendations have been made to further optimize the multimodality phantom setup. It is advised to already start collecting relevant patient and model data for validation purposes in parallel to further expedite phantom development.

In conclusion, the foundation is paved for the development of a multimodality validation phantom for ground truth perfusion measurement in quantitative MPI. Broad application of this phantom can provide valuable insight into the evolving MPI field in a controlled, and patient representative environment. Functional imaging phantoms in general have many application possibilities that merit further exploration. We encourage a future perspective wherein the use of functional imaging phantoms becomes incorporated in clinical guidelines to ensure quality of quantitative perfusion imaging procedures. These clinically dedicated models may be even characterized as next generation imaging phantoms because of their envisioned added value in more effectively connecting technical and medical disciplines, thereby enriching the evolving medical imaging domain through synergy.

Samenvatting

Het doel van dit proefschrift is een bijdrage te leveren aan de (lokale) validatie en standaardisatie van kwantitatieve beeldvorming van de bloeddoorstroming van de hartspier (myocard perfusie of MPI). MPI is essentieel voor het kunnen stellen van een adequate diagnose en prognose van patienten met (een verdenking op) kransslagaderlijden. De aanwezigheid van myocardiale ischemie is een belangrijke indicatie voor de te bepalen behandelstrategie. Bij kwantitatieve MPI is het noodzakelijk om de verdeling van een toegediend contrastmiddel (of radiofarmacon) af te beelden gedurende een bepaalde scantijd. Met behulp van een dergelijke dynamische afbeeldingsreeks van het contrastmiddel kan de regionale weefseldoorbloeding (in mL/g/min) worden bepaald met zogenaamde kinetische modellen. Deze waardes kunnen worden toegevoegd aan de huidige visuele beoordeling en kunnen leiden tot een verbeterde diagnostiek met name bij patiënten met gebalanceerde ischemie en microvasculair lijden. Tevens biedt kwantitatieve MPI de mogelijkheid tot een meer objectieve – te standaardiseren – vorm van evaluatie van de doorbloeding van de hartspier.

Er zijn echter nog de nodige uitdagingen om een dergelijke innovatie veilig en adequaat te kunnen integreren in de klinische praktijk. Voordat bijvoorbeeld een clinicus kan vertrouwen op kwantitatieve (of zelfs absolute) perfusie waardes, zal eerst aangetoond moeten worden dat de meettechniek betrouwbaar en robuust is. Vanwege de grote diversiteit in scanners en software technologie is validatie en standaardisatie erg lastig te realiseren, zeker met alleen patiëntstudies. Functionele fantomen voor beeldvorming zouden in deze klinische behoefte kunnen voorzien. Een dergelijk fantoom zal nooit de anatomie en (patho-)fysiologie van een patiënt volledig kunnen nabootsen, maar het zou wel referentiewaardes kunnen opleveren in een gecontroleerde klinische omgeving. Op deze manier kunnen we meer inzicht en grip krijgen op de verschillende kwantitatieve MPI procedures. De implementatie van geharmoniseerde drempelwaarden kunnen bijdragen tot een betere besluitvorming voor eventuele behandeling van de patiënt: wel of niet invasief behandelen, of juist helemaal geen behandeling.

Onze eerste onderzoeksdoelstelling betrof het bestuderen van de bruikbaarheid van hedendaagse flow / perfusie fantoom modellen voor referentie perfusiemetingen in kwantitatieve MPI. **Hoofdstuk 2** beschrijft daarom een systematisch review waarin bestaande perfusie fantoom opstellingen voor kwantitatieve beeldvorming worden beschreven. De resultaten laten zien dat de geïncludeerde fantoomstudies zich voornamelijk richten op het valideren van beeldvormende technologie, en regelmatig gebruik maken van op maat gemaakte analyse software voor evaluatie van MPI. Bovendien wordt weefseldoorbloeding gesimuleerd door één of hoogstens twee fysieke compartimenten, waarbij uitgebreide fantoom modellen ontbreken. Omdat de controle over de contrastopname en -retentie zeer beperkt is in deze fantoom opstellingen, zijn de toepassingsmogelijkheden relatief klein. Op basis van deze bevindingen kunnen wij concluderen dat de huidige beschikbare fantomen ontoereikend zijn voor het doel dat wij voor ogen hebben. Desalniettemin heeft het review geholpen om inzicht te krijgen in mogelijk fantoom ontwerp, fabricage en evaluatie methoden voor de ontwikkeling van een specifiek fantoom voor myocard perfusie en geschikt voor meerdere modaliteiten.

Ook onderzoeksdoel 2 is behaald en bestaat uit het definiëren van het eisenpakket. Dit functionele, multimodale fantoom vereist: i) afdoende nabootsing van de fysieke geometrie van het hart, voornamelijk van de linker hartkamer, om zo fantoom compatibiliteit te verkrijgen met MPI hardware en software, ii) adequate nabootsing van gestandaardiseerde arteriële flow om dynamische contrastmeting over tijd na te bootsen, en iii) geavanceerde nabootsing van gestandaardiseerde myocardiale perfusie om dynamische contrastmeting te realiseren, zowel binnen als buiten de normaalwaarden.

Het overkoepelende onderzoeksdoel, namelijk fantoom ontwikkeling voor multimodaal gebruik, is grotendeels behaald. Tijdens dit empirische en iteratieve ontwikkelproces zijn de fantoomeisen vertaald naar een proof-of-concept fantoom ontwerp, waarna dit ontwerp is gerealiseerd, getest en geëvalueerd met dynamische SPECT-MPI (**hoofdstuk 3**). Daarna hebben we het fantoom model verfijnd, gevolgd door aanvullende testen en evaluatie (**hoofdstuk 4**). Dit fantoom ontwerp maakt gebruik van de voordelen van 3D-print technologie om de geometrie van een generiek linker hartkamer te incorporeren. Vanwege dit ontwerp is het gelukt om de doorbloeding in het fantoom te meten met een SPECT scanner en te analyseren met klinische software. Daarnaast hebben we een nieuw concept geïntroduceerd om compartimentale contrast kinetiek na te bootsen, door de myocardiale compartimenten in het fantoom te vullen met verschillende samenstellingen van sorptie materiaal. Daaropvolgende fantoom metingen in dynamische SPECT-MPI toonden aan dat het type en de hoeveelheid gebruikte sorbent de kinetiek van het passerende contrastmiddel in dit fantoom compartiment beïnvloedde. De resulterende tijd-ac-

tiviteits curves kwamen goed overeen met die van een patiënt. Deze bevindingen impliceren dat het mogelijk is om lokaal, patiënt representatieve contrast kinetiek na te bootsen. Sorptie processen, waaronder ionenuitwisseling en adsorptie, zijn van bijzonder belang omdat deze in essentie: i) vrij diffundeerbare contrast kinetiek in weefsel, ii) reversibele binding van contrast media, en iii) onomkeerbare binding van contrast media aan cellen kunnen nabootsen. In **hoofdstuk 5** wordt aangetoond dat dit op sorptie gebaseerde concept vergelijkbaar is met (hogere orde) contrast kinetiek modellen. Dit proefschrift wordt afgesloten met een haalbaarheidsstudie van de fantoom opstelling voor multimodaal gebruik, inclusief metingen met PET, CT en MRI (**hoofdstuk 6**). De resultaten vertoonden compatibiliteit met deze scanners en softwarepakketten en benadrukten mogelijkheden voor multimodaal fantoom gebruik. We voorzien dat de combinatie van membraan- en sorptietechnologie het nabootsen van weefselperfusiedynamiek in multimodale perfusie fantomen verder kan verbeteren. In MPI wordt dit beoogd tot op het niveau van absolute referentie metingen voor myocardiale perfusie. Momenteel meten we met het fantoom een verschil tussen referentie perfusie (1.5 mL/g/min) en klinisch geschatte perfusie van respectievelijk 0.4, 0.1 en 0.1 mL/g/min voor de drie myocardiale fantoom compartimenten (die de drie kransslagader stroomgebieden voorstellen). Dit nieuwe concept van weefsel nabootsing dient verder onderzocht en gevalideerd te worden voor de verschillende contrastmiddelen. Tevens zijn er aanbevelingen gedaan om de multimodale fantoom opstelling verder te ontwikkelen.

In deze thesis is de basis gelegd voor de (verdere) ontwikkeling van een multimodaal validatie fantoom voor referentie perfusiemetingen in kwantitatieve MPI. Brede toepassing hiervan kan waardevolle inzichten verschaffen in het innovatieve MPI werkveld in een gecontroleerde en patiënt representatieve omgeving. Wij voorzien een toekomst waarin het gebruik van dit soort functionele fantomen wordt opgenomen in klinische richtlijnen om zo de kwaliteit van kwantitatieve perfusie beeldvorming te waarborgen. Deze klinisch georiënteerde modellen kunnen zelfs worden gekarakteriseerd als de “volgende generatie” fantomen. Door de beoogde toegevoegde waarde in het effectiever verbinden van technische en medische disciplines vormen dergelijke fantomen een verrijking van het medische beeldvormingsdomein.

Dankwoord

De afgelopen jaren heb ik kennisgemaakt met veel inspirerende personen die mij hebben geholpen met de totstandkoming van dit onderzoek en proefschrift. Al met al zijn er legio collega's, studenten, vrienden en familieleden die maken dat ik terugblik op een ontzettend leuke en leerzame periode!

Allereerst wil ik mijn promotoren en copromotor bedanken voor hun begeleiding. Ik ben jullie alledrie erkentelijk voor de vrijheid die jullie mij hebben gegeven om zelf sturing te geven aan dit onderzoek en het vertrouwen dat jullie daarbij uitstraalden. **Riemer** en **Marcel**, jullie input tijdens onze twee-wekelijkse meetings heb ik zeer gewaardeerd. Mijn last minute review deadlines waren nooit een issue, ik kon altijd rekenen op jullie feedback. Daarbij heb ik genoten van het uitvoeren van de fantoommetingen in het UMCG, want daar komt de relevantie van dit onderzoek pas echt tot leven! Bedankt hiervoor. **Kees**, wat heb ik veel van jou geleerd en dat besef groeit met de jaren. Ik heb bewondering voor jouw typerende begeleidingsstijl. Je geeft de ruimte om zelf te ontdekken en te groeien en stuurt (meestal) alleen door te vragen. Dat is precies de stimulans die ik nodig heb om het beste uit mijzelf te halen en maakt dat ik heb geleerd een eigen koers te varen en daarop te vertrouwen. Ik hoop deze vaardigheid in het begeleiden ook ooit eigen te maken.

Hoog op het bedank-lijstje staan ook alle technici en laboranten die mij veelvuldig hebben geholpen bij het ontwerpen, realiseren, testen en evalueren van de diverse fantoomopstellingen. **Henny**, bedankt voor je tomeloze inzet. Zonder jouw brede expertise in het ontwerpen en bouwen van flowopstellingen (en in de meet- en regeltechniek die daarbij komt kijken) waren we nooit zo ver gekomen. Je bent een fijne collega om mee samen te werken! Dat geldt tevens voor **Johan**, **Sander** en **Wim**. Jullie zijn zeer bereid mee te denken in oplossingen en jullie kritische, ervaren en praktische kijk op zaken is zeer waardevol. Bedankt voor jullie hulp en input bij de de nuttige en gezellige brainstorm sessies. **Jacqueline**, wat heb jij veel voor mij gedaan in het ZGT en wat ben ik je daar dankbaar voor. Jouw enthousiasme, behulpzaamheid en interesse voor onderzoek en innovatie maakt dat ik altijd met heel veel plezier in een volgeladen auto jullie kant op reed. **Marloes**, ook jij hebt mij

heel erg geholpen! Ik zal nooit vergeten hoe adequaat jij hebt gehandeld tijdens het eenmalige (ietwat radio-actieve) waterballet. Jullie samen zijn een super team in het praktisch meedenken en kunnen dit onderzoek heel goed linken aan de klinische praktijk. Binnen TechMed heb ik ook hulp gehad van **Jaap** en **Remco**. Ondanks jullie voorliefde voor MRI, hebben jullie dikwijls geholpen met de fantoomtesten op de X-ray systemen. Naast dat jullie mij met verve hebben bijgestaan in het X-ray praktijkonderwijs, ben ik jullie ook heel erg gaan waarderen in de rol van onderzoekers. Ik hoop dat jullie daarmee door gaan.

De afgelopen jaren heb ik met verschillende experts kennisgemaakt die ik in al mijn enthousiasme een soort van zijdelings betrokken heb bij dit promotie onderzoek en die altijd paraat stonden met waardevolle adviezen. **Willem van Meurs**, ik heb onze discussies over het nut van (fysieke) modellen en de verificatie en validatie daarvan als zeer inspirerend ervaren. **Klaus Schäfers**, I really enjoyed our elaboration on how to incorporate tissue-mimicking properties in dynamic/stationary myocardial perfusion phantoms. **Srirang Manohar**, bedankt voor je interesse in mijn onderzoek. Mede door jouw sturing lukte het om een fijnere balans te vinden tussen onderzoek en onderwijs. Ook heb ik dankzij jou kennisgemaakt met alle hordes die komen kijken bij een patentaanvraag. **Wiebe de Vos**, bedankt voor onze gesprekken over membraan en sorptie technologie en alle extra hulp die je daarbij geboden hebt. **Jutta Arens**, I have really appreciated our regular lunch meetings and I look forward to continuing these in the future. You are like a mentor to me, whom I can always turn to for good advice.

Natuurlijk wil ik ook iedereen bedanken van de **afdeling Nucleaire Geneeskunde** in het ZGT. Ik heb me altijd heel erg welkom gevoeld en jullie hebben mij van alles bijgeleerd. Ik ken trouwens geen afdeling waarbij er zoveel lekkers met elkaar gedeeld wordt als bij jullie in de koffiekamer. **Ali**, **Leo** en **Nils**, bedankt voor jullie klinische input. **Marjolein**, onze gesprekken waren altijd interessant én gezellig. Het toppunt was voor mij toch wel het EANM congres in Barcelona waar we als delegatie naartoe gingen. Erg leerzaam natuurlijk, maar wat hebben we ook een lol gehad daar! Jullie enthousiasme en betrokkenheid destijds heeft mij enorm gemotiveerd.

De afgelopen jaren heb ik het enorm naar mijn zin gehad bij verschillende groepen op de UT, zowel bij **RaM**, het **ECTM**, de opleidingen **TG** & **BMT**, als bij **M3I**. Het wordt wat veel om iedereen bij naam te noemen, maar dit neemt niet weg dat ik jullie allemaal heel erg waardeer als collega's. **Jolanda**, bedankt voor alles. **Anique**, je bent een top collega en ik ben trots op wat jij neerzet. **Frank**, wie weet word jij ooit cool genoeg om je aan ioniserende straling te wagen en **Erik GJ**, ik vertrouw erop dat jij flowopstellingen ingebed houdt binnen de vakgroep. **Eline**, **Lex**, **Jordy**, **Mathilde** en **Tim**, jullie als mede WijTGers waren een fijn team om op te bouwen. **Selma**, **Marleen**, **Esmeralda**, **Michelle**, **Sebastiaan**, en **Heleen**, ik kijk terug op leuke en leerzame ge-

sprekken met jullie. **Erik K**, **Tim**, **Hadi**, en **Jaimy**, betere kamergenoten had ik mij niet kunnen wensen! **Astrid**, **Eliane** en **Melissa**, bedankt voor de nuttige schrijfsessies en andere leuke dingen die we samen ondernamen. Ook wil ik alle **studenten** bedanken die hebben bijgedragen aan dit onderzoek en de **PhD's en postdocs bij RaM en M3I** voor alle gezelligheid. Last but not least, **Arthur**, bedankt voor alles wat jij de afgelopen jaren voor mij hebt gedaan. Ik waardeer jou heel erg als collega. De vormgeving van dit proefschrift is prachtig en dat komt door jou.

Eliane en **Jaimy**, fijn dat jullie mijn paranimfen wilden zijn. Jullie zijn super collega's met wie je lief en leed kan delen. Het duurt niet lang meer en dan zijn jullie aan de beurt... Succes! **Xenia**, **Joannet**, **Marit**, **Esther** en **Rayke**, ik bof met vriendinnen zoals jullie. Naast het genieten van lekker eten, drinken en de nodige humor, kan ik ook altijd bij jullie terecht voor serieuzere zaken. Jullie zijn een luisterend oor en goede adviseurs. Lieve **papa**, **mama**, **Gert-Jan** en **Evelien**, ik houd ontzettend veel van jullie. Ook jullie hebben vaak genoeg mijn verhalen aangehoord en staan altijd voor mij klaar. Ik ben opgegroeid in een warm gezin en daar ben ik jullie dankbaar voor. Ook waardeer ik het hoe jullie als ouders mij gestimuleerd hebben om te leren en om doorzettingsvermogen te tonen.

Jaap, hierbij een ode aan jou, want jij hebt het de laatste tijd niet gemakkelijk gehad. Jij staat al meer dan twaalf jaar voor mij klaar, vult mij goed aan en maakt mij gelukkig. Je bent rustig, evenwichtig en ook nog eens een fijne sparringspartner. Jij kan gemakkelijk hoofd- van bijzaken onderscheiden en mij op de nodige momenten aansporen om te relativeren. Met jouw humor en positieve blik weet je altijd een lach op mijn gezicht te toveren. Met de kleine man erbij kan ons geluk niet op. Lieve **Ruben**, je bent nu 1,5 jaar oud en het is een feestje om jou te zien opgroeien. Je bent een vrolijk kereltje, niet bang, vol energie en al een tikkeltje eigenwijs. Samen gaan we de toekomst met een lach tegemoet!